

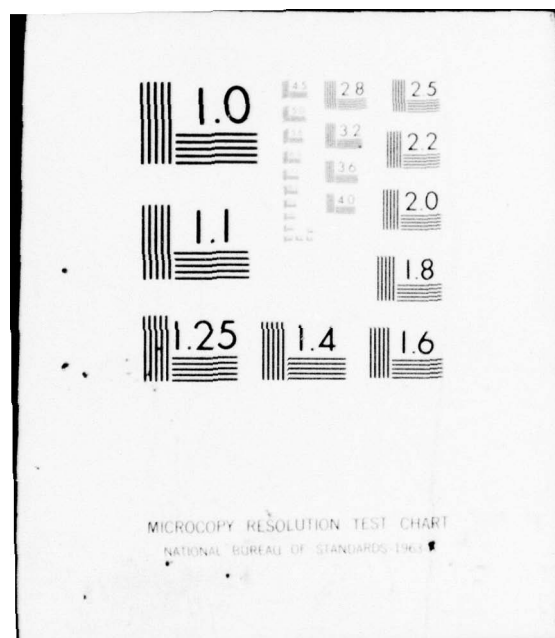
AD-A033 737

SINGER CO LITTLE FALLS N J KEARFOTT DIV
NOISE SOURCES IN NMR OSCILLATORS AND RELAXATION PHENOMENA IN OP--ETC(U)
AUG 76 D S BAYLEY, I A GREENWOOD, J H SIMPSON F44620-72-C-0047
KD76-31 AFOSR-TR-76-1418 NL

UNCLASSIFIED

1 OF 2
AD
A033737





ADA033737

FOSR - TR - 76 - 1418

KD-76-31

[Handwritten signature and circled number 12]

NOISE SOURCES IN NMR OSCILLATORS
AND
RELAXATION PHENOMENA IN OPTICALLY PUMPED
MERCURY ISOTOPES

**Research
Center**

Contract No. F44620-72-C-0047

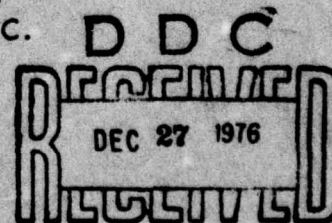
Final Scientific Report
June 1972 to July 1976

prepared by:

Donald S. Bayley, Ivan A. Greenwood, James H. Simpson

prepared for:

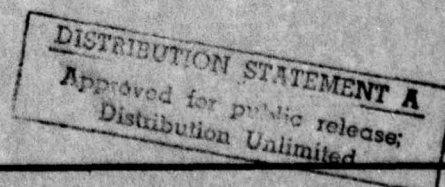
Air Force Office of Scientific Research
Bolling AFB
Washington, D.C.



August 31, 1976

[Handwritten initials] A

SINGER
KEARFOTT DIVISION



AIR FORCE OFFICE OF SCIENTIFIC RESEARCH (AFSC)
NOTICE OF TRANSMITTAL TO DDC
This technical report has been reviewed and is
approved for public release IAW AFR 190-12 (7b).
Distribution is unlimited.

A. D. BLOSE
Technical Information Officer

KD-76-31

NOISE SOURCES IN NMR OSCILLATORS
AND
RELAXATION PHENOMENA IN OPTICALLY PUMPED
MERCURY ISOTOPES

Contract No. F44620-72-C-0047

Final Scientific Report
June 1972 to July 1976

prepared by:

Donald S. Bayley, Ivan A. Greenwood, James H. Simpson

prepared for:

Air Force Office of Scientific Research
Bolling AFB
Washington, D.C.

August 31, 1976

THE SINGER COMPANY
KEARFOTT DIVISION
LITTLE FALLS, NEW JERSEY

THE SINGER COMPANY • KEARFOTT DIVISION

ACCESSION for	
NTIS	Write Section <input checked="" type="checkbox"/>
DOC	Out Copies <input type="checkbox"/>
UNANNOUNCED	<input type="checkbox"/>
JUSTIFICATION	
BY	
DISTRIBUTION AVAILABILITY CODES	
DIR	AVAIL. AND OF SPECIAL

A

1. INTRODUCTION AND SUMMARY

1.1 INTRODUCTION

This final scientific report describes the accomplishments and activities supported by the AFOSR Contract No. F44620-72-C-0047 from June 1972 to July 1976. The effort consisted of two separate investigations, namely, the effects of noise in nuclear magnetic resonance (NMR) oscillators and the relaxation phenomena that randomize the spins of mercury nuclei after initial orientation or alignment by an optical pumping beam.

1.2 NOISE IN NMR OSCILLATORS

The purpose of this portion of the effort was to develop models of possible noise sources, to expand the noise-free model of the NMR oscillator by introduction of these noise models, and to verify the predictions of this extended model by an experimental study of the output of such an oscillator.

It was found that a suitable model was provided by white-noise forcing of an NMR oscillator based on linearized Bloch equations. Experimental confirmation of the theory down to the microhertz level was obtained. This analysis and the experimental results are described in Section 2.

1.3 RELAXATION OF OPTICALLY PUMPED MERCURY ISOTOPES

This portion of the investigation represents four years of effort toward the goal described below. Its continuation is being supported under the AFOSR Contract No. F44620-76-C-0009.

The goal of the investigation is to obtain a better understanding of the following:

- a) Spin-relaxation interactions between optically pumped Hg nuclei and the walls of the cell.

THE SINGER COMPANY • KEARFOTT DIVISION

- b) Interactions between Hg atoms and the cell wall that cause anomalous changes in Hg vapor density and affect the nuclear-spin relaxation by changing the activation energies associated with cell-wall relaxation mechanisms.
- c) The effects of cell material, cell preparation and heat treatment, cell-wall coating and irradiation, and buffer gases on the mechanisms that cause spin-relaxation and control the Hg vapor density.

The apparatus, cell preparation and filling, lamp fabrication and spectra are described in Sections 3, 4, and 5, respectively.

Section 6 is concerned with interactions between Hg atoms and the cell walls or with gaseous impurities within the cell. The realization that such interactions could have a pronounced effect on the investigation of nuclear spin-relaxation occurred early in the program. It arose from observations of anomalies in the temperature dependence of the Hg vapor density as monitored by the transmission of the cell for a beam of resonance radiation.

For cells made of glass the results showed that some of the anomalous changes in Hg vapor density could be caused by a foreign gas. This led to the use of a hotter and longer bake-out during preparation of the cells. Measurements of the transmission of Hg resonance radiation through one fused silica cell showed that after several heat treatments, and at temperatures well below that at which it was sealed off from a liquid mercury reservoir, the cell no longer contained mercury in the liquid phase. Instead there appeared to be three different Hg-wall states each of which had a different Hg-wall bond strength, and all of which were stable and reversible at temperatures below $\sim 320^{\circ}\text{C}$, except when the cell was exposed to Hg resonance radiation. Resonance radiation was found to cause and be required for transitions between these states. A possible model for explaining these results is described below.

THE SINGER COMPANY • KEARFOTT DIVISION

Crystalline silica is known to have at least 22 different phases and sub-phases and vestiges of these structures can appear on the surface of fused silica. It is possible that the three Hg-wall binding states correspond with three different types of surface structure. Mercury atoms excited by the resonance radiation could then transfer energy to one type of the surface structure and by breaking bonds cause a reconstructive transition to another type of structure.

Further experiments showed that heat treatments designed to make the surface of a fused silica cell more like quartz than tridymite so increased the Hg-wall attraction that most of the Hg atoms were removed from the vapor phase.

The relaxation measurements are described in Section 7. The results are summarized below.

- a) The relaxation rate of ^{199}Hg on glass was less than on fused silica. For glass the largest observed transverse relaxation time $\tau_2(\text{max}) = 40.5 \text{ min}$ (at $\sim 300^\circ\text{C}$), whereas for fused silica $\tau_2(\text{max}) = 11 \text{ min}$ (at $\sim 200^\circ\text{C}$).
- b) The relaxation rate of ^{201}Hg on fused silica was less than on glass. For fused silica $\tau_2(\text{max}) = 100 \text{ sec}$ (at $\sim 400^\circ\text{C}$), and for glass $\tau_2(\text{max}) = 50 \text{ sec}$ (at $\sim 300^\circ\text{C}$).
- c) In glass cells the relaxation times of ^{199}Hg and ^{201}Hg increased smoothly with cell temperature. The long ^{199}Hg relaxation times show that the relaxing magnetic dipole interaction was very weak. The much shorter ^{201}Hg relaxation times show that the relaxation was caused primarily by an electric quadrupole rather than a magnetic dipole interaction. The temperature dependence shows that the sources of both relaxing mechanisms were intrinsic to the cell.
- d) In most fused silica cells a completely different situation was found. The temperature dependence of the relaxation time, particularly for ^{199}Hg , not only did not continue increasing with temperature but also depended on whether the cell was being heated or cooled and the extent and nature of the heat treatments applied to the cell after it had been prepared.

THE SINGER COMPANY • KEARFOTT DIVISION

For ^{199}Hg the temperature dependence of the relaxation time showed a large maximum, whose magnitude and location in the region below 300°C depended upon whether the cell was in a heating or cooling cycle. Successive heating and cooling cycles between 25°C and 600°C removed this maximum and tended to stabilize the temperature dependence. Further heat treatments restored the maximum, and exposure to uv radiation during the heat treatment enhanced it and rendered it less sensitive to further heating and cooling cycles. A similar maximum was found in the temperature dependence of the ^{201}Hg relaxation time. Comparison of the ^{199}Hg and ^{201}Hg results showed that as both relaxation times decreased with temperature that for ^{199}Hg in some cases dropped more rapidly and became appreciably less than that for ^{201}Hg .

- e) The maxima in the temperature dependence of the ^{199}Hg and ^{201}Hg relaxation times show that in most fused silica cells there is at least one additional relaxation mechanism which as the cell temperature is increased, overcomes the weaker magnetic and electric interactions that occur in glass cells. The observation that the relaxation time of ^{199}Hg could become less than that of ^{201}Hg provides strong evidence for an additional strong magnetic dipole interaction whose source is intrinsic to the cell and whose strength increases rapidly with temperature (at least in the region up to 400°C). That the strength of this interaction does not depend upon the OH concentration of the fused silica was demonstrated by measurements on cells with widely different OH concentrations. That it may be associated with differences in the surface structure of the cell walls is shown by (1), measurements on the fused silica cell that apparently had three different Hg-wall binding states, (2), measurements of the ^{199}Hg relaxation time in one cell made from the GE204 grade of fused silica which did not show a maximum in the temperature dependence and (3),

THE SINGER COMPANY • KEARFOTT DIVISION

measurements by Bonnot and Cagnac (Ref. 14) which showed that in a cell made from flame-fused silica both ^{199}Hg and ^{201}Hg relaxation times increased with temperature up to respective values of 30 min and 1.5 min at 600°C .

- f) The light induced quadrupole splitting of the ^{201}Hg resonance, that causes the nuclear-spin relaxation to differ from a single exponential function of time, was investigated. Previous measurements by Cagnac (Ref. 15) were made by carefully controlling the magnitude and frequency, respectively, of the dc and rf magnetic fields so that the NMR line width became small enough to observe an .06Hz — splitting of the resonance. The measurements reported here did not require such precise control because they were made by observing the associated beats in the decay of the free precession signal. The increased sensitivity not only allowed more precise confirmation that the splitting disappeared when the light was polarized at $\sim 55^{\circ}$ with respect to the direction of the dc magnetic field H_0 , but also showed that as the light intensity approached zero there remained a cell-intrinsic quadrupole splitting of .0065Hz. It was then found that the magnitude of this intrinsic quadrupole splitting depended on the orientation of the cell axis (the axis of the small seal-off tip) in the same way as the light induced splitting depended on the orientation of the plane of polarization. This splitting could not be observed when the cell axis was oriented at $\sim 55^{\circ}$ with respect to the H_0 field direction. The cell-intrinsic quadrupole splitting of .0065Hz was observed in a fused silica cell. In a larger and more cylindrical glass cell a splitting of .017Hz was measured.
- g) It was found that exposure of a cell made from the GE204 grade of fused silica to uv irradiation increased the ^{199}Hg relaxation rate. At least three exponential time constants, the longest of which is 25 min, are required to describe the recovery (reduction in relaxation rate) of the cell walls after the radiation is removed. These results are similar to those reported by

THE SINGER COMPANY • KEARFOTT DIVISION

French authors (Ref. 20). However our results also showed that the relaxation rate was enhanced by about 30% when the uv radiation contained hyperfine components that could excite the ^{199}Hg atoms in the cell. Exposure of two fused silica cells containing ^{199}Hg and ^{201}Hg to high energy irradiation by β and γ rays and neutrons caused no observable changes in relaxation time or appearance of the cells.

2. NOISE IN NMR OSCILLATORS

2.1 INTRODUCTION

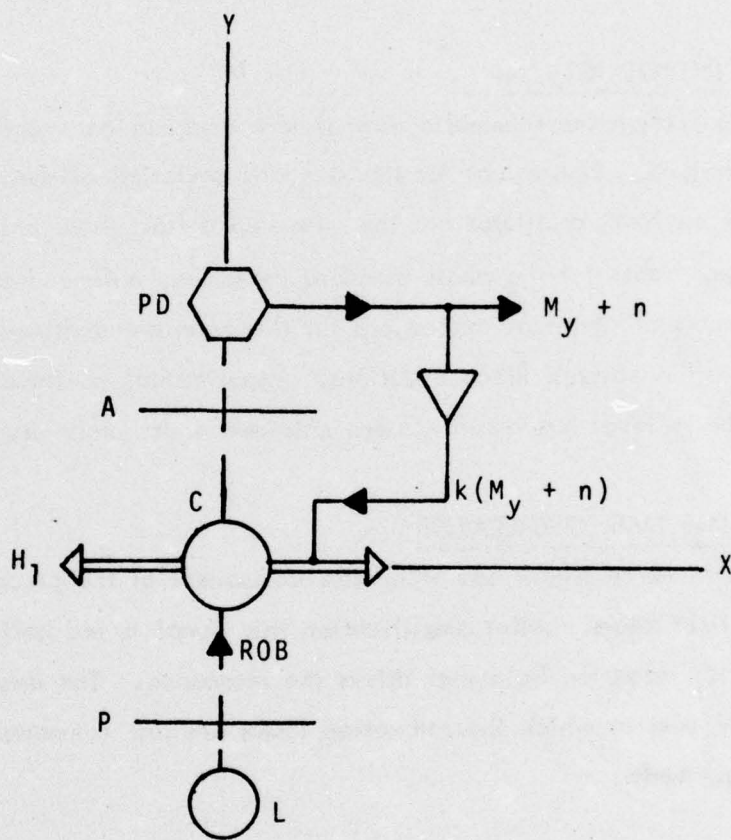
In this section the schematic arrangement of a nuclear magnetic resonance (NMR) oscillator is described. Expressions for the standard deviation of the observed phase angle of the output of an NMR oscillator are then developed from three points of view. The equivalence of the approaches for the phase standard deviation, a time dependent function, is indicated by the fact that identical expressions for this term are obtained. All three approaches are based on linearized Bloch equations. Experimental confirmation of the theory down to the microhertz level has recently been obtained under other programs.

2.2 THE NMR OSCILLATOR

In the NMR oscillator one transverse component of the precessing magnetization is read out by a light beam. After amplification this signal is fed back positively to energize the transverse H_1 magnetic field that drives the resonance. The amplitude of the oscillation adjusts to the level at which the relaxation losses are just compensated by the action of the optical pumping beam.

The frequency of oscillation is determined primarily by the magnitude of the H_0 static magnetic field. This field and the optical pumping beam are directed along the Z axis of the rectangular coordinate system whose X and Y axes are shown in Figure 2-1, which illustrates schematically an NMR oscillator utilizing Faraday-rotation read out. The Y component of the transverse magnetization modulates the output of the photodetector PD and after amplification this signal is fed back positively to the coils (not shown) that produce the H_1 magnetic field.

For convenience in the analysis the output from the photodetector is written as a magnetization and the gain constant k includes all the factors that convert this signal to a magnetic field. This time-dependent output includes the noise $n = n(t)$ which in the analysis will be



A: Analyser
 C: NMR Cell
 k: Gain Constant
 L: Read Out Lamp

P: Polarizer
 PD: Photodetector
 ROB: Read Out Beam

H_1 : Oscillating Transverse Magnetic Field
 $M_y + n$: Transverse Magnetization Component Plus Noise

FIGURE 2-1: The NMR Oscillator

assumed to be the white (shot) noise generated at the photodetector by the photons of the read out beam.

The actual output of the NMR oscillator is the phase of the output signal $M_y + n$, and the analysis will determine the standard deviation of this phase. It will be shown that this can be written as the sum of two terms. The first of these is a constant readout error and corresponds to the phase standard deviation that would be obtained if the feedback path were opened and the H_1 coils driven by an external oscillator. The second is a time-dependent random walk and is caused by white-noise forcing when the feedback path is closed.

2.3 NOMENCLATURE

t = time period over which the phase wander of an NMR oscillator is to be computed.

t_{av} = averaging interval for readout measurement.

τ_1, τ_2 = longitudinal, transverse relaxation times of an optically pumped NMR oscillator after the feedback loop is opened.

M_0 = Z-axis magnetic dipole moment which would be present in the absence of a transverse magnetic field drive.

$M_z \equiv z$ = Z-component of magnetization with transverse drive.

$M_y \equiv y$ = Y-component of transverse magnetization in the laboratory coordinate system.

u, v = orthogonal components of transverse magnetization in the rotating coordinate transformation of the Bloch equations. The directions of H_1 and u are parallel.

y_{nf} = noise-free in-phase moment.

γ = gyromagnetic ratio.

H_1 = transverse magnetic field.

H_0 = Z-axis static magnetic field.

ω = angular frequency.

THE SINGER COMPANY • KEARFOTT DIVISION

$\omega_o = \gamma H_o$ = free precession frequency.

ω_s = undamped natural frequency.

$\omega_2 = 1/\tau_2$.

$n(t)$ = noise amplitude function of time.

$P_n(\omega)$ = noise power per unit (radian/sec) bandwidth.

N/B = noise power per unit (hertz) bandwidth.

S = signal power.

ϕ = a phase angle.

θ = NMR oscillator phase or measured phase.

k = gain constant of NMR feedback path.

σ^2 = variance.

σ = standard deviation = (variance)^{1/2}.

p = operator $d()/dt$.

$L[], L^{-1}[]$ = direct, inverse Laplace Transforms.

$\tau, \lambda, \alpha, \beta$ = dummy integration variables.

f_1, f_2 = time functions.

F_1, F_2 = transforms of f_1, f_2 .

$\delta()$ = delta function (unit impulse function).

C = constant in function used to fit experimental results.

2.4 TIME-DEPENDENT ERROR, METHOD I

An NMR oscillator in the presence of a phase angle, $-\phi$, in its feedback loop runs at a frequency offset $(\omega - \omega_o)$ such that an equal and opposite phase angle, $+\phi$, is generated by the resonance process. From the steady state Bloch equations in a rotating coordinate system rotating at ω relative to the laboratory framework, and neglecting noise,

$$\tan \phi = \frac{u}{v} = \tau_2(\omega - \omega_0). \quad (2-1)$$

Noise added to the feedback signal which drives H_1 , the transverse magnetic field, is averaged over the full running time t , and treated as an average phase perturbation. The phase error of a signal in additive noise averaged for t seconds is

$$\phi_{n,t} = \left(\frac{N/B}{S} \right)^{1/2} t^{-1/2}. \quad (2-2)$$

The average angular frequency error is

$$\overline{\omega - \omega_0} = \tan \phi_{n,t} / \tau_2 \approx \phi_{n,t} / \tau_2, \quad (2-3)$$

and after t seconds, the error in θ is

$$\sigma_{\theta,t} = t(\overline{\omega - \omega_0}) = \left(\frac{N/B}{S} \right)^{1/2} \frac{t^{1/2}}{\tau_2}. \quad (2-4)$$

This equation represents a "random walk" in phase.

2.5 READOUT AND TIME-DEPENDENT ERRORS, METHOD II

Assume an NMR Oscillator is started with no errors. Since the spin system, which is the phase information storage, decays at the initial rate of 100% per τ_2 , it must be read out and new spins added in accordance with the measured phase at the same rate. Assume this is done on a step-by-step basis, averaging the noise-contaminated phase over an interval $t_r \ll \tau_2$, during which the spins are in error-free free precession, followed by reinsertion of the fraction t_r/τ_2 of the spins by an appropriate H_1 pulse. The phase error for each such measurement is

$$\sigma_{\theta,t_r} = \left(\frac{N/B}{S} \right)^{1/2} t_r^{-1/2}, \quad (2-5)$$

THE SINGER COMPANY • KEARFOTT DIVISION

and the oscillator internal phase is altered at each insertion by $\sigma_{\theta, t_r} t_r / \tau_2$. This process is continued up to the start of a final readout averaging interval of duration t_{av} ending at time t . The internal phase error at $t - t_{av}$ is the root sum of squares of $(t - t_{av})/t_r$ additions of $\sigma_{\theta, t_r} t_r / \tau_2$. Therefore,

$$\sigma_{\theta, t-t_{av}} = \left(\frac{N/B}{S} \right)^{1/2} \frac{(t - t_{av})^{1/2}}{\tau_2} \quad (2-6)$$

Note that t_r has cancelled out. As $t_r \rightarrow 0$, this model approaches the continuously operating NMR oscillator.

During the final readout process, two additional errors in indicated output accumulate. The first is the noise contribution to the phase measurement, averaged over t_{av} . The second is the phase random walk during the averaging interval t_{av} . Since these terms are correlated, they must be added before rms addition to the statistically independent internal phase error at $t - t_{av}$.

$$\sigma_{\theta, \text{readout}} = \left(\frac{N/B}{S} \right)^{1/2} \left(\frac{1}{t_{av}^{1/2}} + \frac{2}{3} \frac{t_{av}^{1/2}}{\tau_2} \right) \quad (2-7)$$

The final expression for the error in the indicated output at $t = t$ is then

$$\sigma_{\theta, t} = (\sigma_{\theta, t-t_{av}}^2 + \sigma_{\theta, \text{readout}}^2)^{1/2} \quad (2-8)$$

$$\sigma_{\theta, t} = \left(\frac{N/B}{S} \right)^{1/2} \left[\frac{t - t_{av}}{\tau_2^2} + \left(t_{av}^{-1/2} + \frac{2}{3} \frac{t_{av}^{1/2}}{\tau_2} \right)^2 \right]^{1/2} \quad (2-9)$$

$$= \left(\frac{N/B}{S} \right)^{1/2} \left[\frac{t}{\tau_2^2} + \frac{1}{t_{av}} + \frac{12\tau_2^2 - 5t_{av}}{9\tau_2^2} \right]^{1/2} \quad (2-10)$$

For $t_{av} \ll \tau_2$ this reduces to

$$\sigma_{\theta,t} = \left(\frac{N/B}{S} \right)^{1/2} \left[\frac{t}{\tau_2} + \frac{1}{t_{av}} \right]^{1/2}. \quad (2-11)$$

The time dependent part of this result agrees with that found previously, Eq. (2-4). Equation (2-11) was derived earlier by J. Simpson by a similar argument (Ref. 1).

2.6 TIME-DEPENDENT ERROR, METHOD III

In the third derivation, the full equations of the NMR oscillator are used. From these are developed a linear transfer function relating the output error to the noise forcing. The solution for white noise forcing is then found.

The system equations used were taken, with minor modifications, from a study by S. Sherman (Ref. 2). The solution for white noise forcing has drawn on a similar calculation for another problem by H. Strell (Ref. 3).

The equations for the NMR oscillator are found by solving in the laboratory framework for the Y-component of magnetization, assuming that the H_1 transverse magnetic field linearly polarized along the laboratory X-axis is given by

$$H_1 = k[M_y + n(t)]. \quad (2-12)$$

The dynamic equation for $y \equiv M_y$ is then

$$\left[p^2 + \left(\frac{2}{\tau_2} - \gamma kz \right) p + \gamma^2 H_o^2 + \frac{1}{\tau_2^2} - \frac{\gamma kz}{\tau_2} \right] y = \gamma kz (1/\tau_2 + p) n(t). \quad (2-13)$$

In the steady state, the coefficient of the py damping term vanishes. Therefore

$$\gamma k \bar{z} = 2/\tau_2 \equiv 2\omega_2.$$

The equation may then be simplified and written as a linear transfer function

$$\frac{y(p)}{n(p)} = \frac{2\omega_2 (p + \omega_2)}{p^2 + \omega_s^2}, \quad (2-14)$$

in which

$$\omega_s^2 = \omega_o^2 - \omega_2^2, \text{ and}$$

$$\omega_o = \gamma H_o.$$

The NMR oscillator is now assumed to be in steady state oscillation, and the effect of in-phase noise is ignored since it does not lead directly to a phase change. The buildup with time of a very small orthogonal oscillation mode $y(t)$ forced by noise and the resulting perturbation of the noise free phase will be found. These assumptions linearize the equations by excluding the perturbation of z forced by the noise.

The convolution theorem*,

$$\int_0^t f_1(\lambda) f_2(t - \lambda) d\lambda = L^{-1}[F_1(p) F_2(p)], \quad (2-15)$$

where $F_1 = L[f_1]$, and $F_2 = L[f_2]$, provides the next step. The function $y(t) = L^{-1}[y(p)]$ is obtained from equation (2-14) by letting

$$F_1(p) = \frac{2\omega_2 (p + \omega_2)}{p^2 + \omega_s^2}, \text{ and}$$

$$F_2(p) = n(p).$$

*This is also known as Borel's theorem. See, for instance, Ref. 4, p.121.

THE SINGER COMPANY • KEARFOTT DIVISION

Then

$$f_1(\lambda) = 2\omega_2(\cos \omega_s \lambda + \frac{\omega_2}{\omega_s} \sin \omega_s \lambda), \text{ and}$$

$$f_2(t - \lambda) = n(t - \lambda).$$

An NMR oscillator is usually operated under conditions such that $\tau_2 \gg 1/\omega_0$. Thus $\omega_2 \ll \omega_0$ and the above equations can be simplified by substituting $\omega_s = \omega_0$ and neglecting ω_2/ω_s . The result is that after a time t the noise-forced oscillation has an amplitude

$$y(t) = 2\omega_2 \int_0^t n(t - \lambda) \cos \omega_0 \lambda d\lambda. \quad (2-16)$$

and the corresponding variance $\sigma_y^2(t) = [y(t)]^2$. The ensemble average of the time average, $\sigma_y^2 = [\overline{\sigma_y^2(t)}]$ can be written as

$$\sigma_y^2 = 4\omega_2^2 \int_0^t \int_0^t \overline{n(t - \alpha) n(t - \beta)} \cos \omega_0 \alpha \cos \omega_0 \beta d\alpha d\beta. \quad (2-17)$$

From the Wiener-Khintchine theorem (see, for instance, Ref. 5, Section 28),

$$\overline{n(t - \alpha) n(t - \beta)} = \int_0^\infty P_n(\omega) \cos \omega (\alpha - \beta) d\omega, \quad (2-18)$$

where $P_n(\omega)$ is the noise power spectral density. For white noise

$$P_n(\omega) = \frac{N/B}{2\pi} \quad (2-19)$$

where N/B is the constant noise power over a bandwidth of one hertz. Then

$$\overline{n(t - \alpha) n(t - \beta)} = \frac{N/B}{2\pi} \int_0^\infty \cos \omega (\alpha - \beta) d\omega. \quad (2-20)$$

From Ref. 4, Appendix E, eq. 26, the integral in equation (2-20) equals π if $\alpha = \beta$ and equals zero if $\alpha \neq \beta$. Equation (2-20) becomes

$$\overline{n(t - \alpha) n(t - \beta)} = \frac{N/B}{2} \delta(\alpha - \beta), \quad (2-21)$$

where $\delta(\alpha - \beta)$ is the unit impulse function. Substituting this into equation (2-17) and integrating gives

$$\sigma_y^2 = \omega_2^2 (N/B) \left[t + \frac{1}{2\omega_0} \sin 2\omega_0 t \right],$$

or since $t \gg 1/\omega_0$,

$$\sigma_y^2 = \omega_2^2 t N/B. \quad (2-22)$$

The noise $y(t)$ was assumed in quadrature with the noise free signal amplitude y_{nf} . The corresponding perturbation in phase $\Delta\theta(t) = y(t)/y_{nf}$, and

$$\sigma_{\theta,t}^2 = \frac{\sigma_y^2}{y_{nf}^2} = \frac{\sigma_y^2}{S} = \frac{\omega_2^2 t N/B}{S},$$

where S is the signal power.

Since $\omega_2 \equiv 1/\tau_2$,

$$\sigma_{\theta,t} = \left(\frac{N/B}{S} \right)^{1/2} \frac{t^{1/2}}{\tau_2}. \quad (2-23)$$

This agrees with the results found previously, equations (2-4) and (2-11).

2.7 EXPERIMENTAL VERIFICATION OF TIME-DEPENDENT DRIFT

Putting numbers typical of operating mercury NMR oscillators in the above time-dependent drift equation (2-23) leads to very small phase errors. For example, if $\frac{N/B}{S} = -60\text{dB}(10^{-6})$, 1Hz), $\tau_2 = 10$ seconds, and $t = 3600$ seconds,

$$\sigma_{\theta,t} = \frac{(10^{-3})(60)}{10} = 6 \times 10^{-3} \text{ radian} = 0.34^\circ \text{ after one hour.}$$

To observe this directly with a single NMR oscillator would require a magnetic field instability given by

$$\Delta H_0 \gamma t < .34 \text{ deg.}$$

For ^{199}Hg , where $\gamma = 2.7 \times 10^5 \text{ deg/sec/oersted}$, this would require that

$$\Delta H_0 < \frac{.34}{2.7 \times 10^5 \times 3.6 \times 10^3} \sim 3 \times 10^{-10} \text{ oersted.}$$

The independent oscillator (clock) against which the field-stabilized oscillator is compared must have an instability of $< 3 \times 10^{-10}$ if the experiment is operated at $H_0 = 1$ oersted. While the reference oscillator requirement could be met, the ΔH_0 stability requirement is impractical by any normal means, if not impossible. To make matters worse, fluctuations in optical pumping and read out beams would contribute fluctuations in light-induced shifts which would swamp this result.

A pair of intercompared NMR oscillators operating in the same magnetic field could eliminate two requirements, field stability and an independent high stability clock. However, the light-induced frequency shift problem would not be eliminated.

The remaining problems can be solved by using two sets of double oscillators, as in the NMR gyroscope. Effects such as light-induced frequency shifts can be balanced by

THE SINGER COMPANY • KEARFOTT DIVISION

achieving light beam balances and other symmetries.

In recent tests by the contractor of an NMR gyroscope model, the indicated angle output was recorded for long periods, usually a little over an hour. Readings were taken every 2, 4, 8, and 16 minutes, and the standard deviations of the output changes over these intervals computed. These points were fitted to the function $Ct^{1/2}$, and extrapolated to $t = 3600$ seconds. Typical results are shown in Table 2-1.

TABLE 2-1

$\frac{N/B}{S}, \tau_2$	Computed $\sigma_{\theta, 3600}$	Observed $\sigma_{\theta, 3600}$
-45dB, 1 sec	19.3 deg	20 deg
-52dB, 3.9 sec	2.21 deg	3 deg
-54dB, 16 sec	0.42 deg	1 deg

These results are taken as better-than-order-of-magnitude confirmation of the theoretical results presented in the previous sections. Details of these experiments are reported in Ref. 1.

3. DESCRIPTION OF THE APPARATUS

3.1 ARRANGEMENT

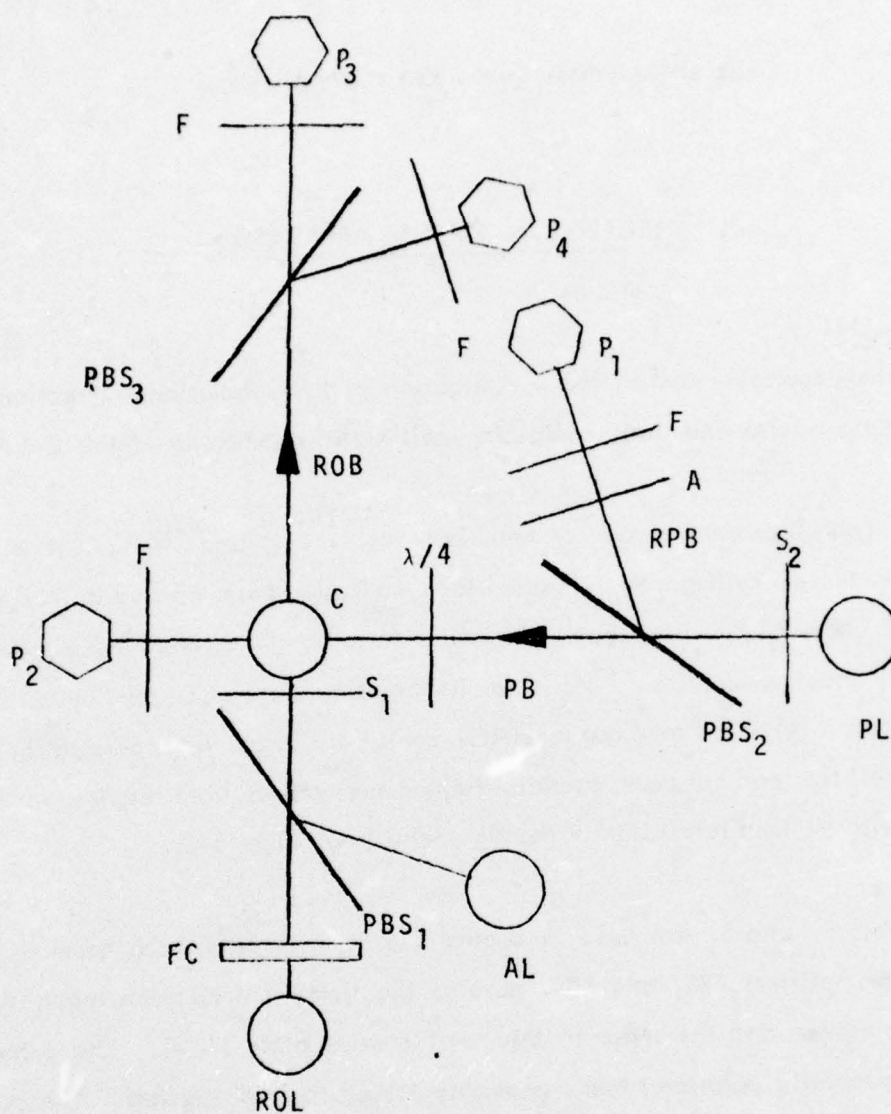
A schematic of the apparatus used in the investigation of the relaxation interactions between optically pumped Hg nuclei and their containing-cell wall is shown in Figure 3-1.

The NMR cell C contains atoms of one or both isotopes, ^{199}Hg and ^{201}Hg . It is mounted at the intersection of two orthogonal uv light beams, a pump beam PB and a read out (Faraday rotation) beam ROB. Each beam originates from an rf - excited Hg discharge lamp. The pump lamp PL usually contains ^{204}Hg since its radiation can be absorbed by both ^{199}Hg and ^{201}Hg (see Figure 5-1). The read out lamp ROL contains ^{202}Hg . After passing through the $^{199}/^{201}\text{Hg}$ filter cell the read out beam contains the non-resonant uv light required for Faraday-rotation read out with minimal relaxation of the Hg nuclei (see Figure 5-3).

Photographic shutters S_1 and S_2 are used to control the "on" time of each beam as desired. The polarizing beam splitters PBS_1 and PBS_2 provide the linear polarization required for Faraday-rotation read out and the input to the quarter-wave plate ($\lambda/4$). The output of the latter is the circularly polarized beam necessary for optical orientation. The polarizing beam splitters each contain a stack of thin fused silica plates mounted at the Brewster angle. The quarter-wave plate is a thin, x-cut, synthetic quartz crystal.

These beam splitters also facilitate illumination of the NMR cell by radiation from the auxiliary lamp AL and generation of the reflected pump beam RPB. The purpose of these provisions is described in Section 3.3.

The polarizing beam splitter PBS_3 in the readout beam serves as the analyzer that converts the Faraday rotation into amplitude modulation. Use of both the transmitted and reflected beams from PBS_3 allows the detected NMR signal to be doubled, as described in Section 3.2.



A: Attenuator
 AL: Auxilliary Lamp
 C: NMR Cell
 F: 253.7nm Filters
 FC: 199/201 Filter Cell
 RPB: Reflected Pump Beam
 $\lambda/4$: Quarter Wave Plate

L: Lamp
 P: Photomultipliers
 PB: Pump Beam
 PBS: Polarizing Beam Splitters
 PL: Pump Lamp
 ROB: Read Out Beam
 ROL: Read Out Lamp
 S: Shutters

FIGURE 3-1 - Arrangement of Apparatus

The photomultipliers P_1 through P_4 measure the light intensities of the various beams. The optical band-pass filters F remove all but the 253.7nm components of the radiation from the lamps. The neutral density attenuator A is used to provide a light intensity at P_1 comparable to the highest intensity at P_2 (see Section 3.3).

3.2 MEASUREMENT OF NMR SIGNALS AND RELAXATION TIMES

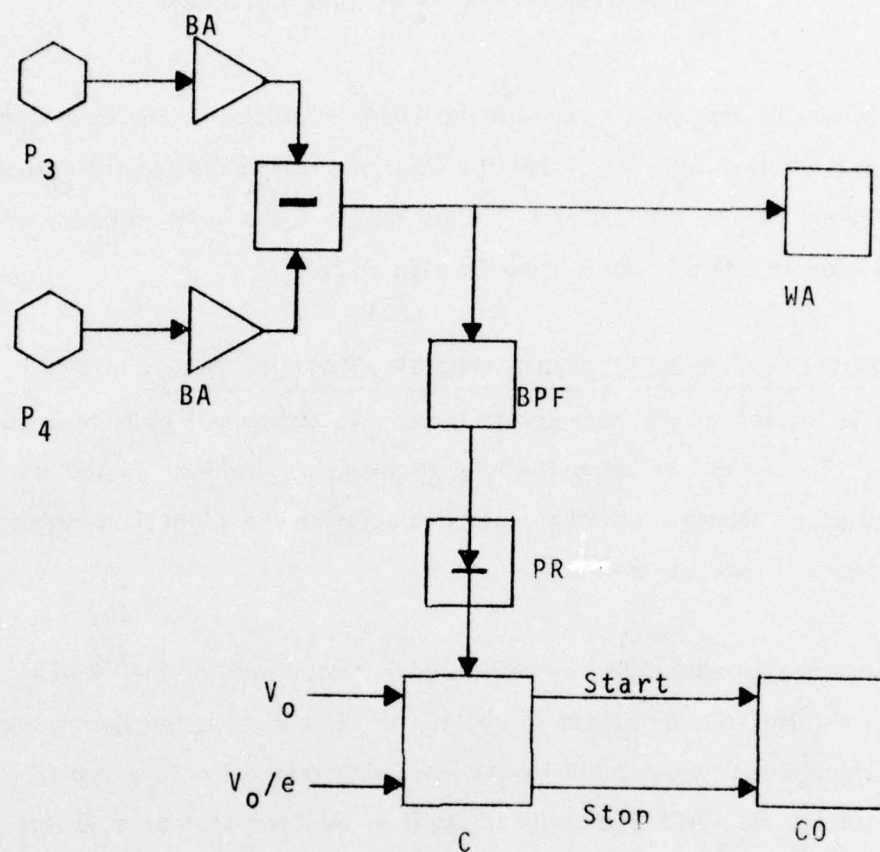
The NMR cell is located at the common center of two orthogonal pairs of coils (not shown in Figure 3-1). These produce respectively a dc magnetic field H_0 in the direction of the pump beam and an ac magnetic field H_1 perpendicular to the plane containing the optical axes of the pump and read out beams.

A magnetic resonance is established by adjusting the magnitude of the field H_0 to equal $2\pi f/\gamma$, where $f = 1\text{kHz}$, the frequency of the H_1 field, and γ is the gyromagnetic ratio of the particular Hg nucleus whose NMR signal level and relaxation time are to be measured. The magnitude of the H_1 field is usually adjusted so that the resonance is just saturated.

The rotating component of the magnetization causes the plane of polarization of the non-resonant read out beam to oscillate at the Larmor frequency (1kHz in this case). The analyzer PBS_3 has its pass axis mounted at 45° with respect to that of the polarizer PBS_1 in the incident read out beam. The intensities of the transmitted and reflected beams from the analyzer are hence modulated at the Larmor frequency and the two modulation signals have opposite phases.

As shown in Figure 3-2, the outputs from the two read out photomultipliers are buffered, subtracted, and fed to a wave analyzer. This input to the wave analyzer has twice the amplitude of the intensity modulation on each output beam from the analyzer PBS_3 .

For measurement of relaxation time with the read out beam "on" continuously the differential output from the read out beam photomultipliers is filtered, rectified, and fed to the comparator C . An adding circuit (not shown) allows the mean value of the rectified noise plus



BA: Buffer Amplifier
 BPF: Band-Pass Filter
 C: Comparator
 CO: Counter
 P_3, P_4 : Read Out Photomultipliers
 PR: Precision Rectifier
 V_0 : Reference Voltage
 WA: Wave Analyzer

FIGURE 3-2- Signal and Relaxation Time Measurement.

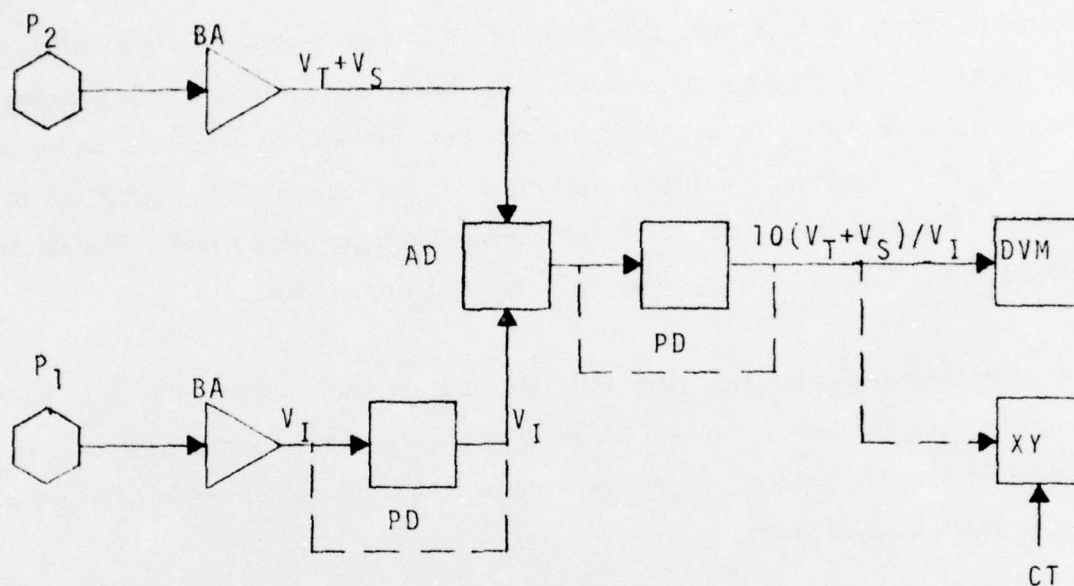
that of any dc offset to be nulled at the output of the precision rectifier PR. The pump beam shutter S_2 (Figure 3-1) is then closed and this operation provides a signal which simultaneously deenergizes the H_1 magnetic field coils. The relaxing magnetization then appears as a corresponding decay in the output of the rectifier. When this reaches a preset reference level V_0 the comparator provides a start signal to the counter CO. After the output has decayed to $1/e$ of this initial value the comparator stops the counter. The relaxation time is read as the time interval between the start and stop signals.

For measurement of relaxation time with the read out beam pulsed, the pump beam and H_1 magnetic field are initially turned off as above. The readout beam shutter S_1 (Figure 3-1) is then operated to produce the minimum pulse width that will provide accurate sampling of the wave analyzer output.

3.3 CELL TRANSMISSION MEASUREMENT

The transmission of the NMR cell C for ^{199}Hg and/or ^{201}Hg resonance radiation is used as a monitor for the Hg vapor density within the cell. In order to make the measurements independent of pump lamp intensity the cell transmission monitor output is developed as a signal proportional to the ratio of the transmitted and incident intensities of the pump beam.

As shown in Figure 3-3, the outputs of the pump beam photomultipliers P_1 and P_2 (Figure 3-1) are buffered and fed as input signals, $V_T + V_S$, and V_I to the analog divider AD whose output is ten times the ratio of its inputs. The signal V_S is generated by light scattered from the read out beam into the transmitted pump beam photomultiplier P_2 . Although the instrumentally scattered light is very small that re-emitted by the H_g vapor can reach nearly 10% of the transmitted pump beam light when the cell is exposed to resonance radiation from the auxiliary read out lamp AL (Figure 3-1). The signal V_S , measured at the output of the ratio detector when the transmitted pump beam is blocked, is applied as a correction to the cell transmission monitor output recorded by the digital voltmeter DVM or the X-Y recorder.



AD: Analog Divider
 BA: Buffer Amplifier
 CT: Cell Temperature
 DVM: Digital Voltmeter
 PD: Peak Detector
 P_1, P_2 : Pump Beam Photomultipliers
 V_I, V_T : Inc.(Trans.) Outputs
 V_S : Output from RO Beam Scat. Light
 XY: X-Y Recorder

FIGURE 3-3 - Cell Transmission Measurement.

THE SINGER COMPANY • KEARFOTT DIVISION

The attenuator A (Figure 3-1) in the reflected pump beam is initially adjusted to hold the maximum output of the analog divider to about 10V. This not only keeps the analog divider within its linear range of operation but also allows the dynodes of both photomultipliers P_1 and P_2 to be operated from the same high voltage supply. As a result the reference input V_1 for the analog divider can be held constant (at 8V) by adjusting the dynode voltage. This greatly reduces the error in the output of this component as compared with operation over the full range (1 to 10V) of this reference signal.

The equipment shown in Figure 3-3 allows cell transmission measurements to be made either when the pump beam is "on" continuously or when it is pulsed via the shutter S_2 (Figure 3-1). The continuous measurements facilitate operation with the X-Y recorder.

For pulsed operation the open time of the shutter S_2 is $\sim .03$ sec. The peak detectors PD shown in Figure 3-3 have rise times of less than 1 msec and decay times greater than 5000 sec. They therefore provide accurate sampling of the inputs and output of the analog divider and hold the latter essentially constant during the time required to fully excite and read the digital voltmeter. It was found that variations in the rapid rise times of the photomultipliers could cause a false peak in the output of the analog divider. This was overcome by increasing the response time of the buffer amplifier fed by photomultiplier P_2 to ~ 5 msec.

An important advantage of the pulsed operation is that it allows the cell transmission to be measured in the "dark" (i.e. without irradiation except during the short pulses), with irradiation by non-resonant light from the filtered ^{202}Hg read out beam, and with resonant radiation either for ^{201}Hg or for both ^{201}Hg and ^{199}Hg , provided by the auxiliary lamp AL (Figure 3-1).

3.4 CELL TEMPERATURE CONTROL

The NMR cells were heated or cooled by an air stream directed at the cell and perpendicular to the read out and pump beams shown in Figure 3-1. The air was heated by passing several times through a coil energized with a Variac fed from the 115V, 60Hz line. Perturbation of the resonance by the heater coil was made negligible by three concentric, cylindrical magnetic shields that surrounded the cell and the coils that produced the H_0 and H_1 magnetic fields. Cooling was accomplished by passing the air through a copper coil immersed in ice water.

The temperature of the cell was measured by a contacting thermocouple (Cu-constantan for temperatures below 400°C , or Pt - (Pt, Rh) for higher temperatures).

4. DESCRIPTION AND PREPARATION OF NMR CELLS

The NMR cells used during the investigation of nuclear spin relaxation were made either from various grades of fused silica or from the uv-transparent Corning 9741 glass. Most of the cells were prepared as "dry" cells, i.e., so that the contained Hg vapor became unsaturated when the cell was heated above the temperature of the Hg reservoir used during the filling and seal-off process. The cells were filled in various proportions with the isotopes ^{199}Hg (86% purity) and ^{201}Hg (82% purity).

Two of the cells, #27 and #49, used in the investigation were prepared several years before this program began. Cell #27 was made from the GE204 grade of fused silica and is a sphere 2.5cm in diameter. Cell #49 was made from Corning 9741 glass and is a cylinder with approximately spherical ends. It is 1.5 cm in diameter and 2.5 cm long. The cells prepared during the program are 1 cm diameter spheres. All cells have seal-off tips which protrude from the spherical region of the surface.

The basic cell preparation procedure was as follows:

- a. One-cm dia. bulbs were blown from stock using a natural gas and oxygen flame. No dessicant was used in the blowing tube.
- b. Several (usually four) cells were attached to a manifold and this was then sealed to a vacuum system equipped with a Vac-Ion pump.
- c. The desired Hg isotopes were held on Au wire in a side arm immersed in liquid N_2 .
- d. The system was evacuated to about 10^{-7} torr and the cell blanks were held at temperatures as high* as 1100°C ($\sim 600^\circ\text{C}$ for the glass cells) for at least 16 hours. The liquid N_2 was periodically removed from the side arm containing the Hg in order to allow trapped vapors to escape.

*Some fused silica cells were baked out at temperatures as low as 950°C . As will be seen the results indicate that the bake out temperature should be as high as possible.

THE SINGER COMPANY • KEARFOTT DIVISION

- e. The Hg was driven into the manifold which was then sealed off from the vacuum system.
- f. The seal-off tip of the manifold was placed in liquid N_2 and all other parts including the cell blanks were flamed lightly to drive the mercury to the cold tip.
- g. One cell blank was flamed for about 5 minutes with the manifold tip in liquid N_2 .
- h. This bulb was placed in water and boiled for 30 minutes while the manifold was placed in another water bath held at the "seal-off" temperature (usually 15° or $30^\circ C$).
- i. The bulb was sealed off from the manifold under the temperature conditions of step h.
- j. Steps g, h, and i were repeated for each bulb on the manifold.

Corning 9741 glass and various grades of fused silica were used in preparing the cell blanks. In order to investigate a possible correlation between the spin relaxation of the Hg nuclei and the OH content of the cell walls qualitative measurements of the strength of the 2.7 - micron OH^- absorption band were made for these materials. The results are shown in Table 4-1. Further testing showed that the OH^- absorption of Spectrosil and GE-204 increase when the material is worked in a flame. In the case of the GE-204, it was found that the absorbing substance existed only in a thin layer at the surface of the material. This layer has been successfully removed either by HF etching or by heating the fused silica to $1100^\circ C$ under high vacuum.

THE SINGER COMPANY • KEARFOTT DIVISION

TABLE 4-1. Absorption of Cell Material at 2.7μ

Material Code Letter	Cell Material	OH Free (per manufacturer)	Observed 2.7μ Absorption		
			0	Weak	Strong
T	Tetrasil				X
S	Tetrasil SE	X		X	
U	Suprasil				X
W	Suprasil W2	X	X		
O or N	Spectrosil			X	
G	GE204	X	X		
F	OH-Free	X			X(!)
P	Coming 9741 (glass)				X

The code letter is used for cell material identification. For instance, W1 indicates the first cell of this new series that was prepared from Suprasil W2. The letters O or N for Spectrosil distinguish between the original and the more recently received stock of the material in our laboratory. Manufacturer's designations are used to describe the cell material.

The experimental results reported herein led to several modifications in the basic procedure used for preparing the NMR cells. The first of these resulted from the indication that an appreciable foreign gas pressure might exist in some cells.

In order to increase the temperature for outgassing of the walls of the Corning Glass cells the cell blanks were placed in a fused silica tube that was then sealed onto the vacuum system. A tube furnace was used to maintain the cell blanks at a temperature just below the softening point. The cell blanks were then baked for 48 hours at a pressure not greater than 10^{-7} torr. They were then removed from the vacuum system and quickly sealed onto

THE SINGER COMPANY • KEARFOTT DIVISION

a pyrex manifold for filling with mercury.

In order to insure that gas was not evolved from impurities in the mercury or on its gold wire holder the mercury was first driven from the wire to a cool spot on the system, the gold wire was removed, and the distilled mercury then exposed to the vacuum system for about four hours. After this some of the mercury from the cold spot was driven into the manifold which together with the cell blanks was then sealed off from the vacuum system.

For the fused silica cells the baking time was increased to 48 hours and the mercury also purified as described above. As previously mentioned it was also found that the bake-out temperature should be as high as possible.

Several special procedures were used in attempts to modify the surface structure of fused silica cell walls. They will be described later, along with the experiments that suggested them.

5. DESCRIPTION AND SPECTRA OF THE MERCURY LAMPS

5.1 DESCRIPTION OF THE MERCURY LAMPS

The 1-cm dia. mercury lamps used in this investigation have the same shape as the 1-cm dia. NMR cells. They were blown from fused silica, evacuated, filled with ~ 2.5 torr of argon and a small drop of the desired Hg isotope, sealed-off, and mounted inside a cylindrical coil that was excited by a 100MHz oscillator. A description of the preparation procedure and the oscillator is given in Ref. 6.

5.2 THE 253.7nm Hg LINE, STRUCTURE AND ZEEMAN COMPONENTS

This subsection provides a brief review of the well known hyperfine and isotopic structure of the 253.7nm Hg resonance line and of the Zeeman components associated with the various hyperfine transitions of ^{199}Hg and ^{201}Hg . Part of it was adapted from information collected by B. Cagnac and described in his doctoral thesis (Ref. 7). It is included to facilitate description of the conditions under which the experiments were performed and as an aid in interpreting some of the results.

The hyperfine and isotopic structure of the 253.7nm Hg transitions, $6^1S_0 \leftrightarrow 6^3P_1$, is shown in Figure 5-1. All line separations are measured in cm^{-1} and referenced against the even isotope ^{200}Hg . The half integers following the odd isotope numbers are the values of the total angular momentum quantum number F for the excited 6^3P_1 state. The letters in parentheses identify the particular hyperfine transition, i.e., 199(A), 201(c), etc. It can be seen that many of the line separations are larger than the Doppler width ($.034 \text{ cm}^{-1}$ at 25°C) for absorption by the Hg atoms in the NMR cell.

Emission spectra of four isotopically different Hg lamps obtained in our laboratory with a scanning Fabry-Perot spectrometer are shown in Figure 5-2. The predominant isotope and its purity are listed to the right of each spectrum, the ^{201}Hg hyperfine transitions are indicated at the bottom of the figure, and the ^{199}Hg hyperfine transitions as well as the emission lines

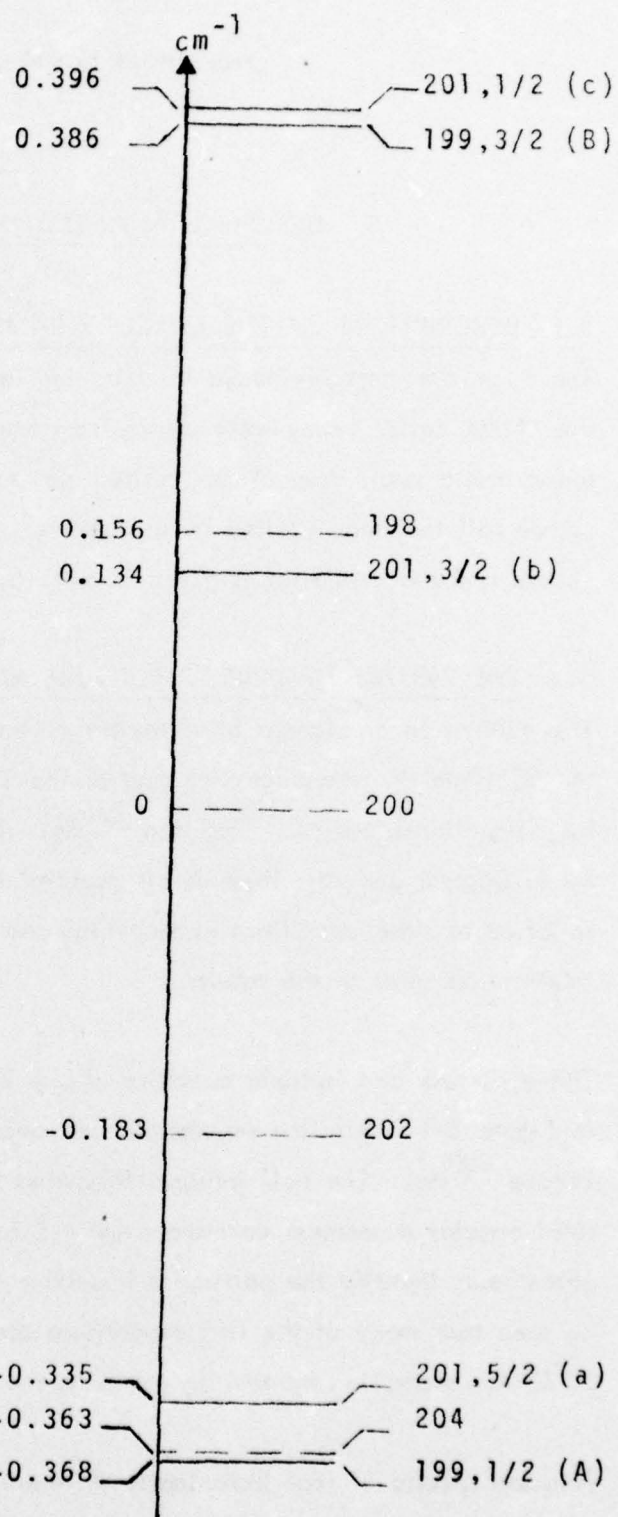


FIGURE 5-1 - Hyperfine and Isotopic Structure of the 253.7 nm Hg Transition, $6^1S_0 \leftrightarrow 6^3P_1$.

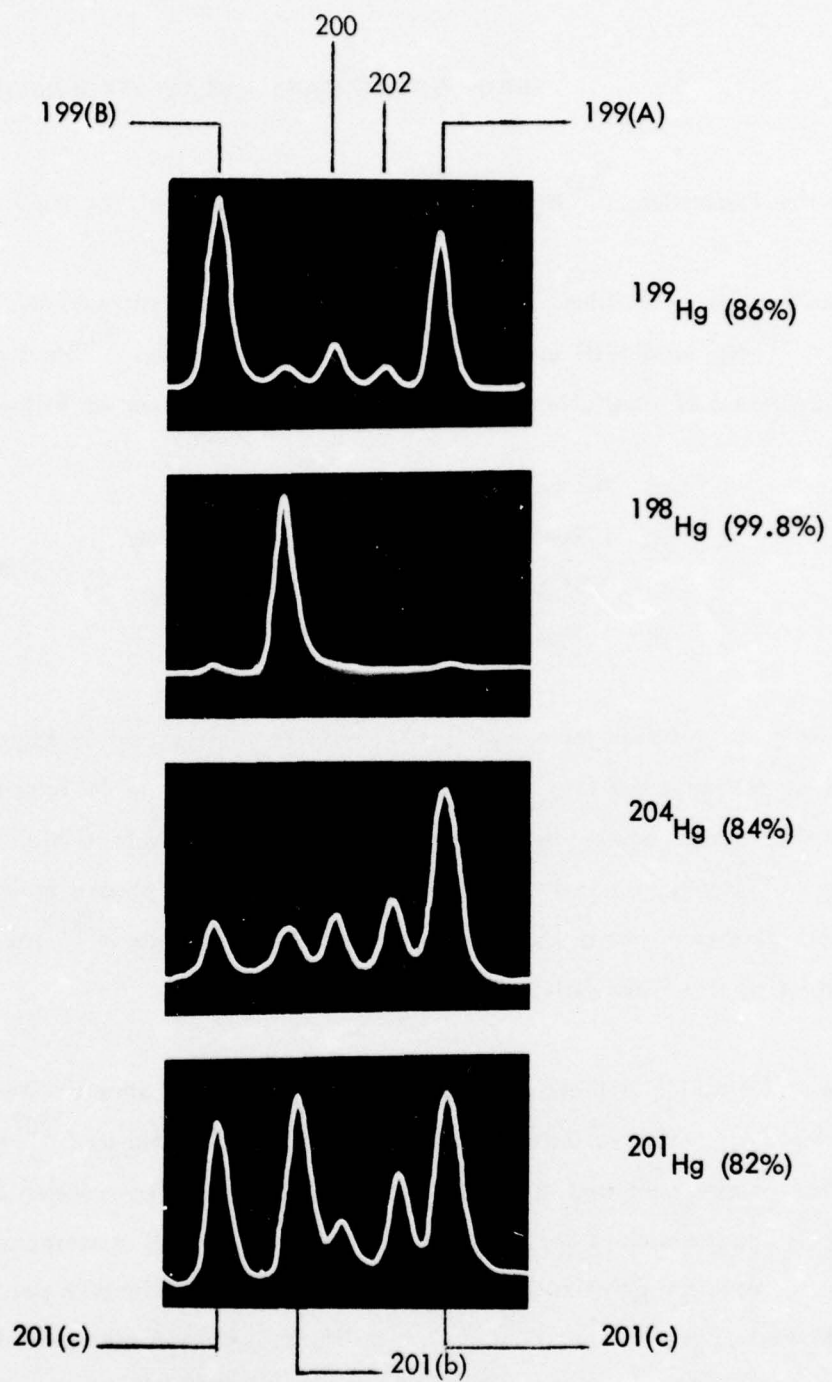


FIGURE 5-2. Hg Lamp Emission Spectra, 253.7nm

from the impurities, ^{200}Hg and ^{202}Hg , are indicated at the top.

In NMR cells containing ^{199}Hg and ^{201}Hg in various proportions, it is seen from Figure 5-2 that a ^{201}Hg lamp will excite the ^{199}Hg as well as the ^{201}Hg hyperfine transitions, and that preferential excitation of these transitions will occur as follows:

- a) All but 201(b) by a ^{199}Hg lamp;
- b) 199(A) and 201(a) by a ^{204}Hg lamp;
- c) 199(B) and 201(c) by a ^{199}Hg lamp and a ^{204}Hg filter cell; and
- d) 201(b) by a ^{198}Hg lamp.

The emission spectrum obtained for a ^{202}Hg lamp is shown in Figure 5-3. It shows the onset of self-reversal for ^{202}Hg and the relative increase in intensity of the impurity emission lines that occur when the air cooling is reduced. Figure 5-3(c) is the spectrum obtained for the ^{202}Hg light when a $^{199}/^{201}\text{Hg}$ filter cell was placed between the lamp and spectrometer. It shows that a large percentage of the ^{199}Hg and ^{201}Hg resonance radiation was absorbed in the filter cell.

Figures 5-4 and 5-5 show the Zeeman components and unnormalized transition probabilities associated with the various hyperfine transitions of ^{199}Hg and ^{201}Hg . The magnetic quantum numbers m' and m correspond respectively to the excited and ground states of the atoms. The transitions for which $\Delta m = m' - m = 1(-1)$ correspond to absorption of $\sigma^+(\sigma^-)$ circularly polarized light. An unpolarized or linearly polarized pump beam can excite both $\Delta m = +1$ and $\Delta m = -1$ transitions. A read out beam linearly polarized parallel to H_0 can excite the $\Delta m = 0$ transitions. An unpolarized read out beam can excite all transitions.

In Figure 5-5, the numbers in parenthesis represent the relative populations of the magnetic sublevels in the ground state that are established by an unpolarized or linearly polarized pump beam. These population distributions correspond primarily to alignment rather than orientation of the ^{201}Hg nuclei.

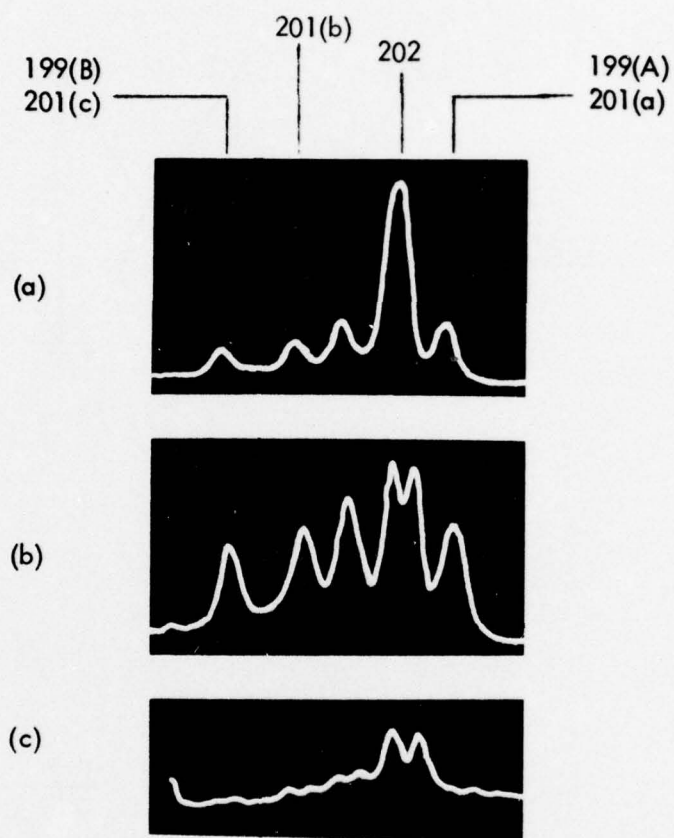


FIGURE 5-3. ^{202}Hg Lamp Emission Spectrum, 253.7nm.
 (a) Strong air cooling.
 (b) Weak air cooling.
 (c) Same as (b) but with 199/201 Hg filter cell.

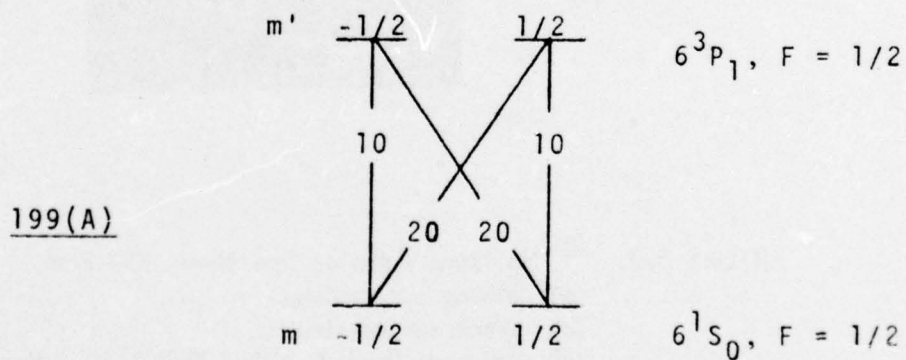
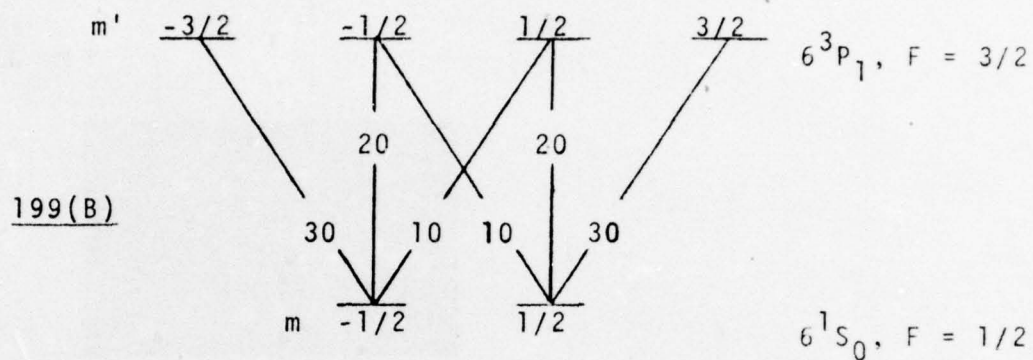
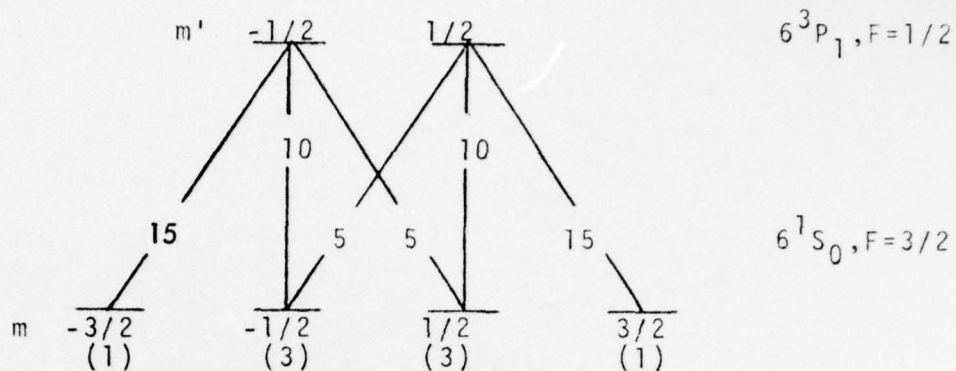
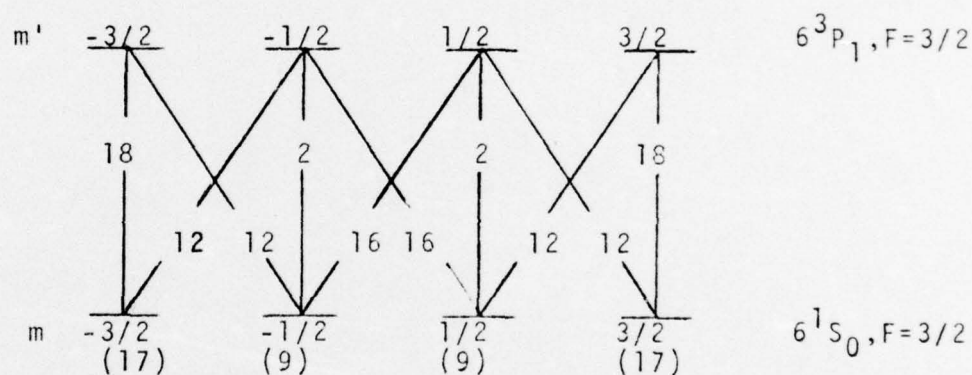


FIGURE 5-4 - Zeeman Components and Transition Probabilities (not normalized), 199(A) and (B) Hyperfine Transitions.

201(c)



201(b)



201(a)

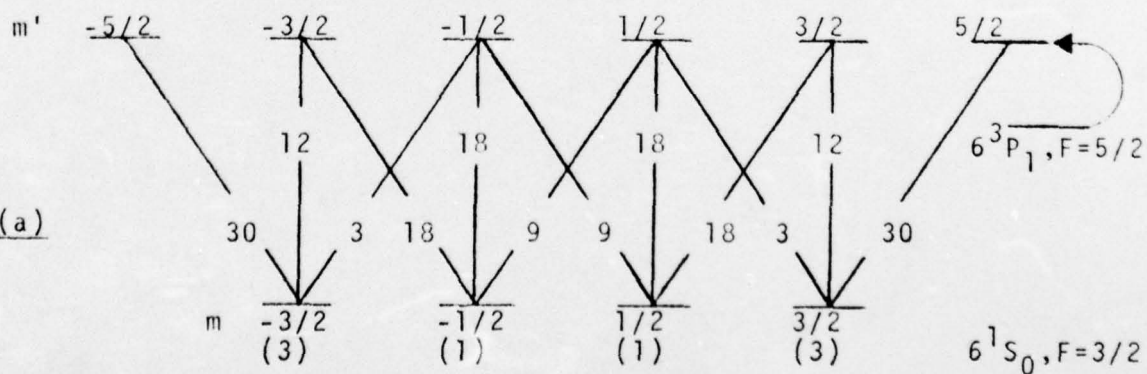


FIGURE 5-5 - Zeeman Components and Transition Probabilities (not normalized). 201(a), (b), and (c) Hyperfine Transitions.

6. MERCURY ATOM INTERACTIONS

6.1 INTRODUCTION

It was found soon after the start of this investigation of the interactions between Hg nuclei and the cell walls that a parallel study of certain Hg atom interactions was necessary.

The strength of the attraction between Hg atoms and the cell walls determines on the average the length of the interval (the "sticking time") during which an Hg nucleus is subjected to forces that can perturb its angular momentum. This attractive force also determines the equilibrium between the Hg atoms bound to the walls and those contained in the vapor phase within the volume of the cell. As will be seen (Section 6.4) certain conditions can cause such a reduction in vapor density that NMR signals can no longer be obtained.

The interactions of excited Hg atoms with the cell walls or impurities thereon may affect the corresponding magnetic dipole and electric quadrupole nuclear spin interactions by causing magnetic and electric changes in the surface structure of the wall. It is very possible that similarly induced modifications in surface structure were responsible for the pronounced changes in Hg vapor density (Section 6.4) that occurred when the atoms in a fused silica cell were exposed to resonance radiation. Finally, the interaction between excited Hg atoms and some gaseous impurity was probably responsible for the anomalous changes in Hg vapor density that were observed (Section 6.3) in a glass cell.

6.2 ANOMALOUS CHANGES IN Hg VAPOR DENSITY

So far the parallel study of Hg atom interactions has been based on conclusions drawn from anomalous changes in the Hg vapor density. This was monitored as described in Section 3.3 by measuring the transmissivity of the cell for a beam of resonance radiation.

In an ideal cell where there is negligible interaction between the mercury atoms and the cell walls the mercury vapor should be in equilibrium with its liquid phase at cell tempera-

tures below that at which the cell was initially sealed off from the liquid mercury reservoir. When the cell is heated the vapor density should increase rapidly until the "dry point", i.e., the temperature at which the liquid phase first disappears, is reached. After this the vapor is unsaturated and, except for the nearly negligible cell expansion, its density should not change with temperature.

Similarly the transmissivity of the cell for a beam of resonance radiation should sharply decrease as the cell is heated and the cell transmission-temperature characteristic should show an abrupt change in slope at the dry point.

It was soon found that the NMR cells were far from "ideal" in this respect. Since the vapor density anomalies observed with Corning 9741 glass cells differed appreciably from those found in fused silica cells the results and conclusions drawn therefrom will be described separately.

6.3 TRANSMISSION OF CORNING 9741 GLASS CELLS

6.3.1 General Characteristics

In general the NMR cells made from Corning 9741 glass approached the ideal cell much more closely than did those made from fused silica. The observed dry points often agreed closely with the seal-off temperatures. At temperatures below the dry point the transmission-temperature characteristic approached a new liquid-vapor phase equilibrium rapidly (several seconds) after the cell temperature was changed.

The principal exceptions were those cells that probably contained gaseous impurities, those made after the preparation procedure was changed to include a long high-temperature bake-out and to provide purer mercury for filling, and the bi-conical "magic angle" cell. (See also Section 7).

The Hg vapor density anomalies in the gas-containing cells occurred at temperatures well above the dry point. These measurements and resulting conclusions are described in greater

detail in the following sub-sections. All cells made with the new procedure were "sticky", i.e. their dry points were all higher than their seal-off temperatures and new liquid-vapor phase equilibria were approached very slowly (after several minutes in some cases). It was concluded that the "cleaner" preparation method increased the attraction of the Hg atoms for the cell walls.

Fabrication of the biconical cell involved blowing molten glass into a considerably colder mold. Cell transmission measurements indicated that the resulting wall surface had a strong attraction for Hg atoms. Not only was there no evidence for a sharp dry point but the Hg vapor density did not reach a maximum until the cell temperature had been increased to $\sim 220^{\circ}\text{C}$. Had there been no wall attraction all the Hg atoms would have entered the vapor phase at the seal-off temperature of 35°C .

6.3.2 Transmission Measurements, Glass Cell P5

Figure 6-1 shows the cell transmission measurements for the ^{199}Hg glass cell P5. The drawing was prepared by tracing low and high temperature portions of the X-Y recording of the cell transmission monitor output vs the emf of the Cu-Constantan thermocouple used for measuring cell temperature. The pump beam produced by a ^{199}Hg lamp was used to monitor the cell transmission. This cell was sealed off at a reservoir temperature of 30° .

The portion (A) of the tracing shows a sharp change in slope at 27.2°C . Thereafter the slope of the characteristic remained small and nearly constant until a temperature of 271°C was reached. As shown by the portion (B) the cell transmission started to rise and after ~ 3 hr leveled off to a higher value at 379°C . The cell was then rapidly cooled (C) from 379°C until it was near room temperature. Ice was then added to water surrounding the coil through which the air used for heating and cooling was passed. Portion (D) represents the X-Y recording obtained during slow cooling of the cell to 17.5°C , at which point it was necessary to interrupt the measurements.

The portion (A) represents the expected variation in cell transmission when the Hg vapor

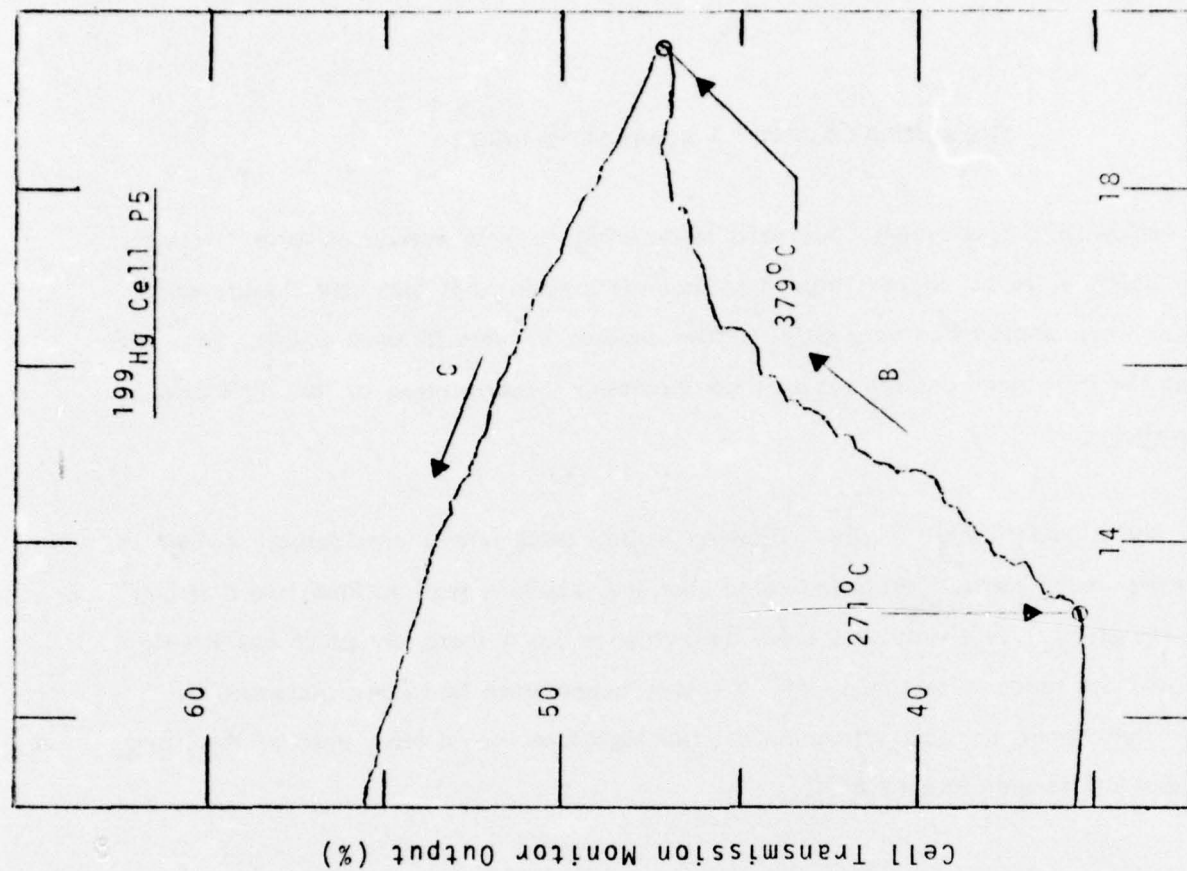
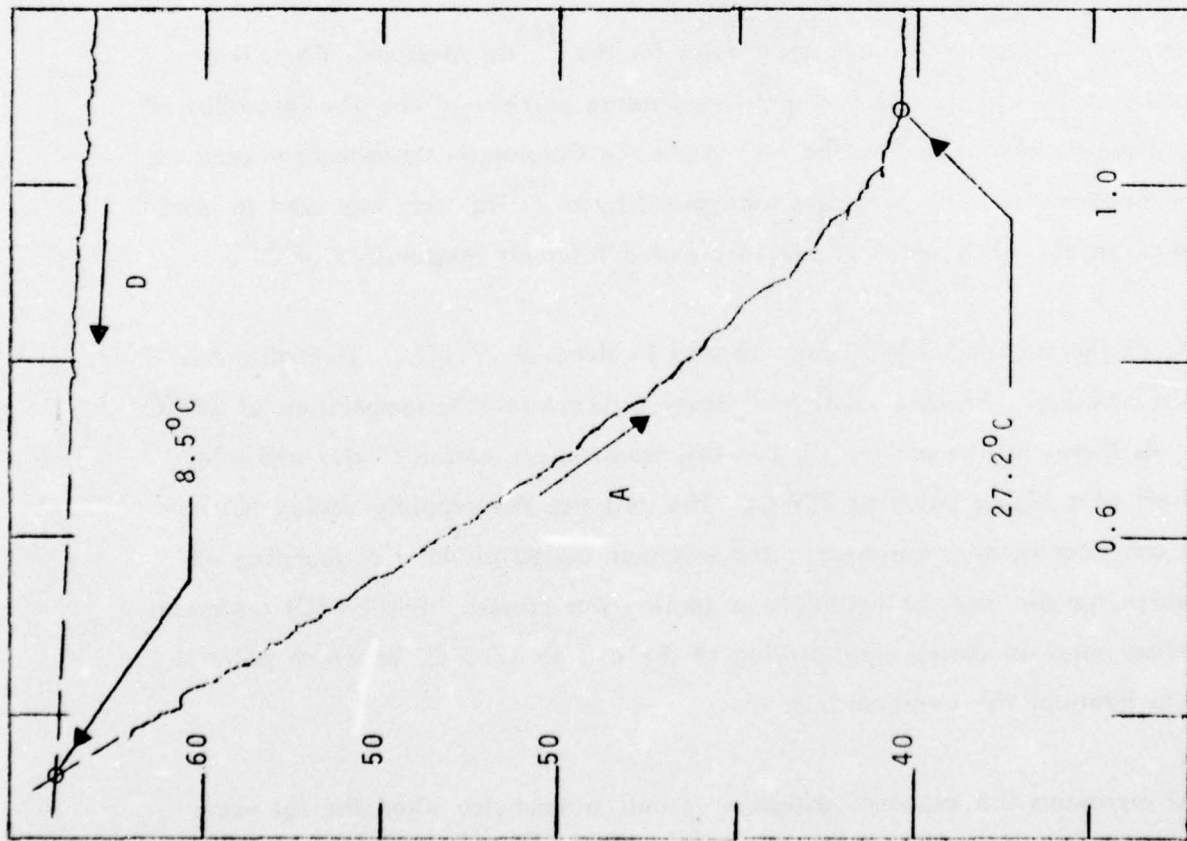


FIGURE 6-1- Depression of Dry Point.

(A): Slow heating to 27°C dry point.

(B): Slow heating from 271°C to 379°C during ~3 hr.

(C): Rapid cooling from 379°C

(D): Slow cooling toward predicted dry point at 8.5°C

THE SINGER COMPANY • KEARFOTT DIVISION

and liquid phases remain in equilibrium. The portion (B) typifies the variations in transmission obtained in several glass cells when anomalous changes in vapor density occur. Since the rise in transmission corresponds to a decrease in vapor density it follows that some process was causing Hg atoms to disappear from the vapor phase in the temperature region between 271 and 379°C.

The portion (D) in the low temperature region shows that the Hg atoms removed from the vapor at high temperatures remain so combined with the cell walls, some impurity, or some impurity-generated product, that they can not re-enter the liquid phase at temperatures well below the initial dry point of 27.2°C. On the assumption that the portion (A) of the characteristic corresponds to a true equilibrium between the liquid and vapor phases, the Hg atoms remaining in the vapor should start to condense as a liquid at the depressed dry point of 8.5°C, i.e., the temperature at which the extrapolation of (D) intersects (A).

TABLE 6-1

T°C	(N/cm ³) × 10 ⁻¹³
8.5	1.41
27.2	6.88

Table 6-1 shows the number densities N/cm³ of Hg vapor at temperatures of 8.5°C and 27.2°C. They were calculated from the known variation of saturated Hg vapor density with temperature. On the assumption that these temperatures are true dry points the results show that ~80% of the Hg atoms disappeared from the vapor phase during the 3 hr period while the cell temperature was above 271°C.

It was also found that the cell transmission would decrease again at temperatures near 400°C if the cell was not exposed to uv irradiation by the pump and read out beams. This result indicates that uv irradiation is required for the reaction that removes Hg atoms from the

THE SINGER COMPANY • KEARFOTT DIVISION

vapor phase and that when this irradiation is stopped the reaction not only ceases but reverses in direction. It follows therefore that the increase in Hg vapor density caused by so heating the cell in the "dark" should lead to an elevation of the dry point. That this is indeed the case is confirmed by the results shown in Figure 6-2.

In this experiment the cell was heated at first rapidly and then very slowly to just above the dry point at 21.3°C (curve A). It was then slowly cooled through a condensation point for the probably slightly super-saturated vapor at 19.8°C (curve B). After this the cell was heated, held in the dark at $\sim 400^{\circ}\text{C}$ for 2 hr, cooled rapidly, and then very slowly as the seal-off temperature of 30°C was approached. The cell transmission observed during the low temperature portion of this cooling cycle corresponds to curve C in Figure 6-2, and shows that the dry point, now 27.7°C , was indeed elevated by the heating process.

In an experiment whose results are plotted in Figure 6-3 the cell transmission was monitored as a function of time while the cell temperature was maintained between 386 and 392°C . The cell was exposed to the ^{199}Hg resonance radiation in the pump (and monitor) beam except during the nearly equal time intervals T_1 and T_2 . During T_1 the cell was exposed only to the off-resonance radiation of the ^{202}Hg read out beam. During T_2 the cell was in the dark. When this experiment was performed the peak detectors (Figure 3-3) had not yet been installed in the circuitry so the transmission could be measured only while the cell was exposed to the monitoring pump beam. The data points in Figure 6-3 were taken from the X-Y recording of transmission vs time.

These results show clearly that resonance radiation is required for, and hence that excited Hg atoms are involved in, this high temperature process that causes Hg atoms to be removed from the vapor phase.

6.3.3 Relaxation Time and Signal Measurements, Glass Cell P5

The ^{199}Hg relaxation time and NMR signal amplitude for cell P5 were measured as a function

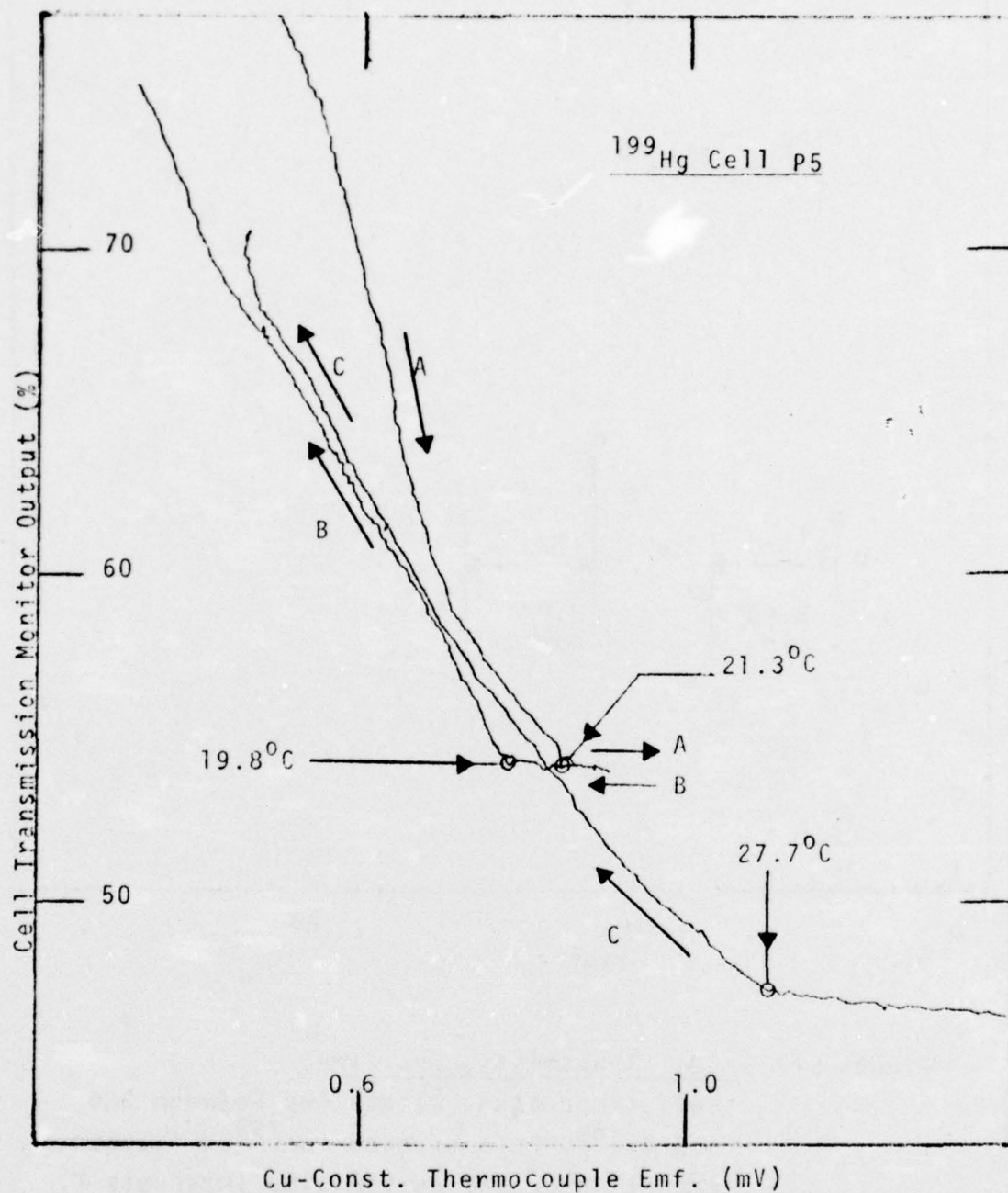


FIGURE 6-2-Elevation of Dry Point.

(A) and (B): Heating to just above initial dry point at $\sim 20^{\circ}\text{C}$ and then cooling.

(C): Cooling after cell was held for 2 hr at -400°C without uv irradiation.

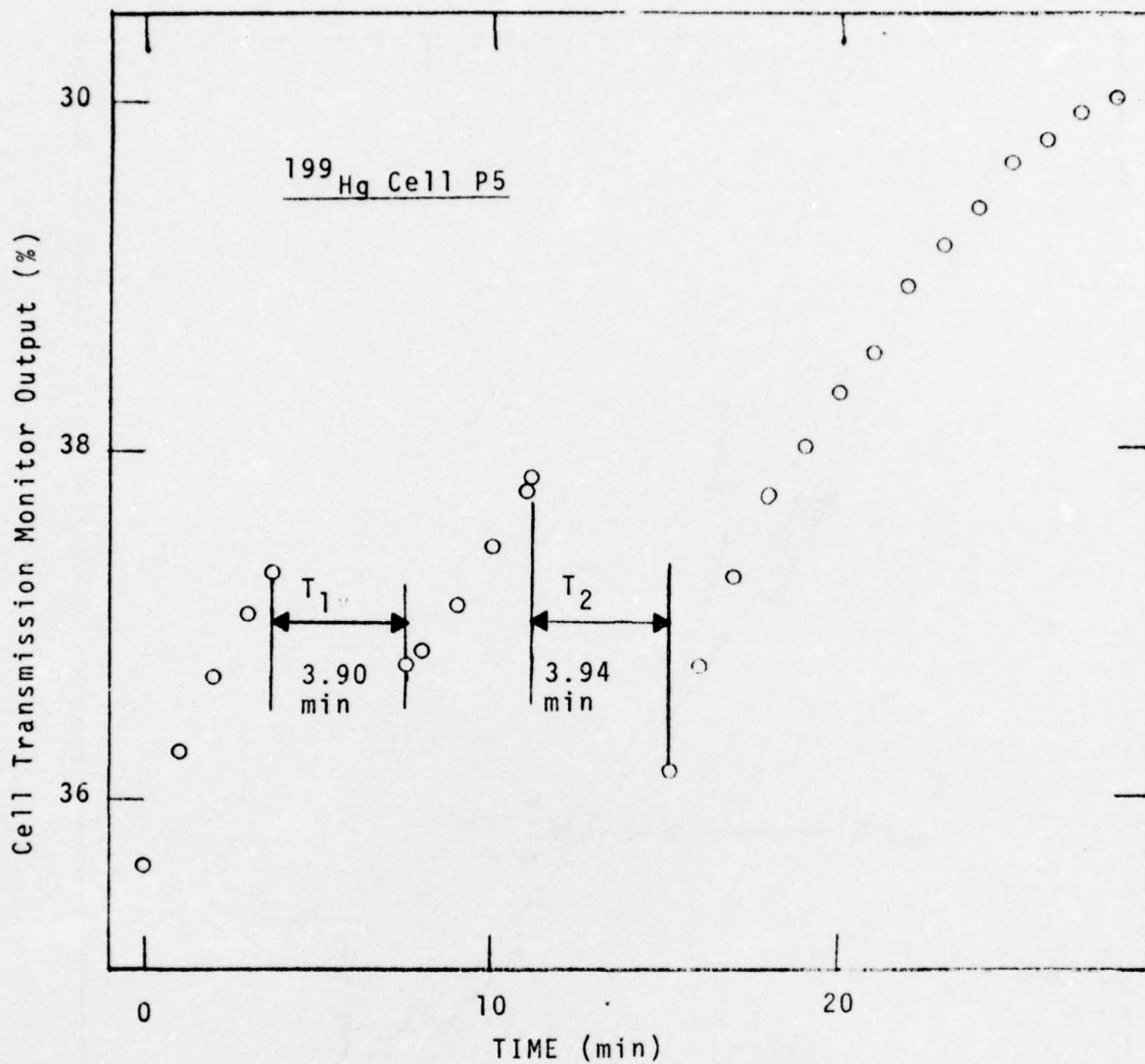


FIGURE 6-3 - Cell Transmission vs Time.

Cell temperature maintained between 386 and 392°C. Cell exposed to ¹⁹⁹Hg resonance radiation except during time intervals T₁ and T₂. Cell exposed to ²⁰²Hg off-resonance radiation during T₁. Cell in dark during T₂.

of temperature, and the following results obtained:

- a) There was no appreciable change in relaxation time during the anomalous decreases in Hg vapor density that occurred at high cell temperatures.
- b) As would be expected, the NMR signal amplitude decreased as vapor density decreased.
- c) At all cell temperatures the insertion of a ^{204}Hg filter cell in the ^{199}Hg pump beam changed the phase of the NMR signal by 180° .

The result (c) shows that the direction of the magnetization set up by the pump beam was reversed by insertion of the ^{204}Hg filter cell. As explained in Section 5.2, only the 199(B) hyperfine transition is excited with the filter cell in the beam, and the reversed magnetization implies that the sign of the ground state population difference was opposite to that set up when both transitions, 199(A) and 199(B), were excited by the pump beam. Such a reversal can not occur unless the populations of the magnetic sublevels in the excited state are being mixed by collisions between excited Hg atoms and the atoms or molecules of a foreign gas.

6.3.4 Excited State Mixing

From the information shown in Figure 5-4 it is evident that a σ^+ circularly polarized ^{199}Hg pump beam will, when excited state mixing and ground state relaxation are negligible, set up a ground state population distribution with nearly all the Hg atoms in the $m = +1/2$ magnetic sub-level. If, however, collisions are causing excited state mixing, i.e., causing excited state magnetic sublevels for which $m' - m$ does not equal $+1$ to become populated, the ground state population distribution will be altered. In particular, when only the 199(B) hyperfine transition is excited, it is easily shown from the transition probabilities that the population of the $m = -1/2$ magnetic sublevel will just exceed that for $m = +1/2$ when the excited state mixing rate per atom just exceeds $1/(2\tau_E)$, where τ_E is the spontaneous

relaxation time of the 6^3P_1 excited state.

On the assumption that one excited state energy transfer occurs for every collision, as defined by the kinetic collision cross sections for Hg and a foreign gas, the foreign gas pressure in a cell at 300°K required for onset of the 180° phase reversal in the $199(\text{B})$ NMR signal was calculated. The results are given in Table 6-2.

TABLE 6-2

Gas	Pressure in torr for 180° phase reversal in $199(\text{B})$ signal.
O_2	1.2
N_2	1.0
CO_2	1.1
H_2	0.4
H_2O	3.1

One conclusion to be drawn from these results is that in this cell as well as in several others including one fused silica cell in which the phase reversal of the $199(\text{B})$ signal was observed, the gas evolved from the cell walls after the cell was prepared.

This conclusion is supported by an experiment with the Corning 9741 glass $^{199/201}\text{Hg}$ Cell P11 which had not been above room temperature since it was prepared. Before the cell was heated it was observed that the NMR signal did not reverse in phase when the ^{204}Hg filter cell was placed in the pump beam. Thereafter the rectified $199(\text{B})$ NMR signal was recorded as a function of cell temperature. During the heating cycle the first occurrence of the phase reversal was indicated by the signal going through a null at 130°C . During the

cooling cycle phase reversal persisted until $\sim 49^{\circ}\text{C}$. It is evident that gas was evolved as the cell was being heated to 130°C and that even more was produced thereafter.

A second conclusion from the above results is that the process causing the anomalous change in Hg vapor density could well be one of the well investigated (see Ref. 8, for instance) reactions generated by collisions of the second kind between gas molecules and excited Hg atoms. Since one of the end products of such reactions is an Hg compound this would explain the reduction in vapor density that persisted when the cell was cooled. Disintegration of the compound at high temperatures would explain the resulting increase in Hg vapor density when the cell was heated in the dark. A possible candidate for this compound is HgO which, in the absence of liquid Hg, has a dissociation pressure of 2.0 torr at 252°C (Ref.9).

These experiments led to a revision (see Section 4) of the cell preparation procedure to provide for a longer bake-out at higher temperature. So far all cells so fabricated have shown no evidence that excited state mixing is occurring. The effects of the new procedure on glass-cell transmission were described earlier (Section 6.3.1). The effects on relaxation time are discussed in Section 7.

6.4 TRANSMISSION OF FUSED SILICA CELLS

6.4.1 General Characteristics

In contrast to the glass cells the fused silica cells show far greater departures from the characteristics of the ideal cell. The earlier measurements of the transmission-temperature characteristics for some cells indicated a dry point more than 50°C higher than the seal-off temperature. Other cells appeared to have multiple dry points and in another group dry points could not be found. Further investigation showed that the transmission-temperature characteristic depended on the past history of the cell, not only as regards the nature of the heat treatments applied after preparation but also as regards the conditions under which a previous transmission measurement had been performed.

In many cases the interaction of the Hg atoms with the cell walls or impurities thereon was so great that it was difficult to maintain sufficient vapor density to observe an NMR signal. The most striking case is that of the fused silica cell W7 made from Suprasil W2 and filled with equal parts of ^{199}Hg and ^{201}Hg .

Measurements of NMR signal amplitude and phase, transmission, and relaxation time were made for this cell as a function of temperature and before and after various heat treatments had been performed in an external oven. The signal measurements showed that the Hg vapor density was the primary factor that determined the signal amplitude and that the cell did not contain sufficient foreign gas pressure to cause excited state mixing. The interesting results of the transmission measurements are reported in the next subsection and the relaxation time measurements in Section 7.

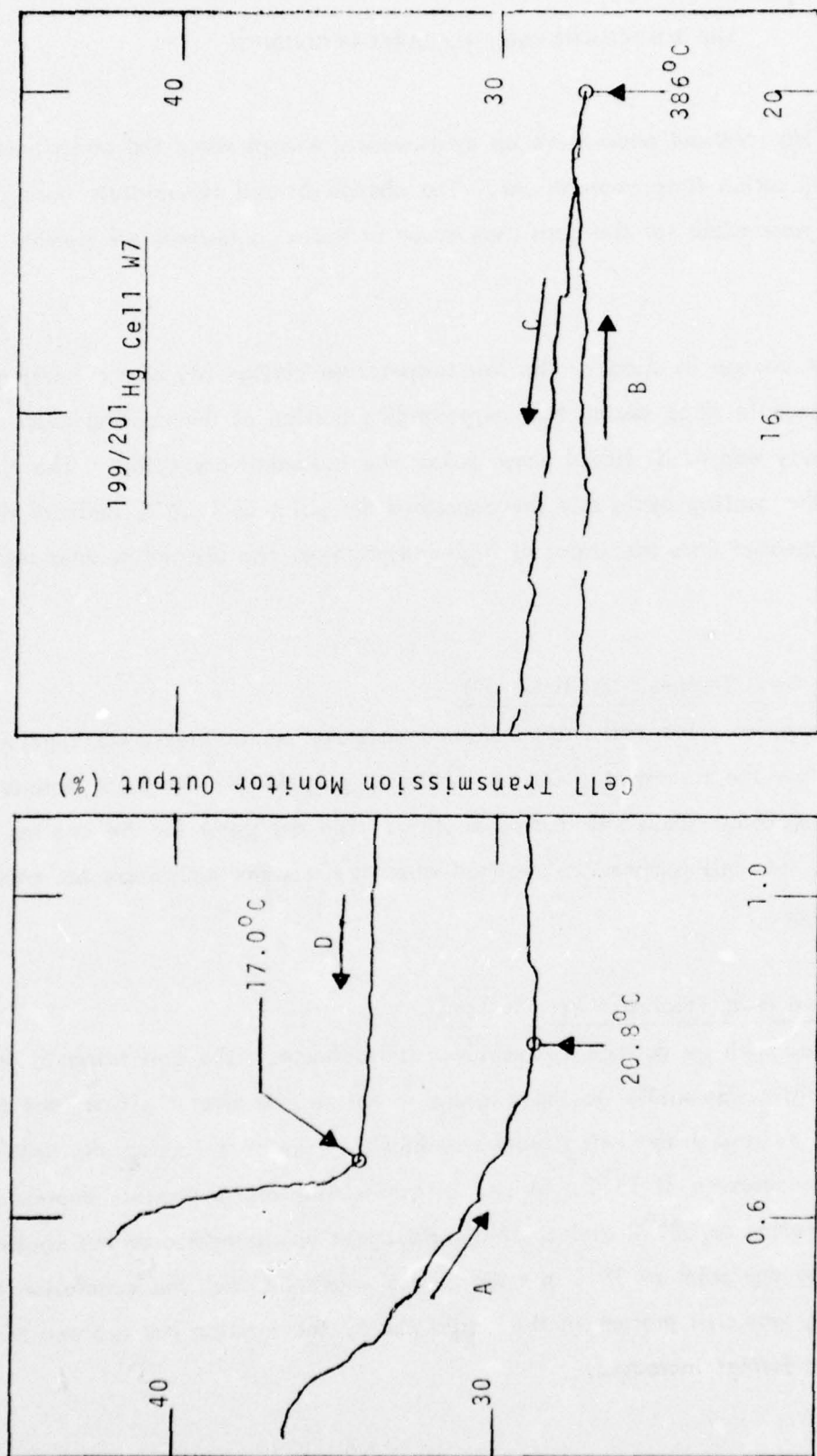
6.4.2 Transmission Measurements, Fused Silica Cell W7

This subsection describes transmission measurements made on the Suprasil W2 cell W7. During preparation this cell was subjected to the outgassing procedure described in Section 4. It was sealed off with the liquid mercury reservoir held at 27°C . The reservoir contained equal parts of ^{199}Hg and ^{201}Hg .

The cell transmission measurements were made as a function of cell temperature before and after each of three successive heat treatments. During each heat treatment the cell temperature was maintained at $\sim 1000^{\circ}\text{C}$ for one hour. During the first heat treatment the cell was not irradiated with uv light. During the second a high pressure Hg arc lamp irradiated the cell during the one-hour heat treatment period. During the third the Hg arc lamp was on only during the first half hour. The results are described below.

6.4.2.1 Before Heat Treatment

Figure 6-4 was traced from portions of the X-Y recording of cell transmission vs the emf of the Cu-Constantan thermocouple used to measure the cell temperature. The ^{204}Hg pump-



Cu-Const. Thermocouple Emf. (mv)

FIGURE 6-4 - Cell W7 Before Heat Treatment. (A) and (B); heating, (C) and (D); cooling.

beam and the ^{202}Hg read out beam were on continuously except when the pump beam was blocked during a relaxation time measurement. The change in cell temperature during such a measurement was responsible for the gaps that occur in the high temperature portion of the X-Y recording.

The somewhat abrupt change in slope of the low temperature portion (A) of the heating cycle and very abrupt change in slope during the corresponding portion of the cooling cycle indicate that some mercury was in its liquid phase below the indicated dry points. The rise in transmission during the cooling cycle and the depressed dry point at 17.0°C indicate that some Hg atoms disappeared from the vapor at high temperatures and did not reenter the liquid phase.

6.4.2.2 After First Heat Treatment (Without uv)

After the first heat treatment the cell transmission-temperature characteristic was similar to that (Figure 6-4) before the treatment. During the heating cycle the dry point occurred at 17°C and the transmission again rose during cooling. The dry point for the cooling cycle was less than 14.6° , the cell temperature reached when the measurements were terminated at the end of the day.

6.4.2.3 After Second Heat Treatment (uv for 1 hr)

Cell W7 was irradiated with uv during the second heat treatment. The cell transmission-temperature characteristic was similar to those measured before and after the first heat treatment except that the average transmission level was higher. However, during the heating cycle a dry point was observed at 19°C . A rise in transmission and a possible depression of the dry point after heating to 381°C and cooling were again characteristic of the cooling curve. Except for the dry point at 19°C the results are consistent with the conclusion that although some mercury was still present in the liquid phase, the fraction not restored to the liquid phase had been further increased.

6.4.2.4 After Third Heat Treatment (uv for first 1/2 hr)

The low and high temperature cell transmission measurements recorded after cell W7 had undergone the third heat treatment are shown in Figures 6-5 and 6-6. It is apparent from Figure 6-5 that the mercury atoms not in the vapor phase are now in a binding state whose temperature characteristic differs appreciably from that shown in Figure 6-1 for the glass cell P5. As discussed in Section 6.2 there is good evidence for assuming that the latter characteristic describes the cell transmission when the vapor and liquid phases are nearly in thermal equilibrium. Furthermore, the high level of cell transmission is not consistent with the mercury vapor density that would exist if the abrupt change in slope at 48.8°C were indeed a dry point.

Figure 6-6 shows the surprising rise in cell transmission that occurred at 357°C . As can be seen from the listed clock times this rise was at first very rapid, then slowed down, and after ~ 1.5 hr leveled off at an approximately 56% higher transmission level. Associated with this rise in transmission was an interesting change in the relaxation times. Both relaxation times increased and that for ^{199}Hg changed from a value less than to a value comparable with that of ^{201}Hg . For a further discussion of this effect see Section 7.

6.4.2.5 Pulsed Transmission Measurements, Cell W7

Since the X-Y recording of cell transmission during the cooling cycle showed a temperature variation that was completely different from any that had been previously observed it was decided to obtain more precise data by pulsing the monitoring ^{204}Hg pump beam and exposing the cell continuously to resonance radiation from the lamp AL that provided the auxiliary read out beam (see Section 3).

The results obtained during a heating cycle are shown in Figure 6-7. The cell was continuously illuminated by an auxiliary ^{198}Hg read out beam. It is apparent from the low temperature data that the mercury in the cell could not have been in the liquid phase. Furthermore the slow but vertical decrease in cell transmission at 63°C would not have

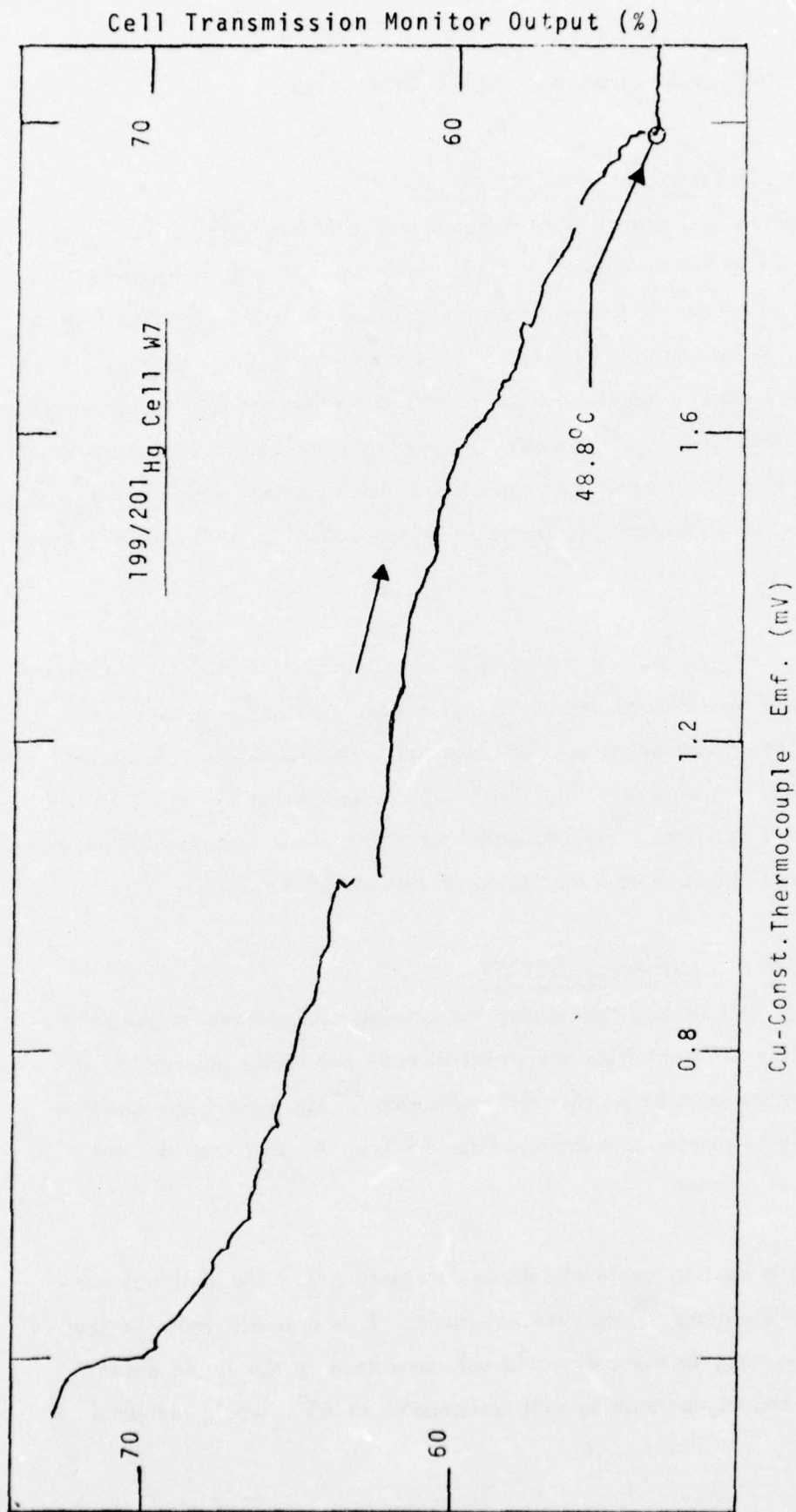


FIGURE 6-5 - Cell W7 After Third One-Hour Heat Treatment at $\sim 1000^{\circ}\text{C}$ (first half hour with uv). Heating at Low Temperatures.

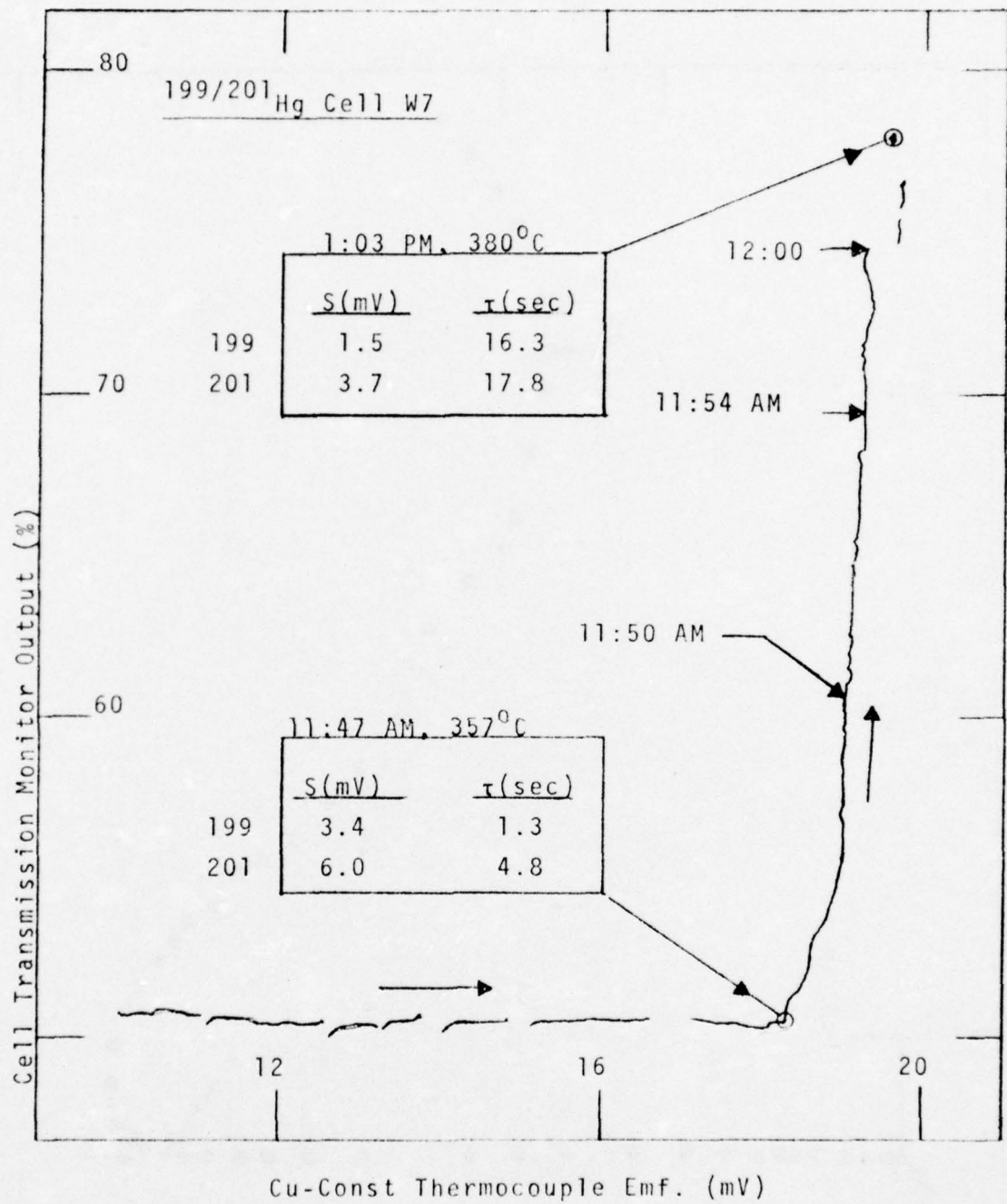


FIGURE 6-6 - Cell W7 After Third One-Hour Heat Treatment at $\sim 1000^{\circ}C$ (first half hour with uv). Increase in Transmission and Associated Increases in Relaxation Times at High Temperatures.

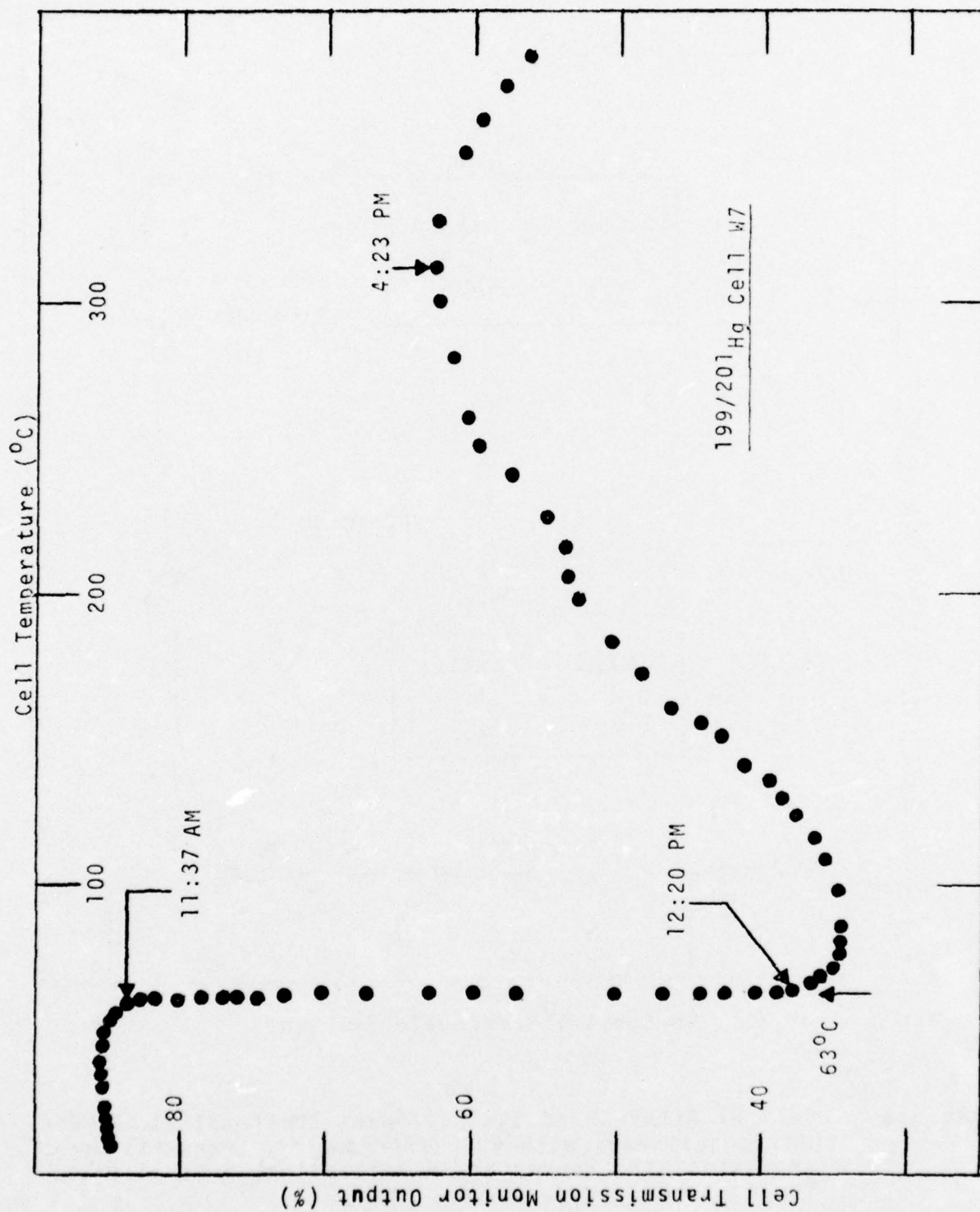


FIGURE 6-7 - Cell W7 After Abrupt Rise in Transmission (Fig. 6-6). Continuous Irradiation by 198Hg Read Out Beam. Pulsed 204Hg Monitor Beam. Heating Cycle.

occurred had the Hg vapor been in thermal equilibrium with some other phase such as a single cell-wall binding state. This change is more characteristic of a phase transition from a type of surface structure with strong Hg-wall binding to a type with appreciably weaker binding.

The remainder of the characteristic above 63°C indicates an equilibrium between competing processes whose rates of change are very slow. This is shown by the long time interval that was required to reach the maximum at $\sim 320^{\circ}\text{C}$ after waiting at each cell temperature for the transmission to become essentially constant.

The characteristic obtained during the cooling cycle was similar to that shown in Figure 6-7 except that between the maximum at $\sim 320^{\circ}$ and 63°C the cell transmission remained above that during heating, and the temperature at which the vertical transition occurred was 49°C rather than 63°C .

In order to determine the influence of excited Hg atoms on the cell transmission characteristic measurements were also made when the cell was illuminated by the non-resonant ^{202}Hg read out beam and when the cell was irradiated only during the $\sim .03$ sec "on" time of the pulsed ^{204}Hg pump beam used to monitor the transmission. It was found that the cell transmission-temperature characteristic obtained with non-resonant radiation did not differ essentially from that observed when the cell was in the dark. It was also found that there were three distinct, stable (below $\sim 320^{\circ}\text{C}$), and nearly reversible cell transmission-temperature characteristics. These are shown in Figure 6-8. It is evident that each of the three characteristics A, B, and C has a different average cell-transmission level.

Below $\sim 320^{\circ}\text{C}$ transitions from one characteristic to another required that the cell be exposed to Hg resonance radiation. The low vapor density characteristic C was always obtained after the cell had been so irradiated at $\sim 300^{\circ}\text{C}$, i.e. near the high temperature maximum of the characteristic for continuous irradiation shown in Figure 6-7. The high vapor density characteristic A always resulted after irradiation at $\sim 100^{\circ}\text{C}$, i.e. near the

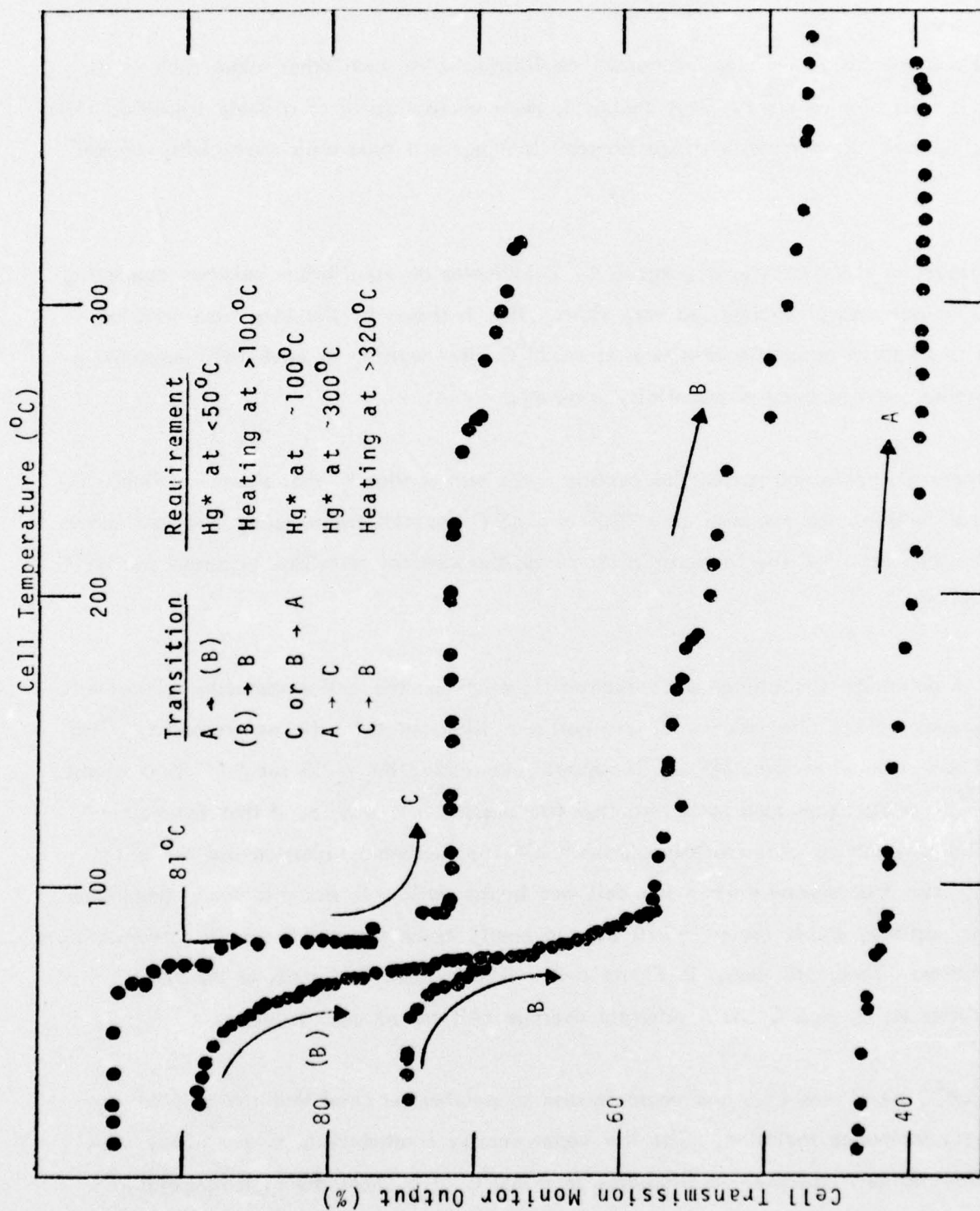


FIGURE 6-8 - 199/201Hg Cell W7: Transmission-temperature Characteristics of Hg-wall Binding States A, B, and C. Pulsed 204Hg Monitor Beam. Heating Cycles.

minimum of that for continuous irradiation.

The intermediate vapor density characteristic B could only be obtained via a transition from the characteristic A. It occurred from A when the cell was exposed to resonance radiation at temperatures below 50°C (the required depression below the transition temperature of 63°C shown in Figure 6-7 has not yet been determined). This at first developed the unstable characteristic (B) which transformed to the stable characteristic B after the cell had been heated above 100°C and then cooled.

The only transition that did not require excited Hg atoms was that from C to B which took place slowly in the dark at cell temperatures above $\sim 320^{\circ}\text{C}$.

It is interesting to note that the Hg vapor density was increased when resonance radiation caused transitions from C or B to A. This is in contrast to the removal of Hg atoms from the vapor that is characteristic of the transitions from A to (B), A or B to C, and the process that caused the rise in transmission in the apparently gassy glass cell P5.

In other experiments it was determined that the transitions between the characteristics were independent of which Hg isotope was absorbing the resonance radiation. For instance, the nature of the transition from A to C near 300°C was not influenced when the $^{199/201}\text{Hg}$ cell was irradiated with the beam from a ^{204}Hg lamp rather than with the ^{198}Hg lamp used for the measurements shown in Figure 6-8. In both cases the cell transmission rose to the same upper value, namely, that of the maximum of the characteristic C. Furthermore, both the ^{199}Hg and ^{201}Hg NMR signal amplitudes decreased together as the mercury vapor density decreased.

If there had been an isotope effect, the upper transmission level should have been lower for irradiation with the ^{198}Hg beam with the ^{204}Hg beam, since the former beam was absorbed only by ^{201}Hg and only atoms of this isotope would then have been removed from the vapor. Similarly only the ^{201}Hg NMR signal should have decreased in amplitude.

6.5 DISCUSSION OF RESULTS, CELL W7

The absence of an isotope effect provides an important clue to the nature of the interaction that involves the excited Hg atoms. It means that there must be more than one step involved in the process that causes the vapor density to change. In the case of a transition involving a decrease in Hg vapor density the first step would utilize the excitation energy of the particular isotope that absorbed the resonance radiation. This would cause such a change in the cell walls or in a foreign gas, if present, that in the next or succeeding steps unexcited Hg atoms could be bound to the walls or combine with a reaction product.

On the assumption that there was a negligible pressure of foreign gas in the cell, as suggested by the lack of evidence for excited state mixing, the three characteristics could correspond to three different states in which mercury was bound to the cell walls. The low transmission, high vapor density characteristic A (Figure 6-8) would result from a loosely bound state and C would result from the most tightly bound state.

A possible model for these cell wall interactions might be developed by relating the three Hg-wall binding states to the various phases (polymorphic forms) of crystalline silica. It is noted in Reference 10 that between 1927 and 1965 the number of known phases of pure silica increased from seven to twenty-two. Transformations between two of these phases are designated as reconstructive when interatomic bonds must be broken, and displacive when the basic structure is distorted rather than changed. Reconstructive transformations occur, for instance, between quartz, tridymite, and cristobalite, whereas that from low to high quartz is displacive.

Among these 22 phases there are six forms of tridymite with phase-transition temperatures between 0°C and 475°C. Of particular interest is the change from tridymite S-I to tridymite S-II whose phase-transition temperature (64°C) is close to that (63°C) at which a pronounced change in cell transmission occurred (Figure 6-7).

It is known that vestiges of these structures can be found in fused silica and it is possible that each structure could differ as regards its capability for binding Hg atoms to the cell walls. It might be then that those transitions which require excited Hg atoms correspond to reconstructive transitions where bonds must be broken. The energy of the excited Hg 6^3P_1 state is 113 kcal/mol and is greater than the bond energy of SiO, namely 106kcal/mol. Similarly displacive transformations might be causing the abrupt changes in cell transmission near 100°C shown in Figure 6-8 along the characteristics C and B.

A second model, or perhaps only a different aspect of the first, was suggested by Ernsberger (Ref. 11), who points out that there are only four ways in which the tetrahedral structural element of four oxygen atoms around one silicon atom can be exposed at the surface of either crystalline or fused silica. These exposure types differ in the number, from 0 to 3, of surface oxygen atoms that are bonded to only one silicon atom. They are designated as exposure types I through IV, numbered in the order of increasing stability of the surface to attack by aqueous solutions. Type I, the least stable, has three oxygen atoms "exposed" at the surface. The author suggests that the four types probably coexist in random patterns at the surface of fused silica, but that in crystals "the exposure type will depend on the crystal plane or planes which constitute the surface." Since it is probable that each exposure type will also differ in the strength of its interaction with mercury this model could well predict the existence and characteristics of several different mercury-silica wall binding states.

6.6 FINAL HEAT TREATMENTS, CELL W7

According to Ref. 10, crystalline silica can exist as tridymite S-VI between 1470°C and 867°C. Rapid cooling then produces metastable "but actually long-lived" tridymite which undergoes transitions from tridymite S-VI to S-I as the temperature drops. However, tridymite changes to quartz if the temperature is maintained for a sufficient time at 867°C.

On the assumption that such a heat treatment might cause the fused silica wall surface to become more like quartz than tridymite, cell W7 was cooled from 900°C to 800°C over a

four hour period. This treatment produced a striking change in the cell characteristics that could not be reversed by any further heat treatments so far devised. The only way that an appreciable Hg vapor density can now be obtained in the cell is to heat it above $\sim 600^{\circ}\text{C}$ and then cool it. However, exposing the cell thereafter to resonance radiation causes Hg to disappear rapidly from the vapor phase. Previously (see, for instance, Figure 6-7) the time constant for such changes was of the order of an hour. The cell now becomes nearly transparent to the monitor beam in less than 10 sec, and NMR signals can not be obtained. These characteristics persist over the temperature range for measurement, 10°C to 400°C .

If the cell surface has indeed become more quartzlike its characteristics below 573°C (Ref. 10) should resemble those of low quartz. According to Ref. 11 the basal plane of low quartz is attacked by aqueous solutions ~ 100 times faster than the prism faces. The former presents a Type II exposure (two exposed O atoms) while the latter presents Type III (one exposed O atom). This model for a fused silica surface would attribute the now greatly increased mercury-wall interaction in Cell W7 to a large increase in the number of Type II exposures on the surface.

6.7 EFFECTS OF VARIOUS MODIFICATIONS IN CELL PREPARATION

Several fused silica (Suprasil W2) cells were prepared in an effort to exploit the more promising of the results obtained with cell W7. One group of the new cells was irradiated with Hg resonance radiation for four hours while being held at room temperature and continuously supplied with the Hg vapor from a room temperature reservoir that contained \sim equal amounts of ^{199}Hg and ^{201}Hg . The cells were then exposed to the vacuum system to remove any gas that may have been produced. After removal from the vacuum system the common Hg reservoir was held at $\sim 20^{\circ}\text{C}$, and the four cells of the set were maintained at a slightly higher temperature for \sim one hour before being sealed off.

The second group of four cells was prepared identically except that the cell temperature was 400°C during the irradiation step.

As shown in Figure 6-7 it was found for cell W7 that Hg resonance radiation apparently caused mercury atoms to disappear from the vapor phase and become bound to the cell walls at temperatures below $\sim 80^{\circ}\text{C}$ and also at temperatures above $\sim 250^{\circ}\text{C}$. The above modifications to the preparation procedure were designed to saturate these low and high temperature vapor-removal mechanisms by continuously supplying new vapor from the Hg reservoir. On the assumption that thereafter the Hg remained bound to the cell walls the additional Hg atoms supplied at seal-off should then remain in the vapor phase during irradiation with the resonance radiation required for optical pumping and hence provide sufficient vapor density to produce strong NMR signals.

It was also found for cell W7 (Section 7) that the strength of the relaxation-time reducing magnetic interaction was apparently diminishing as Hg atoms disappeared from the vapor at temperatures above $\sim 250^{\circ}\text{C}$. The possibility of obtaining sufficient vapor density with the cell walls in this state of low spin-relaxation was a further reason for irradiating the second set of four new cells in this temperature region.

So far, preliminary measurements have been made on cell W13, irradiated at room temperature, and on cells W17 and W19, irradiated at 400°C . The cell transmission measurements made after successive heat treatments show that the cells have not yet become sufficiently stabilized to correlate the results with those obtained for cell W7 nor to distinguish between the effects of pre-seal-off irradiation in the low and high temperature regions. The NMR signal strength measurements show that a stable level of sufficient Hg vapor density has not yet been achieved. The relaxation time measurements show that a cell-wall state of low spin relaxation similar to that of cell W7 has not yet been attained in the new cells. Further heat treatments will be made in an attempt to change these characteristics.

It is possible that the major defect in Cell W7 caused by the special heat treatment (Section 6.6) designed to make its wall surface more quartzlike might be only the lack of sufficient Hg vapor density. It was therefore decided to perform the slow cooling from 900°C to 800°C during the cell preparation process and then expose the cell to Hg resonance

THE SINGER COMPANY • KEARFOTT DIVISION

radiation for about four hours at room temperature and before the cell was sealed off from its Hg reservoir. If the new cell walls were to behave like the now possibly quartzlike walls of W7, this process could provide sufficient vapor density by saturating the walls with Hg before seal off.

Two such cells were prepared from the Suprasil W2 grade of fused silica.

One of these (W25) was sealed off at a reservoir temperature of 25°C . It behaved as though its wall were so saturated with Hg that a large vapor density could be maintained even at low cell temperatures. On a scale where a transmission monitor output of 11V corresponded to 100% transmission, the observed output at 13°C was 6V. As the cell temperature was increased the output dropped to 2.5V at an apparent dry point of 42°C . Resonance radiation had no effect on the transmission at any temperature.

Several heat treatments with and without uv irradiation did not appreciably change the transmission characteristic and after the first heat treatment strong NMR signals were obtained at all temperatures between 90°C and 400°C . However the observed relaxation times were short (<7 sec for ^{199}Hg).

The second cell W26 was sealed off at a reservoir temperature of 0°C . Initially the cell transmission monitor output decreased without an abrupt change of slope from 5.4V at 90°C to 3.2V at 400°C . Resonance radiation did not affect this characteristic.

However after the first heat treatment irradiation at 10°C with a ^{201}Hg beam caused the monitor output to rise from 3.1V to 8.8V in one hour. Further heat treatments not only increased the rate and amplitude of this low temperature rise but also caused the transmission to increase and eventually reach 100% at all temperatures.

After the first heat treatment weak NMR signals were observed in cell W26 as the cell temperature approached 400°C . After the second and successive heat treatments no signals

THE SINGER COMPANY • KEARFOTT DIVISION

could be observed at any temperature. Relaxation times were not measured because of the weak signals. They were estimated as being <0.1 sec.

Although this preparation procedure did lead to a fused silica cell whose vapor density was stable against Hg resonance radiation, the optimum seal-off temperature has not yet been determined nor have long relaxation times been obtained.

7. NUCLEAR-SPIN RELAXATION

7.1 INTRODUCTION

This section describes the results of the investigation of the nuclear-spin relaxation of ^{199}Hg and ^{201}Hg .

It begins (Section 7.2) with a simplified theoretical analysis of the relaxation of these nuclei, a review of the applicable experimental conditions, and a discussion of the light induced frequency shifts that influence the relaxation of ^{201}Hg as observed by the read out beam.

Section 7.3 describes those results obtained with fused silica cells that may lead to correlations with cell material, cell wall structure, cell heat treatment, and cell preparation procedure.

Section 7.4 is concerned with the results obtained with cells made from Corning 9741 glass, Section 7.5 with the interesting results obtained from the measurements of the non-exponential relaxation of ^{201}Hg , and Section 7.6 with the effects of exposing certain fused silica cells to uv radiation, β and γ rays, and neutrons.

7.2 THEORETICAL DISCUSSION

7.2.1 Relaxation

The general theory of optical pumping, read out, and associated relaxation phenomena has been summarized in the review article by W. Happer (Ref. 12). A more detailed theory of the relaxation of ^{201}Hg due to the electric quadrupolar interaction is given by C. Cohen-Tannoudji (Ref. 13).

The investigation reported herein has been concerned with the relaxation of the ground state population distribution established in ^{199}Hg and ^{201}Hg by the optical pumping beam, and observed as a transverse magnetization by means of Faraday-rotation read out. It is convenient, as Happer has shown in Ref. 12, to describe this ground state population as a sum of independent multipole distributions (polarizations). For ^{199}Hg with a nuclear spin of $1/2$ there are only two independent polarizations, i.e., random and (magnetic) dipole. For ^{201}Hg with a spin of $3/2$ there are four, namely, random, dipole, quadrupole, and octopole. Of these only the magnetic dipole and quadrupole contributions can be detected by the read out beam.

The dipole and quadrupole polarizations correspond respectively to orientation and alignment of the nuclear spins. A circularly polarized pump beam is necessary for orientation whereas ^{201}Hg nuclear spins can be aligned even with an unpolarized beam. In general, the dipole and quadrupole polarizations will, for a given perturbation, relax at different rates.

A simplified theory for the relaxation of oriented nuclear spins caused by fluctuating magnetic fields can be developed from the general theory as outlined by Bonnot and Cagnac (Ref. 14). The relaxation of the ground state polarizations is assumed to occur only during a wall collision. An atom on striking the wall does not rebound elastically but may stick to the wall for a time τ_S . The average "sticking" time on the wall is given by

$$\tau_S = \tau_0 \exp(E_a/RT), \quad (7-1)$$

where E_a is an activation energy associated with the sticking process and τ_0 is the sticking time for temperatures much larger than (E_a/R) . The atom on leaving the wall is assumed to traverse the cell in a time τ_v . With no buffer gas in the cell $\tau_v \approx \ell/v$, where ℓ is the diameter of the cell (~ 1 cm) and v is the velocity of the atom ($\sim 10^4$ cm/sec). The time of flight is therefore of the order of 10^{-4} sec. The sticking time τ_S is of the order of 10^{-6} sec. The atom is hence exposed to the relaxing interaction during the fraction $\tau_S/(\tau_S + \tau_v) \sim 10^{-2}$ of the time between wall collisions. The perturbation causing the

relaxation will be assumed to be weak, isotropic, and to have a constant power spectral density for frequencies below $\sim \tau_c^{-1}$, where τ_c is the correlation time which obviously must be less than τ_S . For the Larmor frequency $\omega/2\pi = 1\text{kHz}$, at which the measurements reported here were taken, $\omega^2 \tau_c^2 \ll 1$ even when $\tau_c = \tau_S = 10^{-6}$ sec. Under these conditions the dipole relaxation rate R_M can be shown (see, for instance, Ref. 12) to be

$$R_M = (2/3)(\gamma h_o)^2 \tau_c \tau_S / (\tau_S + \tau_v), \quad (7-2)$$

where γ is the gyromagnetic ratio and h_o is the rms amplitude of the fluctuating magnetic field at the cell wall. The reciprocal of R_M is the intrinsic transverse relaxation time T_2 . To the same approximation of $\omega^2 \tau_c^2 \ll 1$, equation (7-2) also gives the longitudinal relaxation time T_1 .

It is to be noted that the relaxation rate R_M depends on the square of the gyromagnetic ratio and, when subjected to the same fluctuating magnetic field h_o , ^{199}Hg should relax ~ 7.5 times faster than ^{201}Hg . ($\gamma_{201} \sim 0.37\gamma_{199}$.)

Since ^{201}Hg has a nuclear electric quadrupole moment as well as a magnetic dipole moment it can interact with an electric field gradient. Cohen-Tannoudji (Ref. 13) has shown that a fluctuating electric field gradient leads to a relaxation rate for oriented ^{201}Hg nuclei given by

$$R_E = (8\pi/5) (eq Q)^2 \tau_c \tau_S / (\tau_S + \tau_v), \quad (7-3)$$

where Q is the electric quadrupole moment and e the electronic charge. The fluctuating electric field gradient is assumed to have a mean square value of q^2 along an axis of cylindrical symmetry.

7.2.2 Experimental Conditions

The population distributions for the experiments described in this section were produced with a pumping beam, capable of exciting real transitions and directed nominally along the H_0 magnetic field. The pumping beam was either circularly polarized or linearly polarized. In the case of a linearly polarized or unpolarized pump beam the alignment signals correspond most closely with that of a quadrupole polarization. With a circularly polarized beam, the polarization is a mixture; the percentage of each multipole polarization is a function of the pumping rates and relaxation rates.

In all observations, the decay of the transverse components of the magnetization was measured. The initial values of the transverse components were those that were present when a resonant rf field was turned off. In some cases the rf field was applied long enough to generate cw signals, applied as a short " 90° -pulse", or as a longer " 360° -pulse" (for measurement of the longitudinal relaxation time T_1). The action of an rf field is to rotate the various multipole-polarization components without mixing or introducing new ones. Also, it is to be emphasized that during the measurement of decaying signals the spins are in free precession since no rf magnetic fields are applied.

With the pumping beam blocked the magnetization decays due to random magnetic fields, random electric field gradients (for ^{201}Hg) and real transitions excited by the read out beam. The latter can be made negligible by using a filter cell and if necessary reducing the intensity of the read out beam. However, for ^{201}Hg the read out beam in addition can excite virtual transitions and cause a differential change in the spacing of the ground state Zeeman levels and thus constitutes a source for light induced frequency shifts. These are discussed below.

7.2.3 Light Induced Frequency Shift (LIFS)

When the read out beam excites only virtual transitions and is linearly polarized, its effect on the energy levels can be described in terms of an effective electric field gradient. That is, the energy of the levels $m = \pm 1/2$ are shifted by an energy d_1 in one direction and

the levels $m = \pm 3/2$ are shifted by a larger energy d_2 . This is illustrated in Figure 7-1. It is obvious that the spacing between the $+3/2$ and $+1/2$ levels is shifted by an equal but opposite amount to that between the $-1/2$ and $-3/2$ levels.

If the linewidth (proportional to the inverse of the relaxation time τ_2) of the resonance is less than the shift in frequency, the three components of the resonance can be resolved and the magnetization can be described in terms of three independent resonances each with a fictitious spin of $1/2$. In general the free precession signal will exhibit a series of maxima and minima, the envelope of which yields the relaxation time. The period between the beats provides a measure of the difference frequency. Assuming the two displaced components have equal amplitudes, start off in phase, and have the same relaxation times, then S , the amplitude of the transverse signal, decays with time t according to

$$S = (A_1 + 2A_2 \cos \delta t) \exp (-t/\tau_2), \quad (7-4)$$

where δ is $|d_1 - d_2|$. A_1 and A_2 are the amplitudes of the normal and displaced components. Cagnac (Ref. 15) has shown that when the plane of polarization of the transverse beam is at an angle θ of about 55° ($3\cos^2\theta = 1$) with respect to the H_0 magnetic field, the LIFS is effectively zero. (Hanle as quoted in Mitchell and Zemanski (Ref. 8) noted the light scattered from mercury vapor was unpolarized when the incident beam of resonance radiation was linearly polarized at an angle of 55° with respect to the magnetic field).

7.3 RELAXATION OF ^{199}Hg AND ^{201}Hg ON FUSED SILICA

7.3.1 Relaxation of ^{199}Hg on Spectrosil and GE204

The measurements of the temperature dependence of the longitudinal relaxation time T_1 of ^{199}Hg were made in cells prepared before the start of this program and blown from the Spectrosil and GE204 grades of fused silica. These together with those reported for the glass cell #49 in Section 7.4 are the only experiments in which the longitudinal relaxation time was measured. Pulses of the H_1 magnetic field which rotated the longitudinal compo-

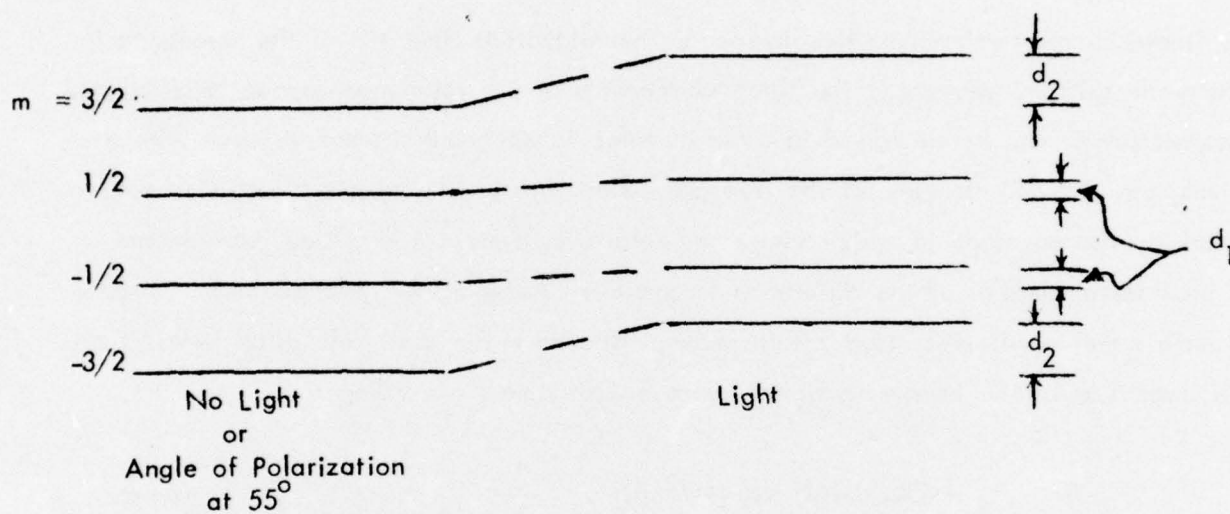


FIGURE 7-1 - Energy Level Displacements Caused by Electric Field Gradient.
 Linearly Polarized, Off-Resonance Read Out Beam can Produce
 Equivalent Shifts.

THE SINGER COMPANY • KEARFOTT DIVISION

ment of the magnetization through 360°C were used for this purpose. It was thereafter found easier and just as accurate to measure transverse relaxation times by using either 90° pulses or continuous H_1 excitation for establishing the initial transverse magnetization component.

The relaxation of ^{199}Hg on Spectrosil is shown in Table 7-1 and the results for GE204 in Table 7-2.

TABLE 7-1. Relaxation of ^{199}Hg on Spectrosil Cell #11

Cell Temp. ($^{\circ}\text{C}$)	T_1 (Seconds)
72	14
86	104
120	207
167	135
210	110
229	96
248	67
266	24
284	12

The measurements show that T_1 increased to 207 sec as the cell temperature was raised to 120°C and thereafter decreased rapidly to 12 sec at 284°C .

TABLE 7-2. Relaxation of ^{199}Hg on GE204 Cell #27

Cell Temp. ($^{\circ}\text{C}$)	T_1 (Seconds)
24	6
50	12
95	47
136	92
176	153
214	190
250	230

It is to be noted that in contrast to Spectrosil the GE204 grade of fused silica does not exhibit a rapid decrease in relaxation time as the temperature is increased. In fact the relaxation time appears to increase monotonically with temperature.

Similar results to those we observed for Spectrosil were obtained for ^{199}Hg by Cagnac and Lemeignan (Ref. 16) in a cell made from Ultrasil, a fused silica manufactured by Heraeus Schott Quarzschmelze and by Amersil. They found that T_1 rose to a maximum of 33 sec at 160°C , decreased to a minimum of 0.3 sec at 360°C , and increased thereafter to ~ 10 sec at 620°C . These authors suggest that the rather sudden decrease in relaxation time at temperatures between 160° and 360°C could be associated with a structural change in the cell wall. They relate their suggestion to the work of Swets et al (Ref. 17) who noted changes in the activation energy and heat of solution for diffusion of He through fused silica at temperatures near 300°C . The latter authors suppose that fused silica may retain some characteristics of the crystalline forms of silica, possibly cristobolite or tridymite whose "volume vs. temperature curves show very pronounced inversions in the temperature range of 160°C to 280°C ."

Similar results to those we obtained for GE204 were found by the French workers, Bonnot and Cagnac (Ref. 14), in a cell made from "silice agglomeree a la flamme" and fabricated by Quartex. For ^{199}Hg they observed a continuous increase in T_1 with temperature and measured $T_1 = 30$ min at 600°C . This is by far the largest relaxation time reported for ^{199}Hg on fused silica. They found a similar temperature dependence for ^{201}Hg and measured $T_1 = 1.5$ min at 600°C . For ^{199}Hg , however, their data showed evidence for a change in activation energy (see Section 7.2) at about 250° , and this they also attributed to a possible structural change in the cell wall.

It is apparent that the mechanism responsible for the anomalous decrease in the relaxation time of ^{199}Hg on Spectrosil and Ultrasil must have a much lower effect in cells made from GE204 and the Quartex flame-fused silica. It is interesting to note that the absorption spectra published by the various manufacturers of these types of fused silica show that

Spectrosil and Ultrasil have a strong OH absorption band corresponding to an OH concentration of ~1100 parts per million. GE204 does not exhibit the OH band and its reported OH concentration is ~10 p.p.M. However, flame fused quartz usually shows a strong OH band.

In order to check whether the OH content of the fused silica or a structural change was responsible for the observed effects on the ^{199}Hg relaxation, a number of cells were prepared from grades of fused silica that had different OH concentrations.

So far our measurements indicate that a structural change may be the more likely candidate. This is evidenced by the results obtained with cells made from Tetrasil which has an OH absorption band and Suprasil W2 which does not (see Table 4-1).

7.3.2 Relaxation of ^{199}Hg on Tetrasil and Suprasil W2

In these experiments the cells were subjected to successive heating and cooling cycles between room temperature and $\sim 600^\circ\text{C}$. During these cycles the cells were in the apparatus and the transverse relaxation time τ_2 was measured as a function of cell temperature.

Except for the intervals during which τ_2 was measured the cells were continuously exposed to the pump beam, and except during measurement of the longer relaxation times, where it was necessary to reduce the relaxation rate caused by the read out light, they were continuously exposed to the read out beam.

The cells were also subjected to a heat treatment in an external oven. This involved heating the cell for 30 to 60 minutes at a temperature which in most cases was held between 950° and 1000°C . In some instances the heated cell was exposed to uv radiation from a high pressure Hg arc lamp.

Before the first heat treatment of a freshly prepared cell the relaxation time changed monotonically and nearly reversibly as the cell was cycled between room temperature and $\sim 600^\circ\text{C}$. The results for the first two cycles of cell T4 are typical and given in Table 7-3. It is to

be noted that the high temperature relaxation times decreased after the first cycle.

TABLE 7-3. Relaxation of ^{199}Hg on Tetrasil, Cell T4. Before
First Heat Treatment.

First Cycle		Second Cycle	
Cell Temperature (°C)	τ_2 (sec)	Cell Temperature (°C)	τ_2 (sec)
27	.001*	50	.07
107	.02	100	.15
208	.05	200	.33
299	.13	300	.57
405	.41	400	2.1
498	4.0	500	3.7
588	10.5	600	6.6
503	4.5	500	3.3
400	1.8	400	1.4
293	.43	300	.21
207	.18	200	.08
114	.12	100	.08
50	.07	50	.06

*Estimated from the condition for saturation of the NMR resonance.

In the cases so far observed the first heat treatment (in these cases, 950°C for ~ 30 min without uv) of a freshly prepared cell causes the low temperature relaxation time to increase by several orders of magnitude. The evidence for this is shown in Table 7-4.

TABLE 7-4. Effect of First Heat Treatment on Low Temperature ^{199}Hg Relaxation Time τ_2 .

Cell Material	Cell Number	BEFORE		AFTER	
		Cell Temperature ($^{\circ}\text{C}$)	τ_2 (sec)	Cell Temperature ($^{\circ}\text{C}$)	τ_2 (sec)
Suprasil W2	W1	33	.02	30	14
Suprasil W2	W2	50	.02	28	10
Tetrasil	T4	50	<.01	50	17

During the first heat treatment the cells were not irradiated with uv. After this heat treatment the variation of transverse relaxation time with temperature was no longer monotonic nor reversible. The results obtained during the first cycle after cell T4 was so heat treated are given in Table 7-5.

As the cells were subjected to successive heating and cooling cycles the peaks (see Table 7-5) in the temperature dependence of the transverse relaxation time gradually disappeared and this function became more nearly repeatable, reversible, and monotonic.

Table 7-6 shows the temperature dependence of the transverse relaxation time τ_2 that was measured during the fifth heating and cooling cycle for cell W2.

TABLE 7-5. Relaxation of ^{199}Hg on Tetrasil, Cell T4. First Cycle After First Heat Treatment.

Cell Temperature (°C)	τ_2 (sec)	
	Heating	Cooling
50	17.1	9.2
100	22.3	10.7
150	16.5	9.9
200	7.9	11.2
250	3.5	5.4
300	1.9	3.0
350	1.7	2.9
400	2.1	3.3
450	3.0	3.7
500	4.0	4.1
550	5.7	4.5
600	7.2	6.0*

*The cell was exposed to the uv light from the read out and pump beams for 10 min before starting the cooling cycle.

TABLE 7-6. Relaxation of ^{199}Hg on Suprasil W2, Cell W2, Fifth Cycle After First Heat Treatment.

Cell Temperature (°C)	τ_2 (sec)	
	Heating	Cooling
50	0.9	0.8
100	1.7	2.1
150	2.3	3.9
200	3.0	4.8
250	2.8	4.1
300	3.8	3.1
350	7.6	4.5
400	8.6	6.4
450	9.9	7.9
500	10.7	8.8
550	11.1	9.7
600	11.3	11.7

THE SINGER COMPANY • KEARFOTT DIVISION

A second heat treatment of the cells (without uv) not only restored but enhanced the relaxation time peaks in the region below 300°C. The results from the first heating and cooling cycle after such heat treatment of cell W2 are given in Table 7-7.

TABLE 7-7. Relaxation of ^{199}Hg on Suprasil W2, Cell W2, First Cycle, Second Heat Treatment.

Cell Temperature (°C)	τ_2 (sec)	
	Heating	Cooling
50	19.0	20.0
100	26.5	28.6
150	21.6	41.6*
200	11.2	45.7*
250	6.9	28.3
300	3.7	14.5
350	3.7	7.0
400	4.9	5.4
450	6.1	5.4
500	7.3	5.2
550	8.3	5.5
600	7.0	5.9**

* Limited by read out light-induced relaxation rate. True values estimated to be approximately twice as large.

** Exposed to uv light from read out and pump beams for ~30 minutes.

Again the temperature dependence of τ_2 became nearly stabilized and reversible after the cell had been recycled several times.

Further heat treatments restored the peaks in τ_2 and increased the height. Measurements made by leaving the cells in the dark except for the ~2 sec time interval necessary for observing the decaying NMR signal amplitude showed a relaxation time peak for cell W1 of 350 sec at a temperature of 237°C. However, after heating to 600°C and cooling, the re-

laxation time at this temperature had decreased to 205 sec.

It was found that exposing a fused silica cell to the uv radiation from a high pressure mercury arc lamp during heat treatment enhanced the relaxation time and may allow the cell to be stabilized with long relaxation times in the region below 300°C. After Cell W1 was so heat treated and irradiated it was subjected to a somewhat random temperature cycling as shown in Table 7-8. All relaxation times greater than 20 sec were measured in the "dark".

TABLE 7-8. Relaxation of ^{199}Hg on Suprasil W2, Cell W1, Heat Treatment With UV Irradiation.

Cell Temperature (°C)	τ_2 (sec)
28	27 (e)
115	310
158	470 (a)
276	38
403	12
488	18
644	15
156	520 (b)
196	640
208	570 (c)
81	240
598	14
208	660 (d)
32	100 (f)

It is to be noted that the peak relaxation time is now 660 sec as compared to 350 sec before the heat treatment and uv irradiation. The 470 sec value (a) for τ_2 at 158°C was enhanced to 520 sec (b) after heating the cell to 644°C and returning to 156°C. Similarly, the value for τ_2 at 208°C was increased from 570 sec (c) to 660 sec (d) after the second

heating to 598°C. Furthermore, the relaxation time at 28°C was changed from 27 sec (e) to 100 sec (f) after the cell was finally cooled to 32°C.

7.3.3 Relaxation of ^{199}Hg and ^{201}Hg on Suprasil W2

This subsection describes measurements of the relaxation of ^{201}Hg as well as ^{199}Hg in the Suprasil W2 cells W2 and W7.

For Cell W2 the temperature variation of the transverse spin-relaxation times of these nuclei is shown in Figure 7-2. It is to be noted that at all cell temperatures the relaxation time of ^{199}Hg either exceeded or was comparable with 10 times that of ^{201}Hg . In the temperature region between 200 and 360°C the ^{199}Hg relaxation time was greater during the cooling cycle than at the same temperature during the heating cycle. This effect was found repeatable during succeeding heating and cooling cycles. The relaxation time for ^{201}Hg did not show such an effect and the results for a heating cycle only are shown in Figure 7-2.

It is also to be noted that the relaxation times were measured as described in Section 3 with the ^{202}Hg read out beam on continuously. As a result the larger values of the ^{199}Hg relaxation time shown in Figure 7-2 are from 1/2 to 1/3 (as determined in other experiments) of those that would have been measured with a pulsed read out beam. Similarly, as described in Section 7.2, the non-resonant read out beam causes virtual light-induced shifts in the Larmor frequency of ^{201}Hg which appear as low frequency beats in the amplitude of the relaxing ^{201}Hg signal. The time required for the signal to reach 1/3 of its initial value can hence differ, especially for the longer times, from the true relaxation time. The anomalously high value of ~15 sec measured at ~340°C, as well as the fluctuations observed between 200°C and 300°C may be the result of this effect.

Cell W7 was prepared and subjected to various heat treatments as previously described in Section 6.4. Before the first heat treatment all relaxation times were small. The largest values measured for ^{199}Hg and ^{201}Hg were respectively, 0.6 and 1.5 sec at a cell temperature of 385°C.

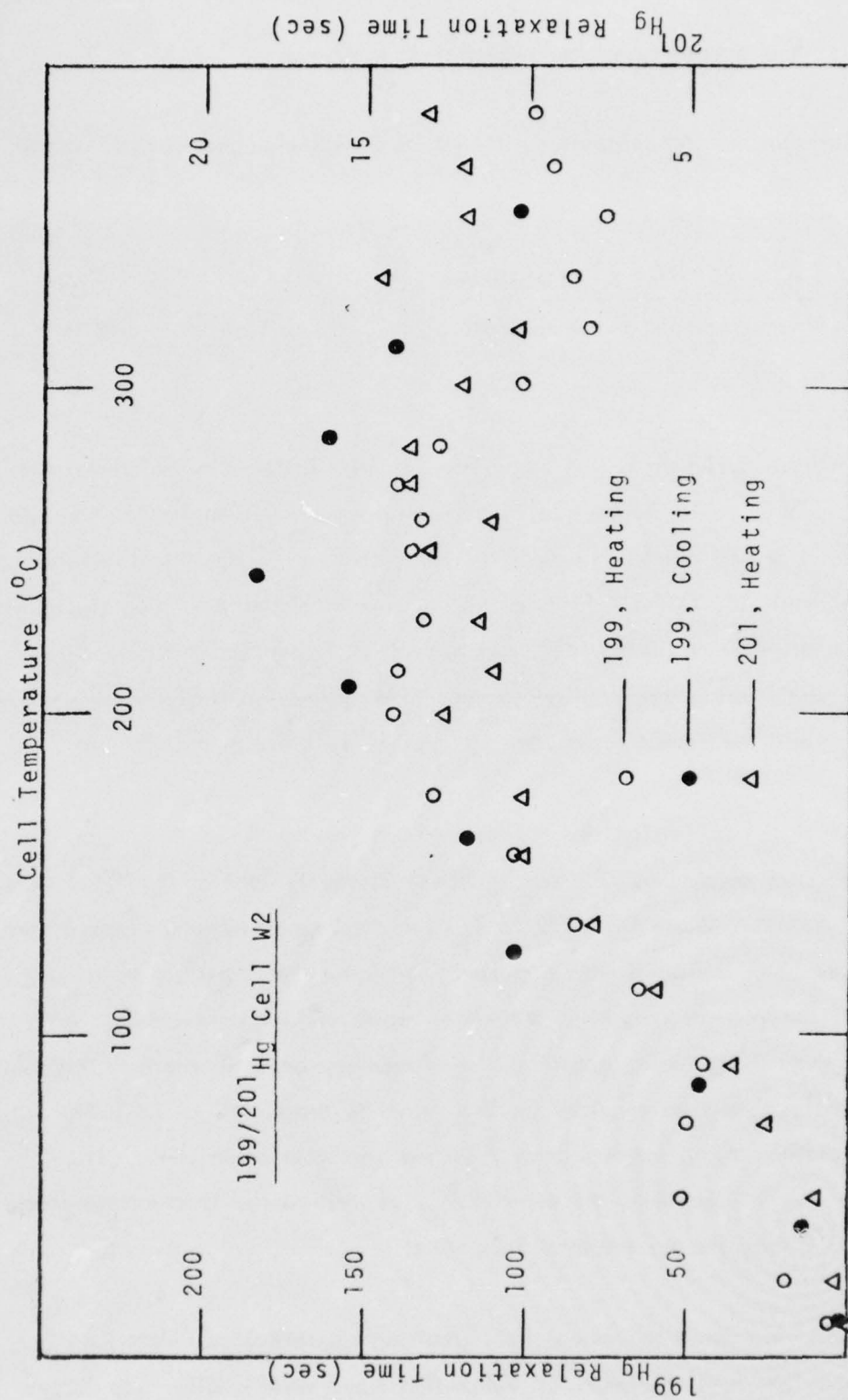


FIGURE 7-2 - Relaxation Time vs Temperature. Heating and Cooling Cycles After Several Heat Treatments.

Figures 7-3 and 7-4 show the variation of relaxation time with temperature during the heating and cooling cycles. The most striking characteristic of these results is that over most of the temperature region the relaxation time for ^{199}Hg was appreciably less than that for ^{201}Hg . This is in distinct contrast to the results shown in Figure 7-2 for Cell W2, where the 199/201 relaxation time ratio was approximately ten to one.

Such a reduction in the 199/201 relaxation time ratio could be caused by a magnetic interaction. As described in Section 7.2, the mercury nuclei in the presence of a fluctuating magnetic field are subject to an interaction through their magnetic dipole moments which causes an initial orientation to relax at the rate given by equation (7-2). Since this relaxation rate is proportional to the square of the gyromagnetic ratio γ , the magnetic interaction should cause ^{199}Hg to relax ~ 7 times faster than ^{201}Hg . In the temperature region above 300°C the measured ^{199}Hg relaxation time is $\sim 1/7$ that of ^{201}Hg .

As will be described in Section 7.4 a ^{199}Hg relaxation time of ~ 40 min was observed with this apparatus in the glass cell P26. The instrumental contribution to the relaxation is hence negligible compared to the cell-inherent contribution that limited the ^{199}Hg relaxation time to ~ 3 sec (Figure 7-4). However, any model for such a relaxing mechanism must include provisions for achieving a strong temperature dependence of the fluctuating magnetic field in order to account for the sharp reduction in both the ^{199}Hg and ^{201}Hg relaxation times that occurred above 200°C .

After the second heat treatment (with uv) the relaxation time measurements made during the heating cycle are shown in Figure 7-5. Those obtained during the cooling cycle are not shown because they did not differ appreciably from those of the heating cycle. A comparison with those measured after the first heat treatment (Figures 7-3 and 7-4) shows that three changes were introduced by the second heat treatment. The first is the general increase in average relaxation time. The second is that below $\sim 240^\circ\text{C}$ the ^{199}Hg relaxation time was greater than that for ^{201}Hg . The third is the greatly increased rate at which the ^{199}Hg relaxation time decreased with temperature in the region between 200° and 300°C .

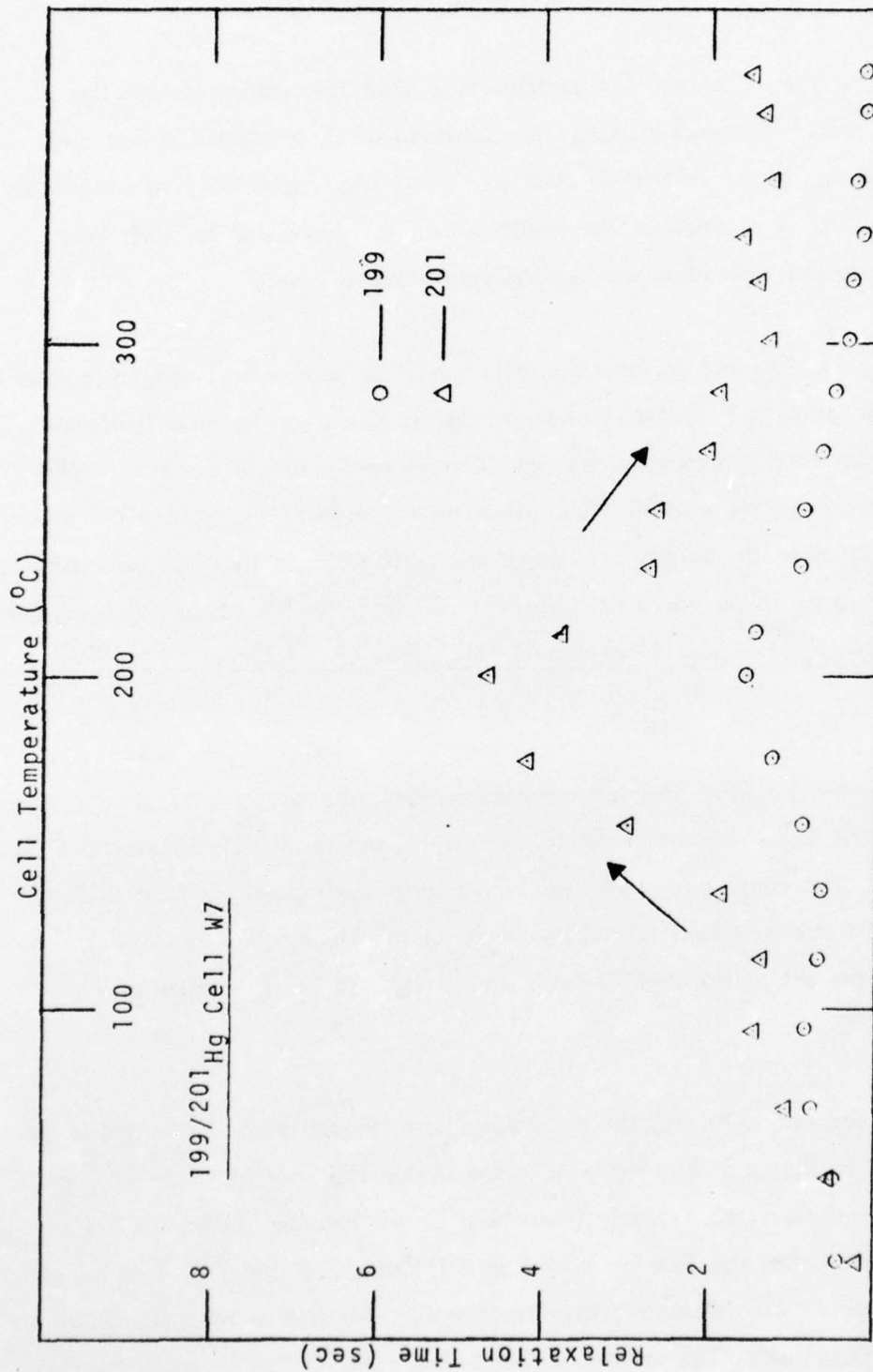


FIGURE 7-3 - Relaxation Time vs Temperature. Heating Cycle After First Heat Treatment. (1000 $^{\circ}\text{C}$ for 1 hr. No uv.)

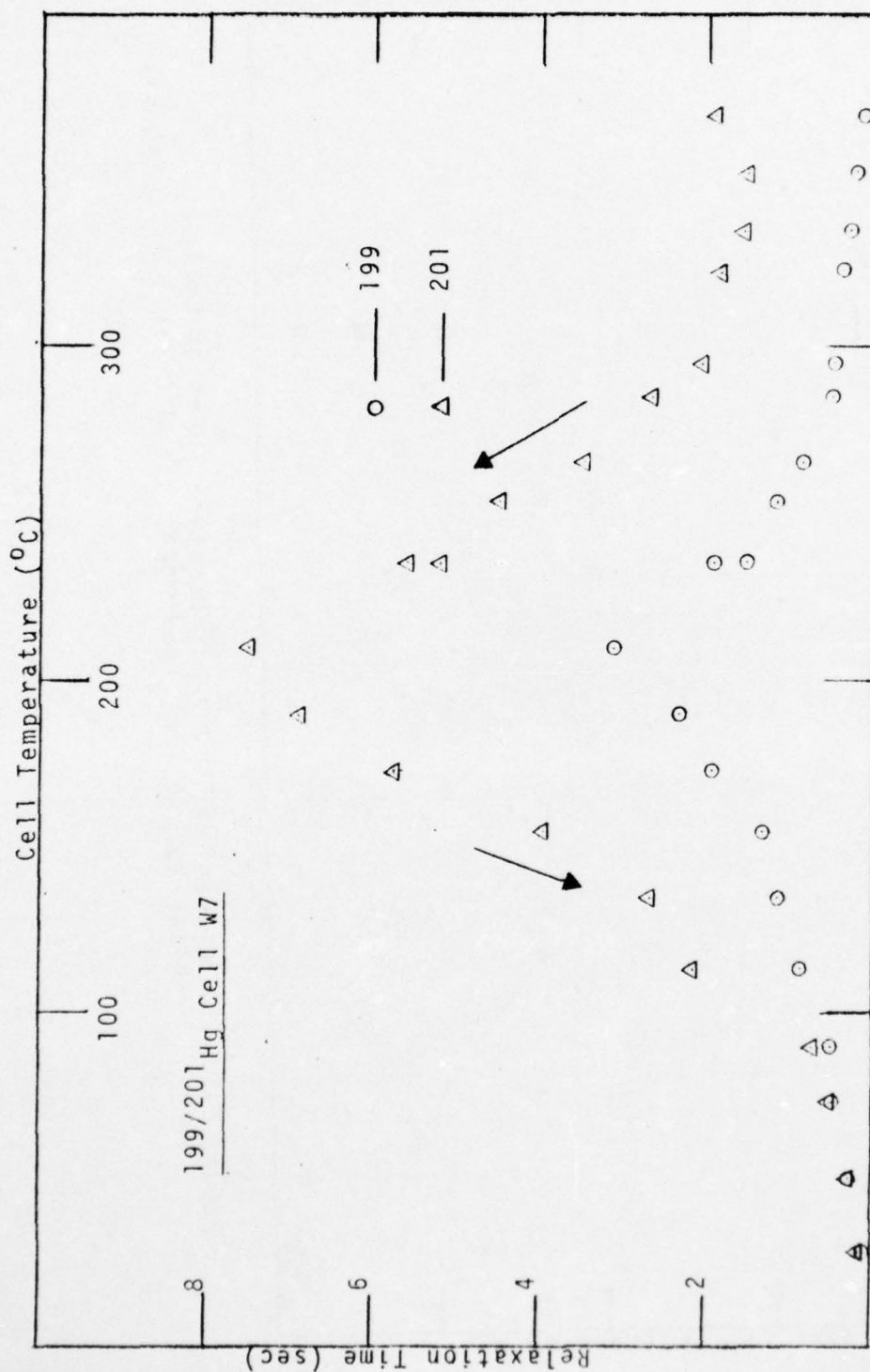


FIGURE 7-4 - Relaxation Time vs Temperature. Cooling Cycle After First Heat Treatment. (1000 $^{\circ}\text{C}$ for 1 hr. No uv.)

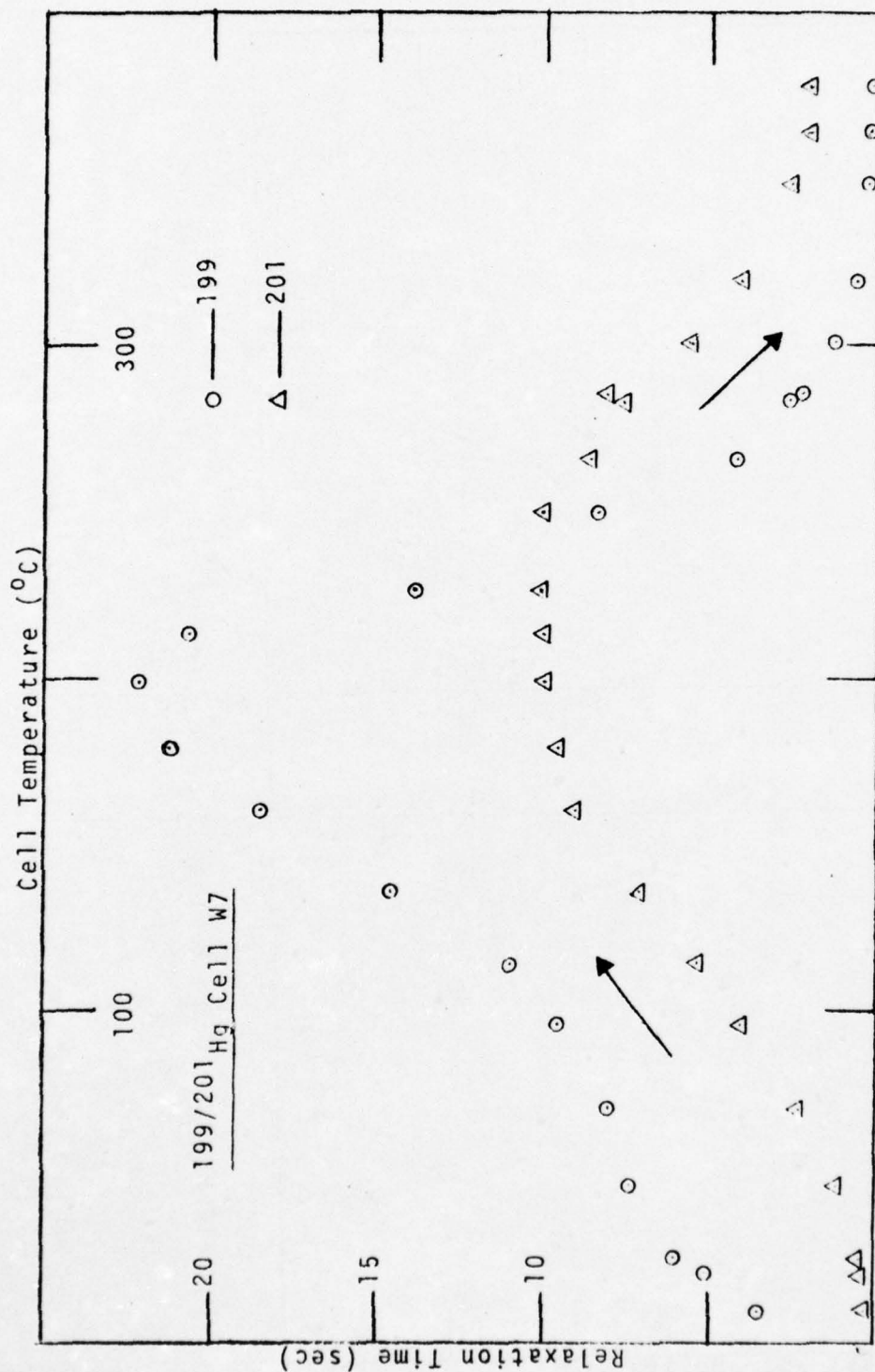


FIGURE 7-5 - Relaxation Time vs Temperature. Heating Cycle After Second Heat Treatment. (1000°C for 1 hr. with uv.)

In contrast there was an inappreciable change in this rate for ^{201}Hg . As after the first heat treatment the ^{199}Hg relaxation time approached 1/7 of that for ^{201}Hg .

The results show that the strength of the interaction that causes the high temperature relaxation time decrease has now been greatly reduced at temperatures below 200°C .

After the third heat treatment (uv for the first half hour) there occurred the surprising change in cell transmission described in Section 6.4.2.4. Associated with this was an interesting change in the relaxation times. Both relaxation times increased and that for ^{199}Hg changed from a value less than to a value comparable with that of ^{201}Hg . It is apparent that the relaxing magnetic dipole interaction was appreciably reduced in magnitude by whatever process caused the rise in cell transmission.

Figure 7-6 shows the variation of relaxation times with temperature observed during the heating cycle. Before the rise in cell transmission occurred (at 11:47 AM) the characteristics are seen to be very similar to those shown in Figure 7-5 for the previous heating cycle. After this change the characteristics were considerably different, as shown in Figure 7-7 for the cooling cycle. It is apparent that the temperature for first appearance of the strong relaxing magnetic dipole interaction has been increased from ~ 200 to $\sim 270^{\circ}\text{C}$ and the temperature for equal ^{199}Hg and ^{201}Hg relaxation times increased from ~ 260 to nearly 400°C .

7.3.4 The Intrinsic Magnetic Dipole Interaction

The simplified theory of relaxation described in Section 7.2 indicates that if the amplitude h_0 of the fluctuating magnetic field remains constant the relaxation time should increase continuously with cell temperature because of the corresponding decrease in "sticking" time predicted by equation (7-1). The results described above in which the relaxation time at first increased and then decreased with cell temperature require that in this model of the relaxation mechanism the magnetic field amplitude h_0 had to be increasing (very rapidly in some cases) with temperature. They also show that the source of the fluctuating magnetic field was a magnetic field gradient that was not instrumental but was instead intrinsic to

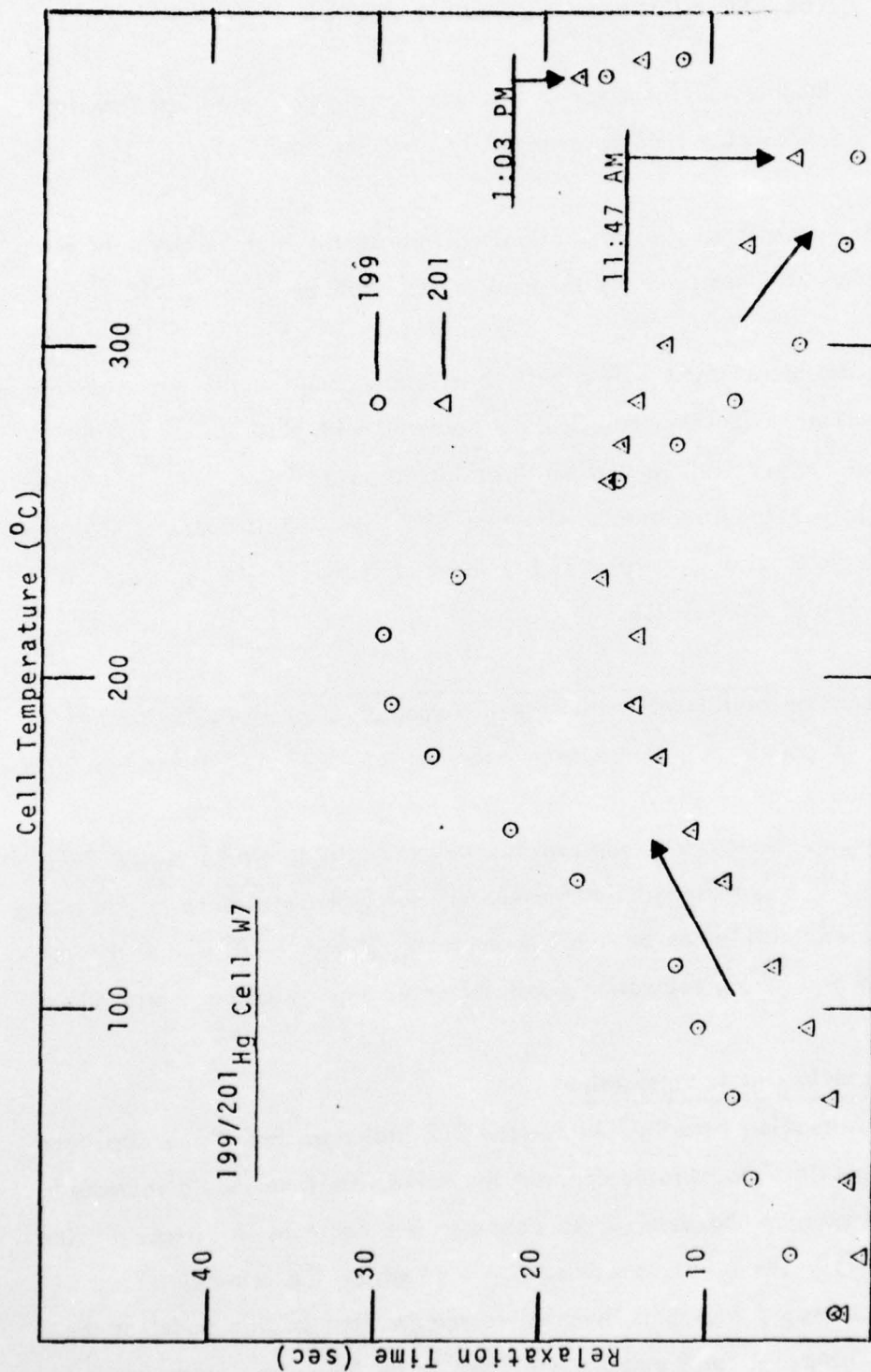


FIGURE 7-6 - Relaxation Time vs Temperature. Heating Cycle After Third Heat Treatment. (1000°C for 1 hr. UV for 1/2 hr.)

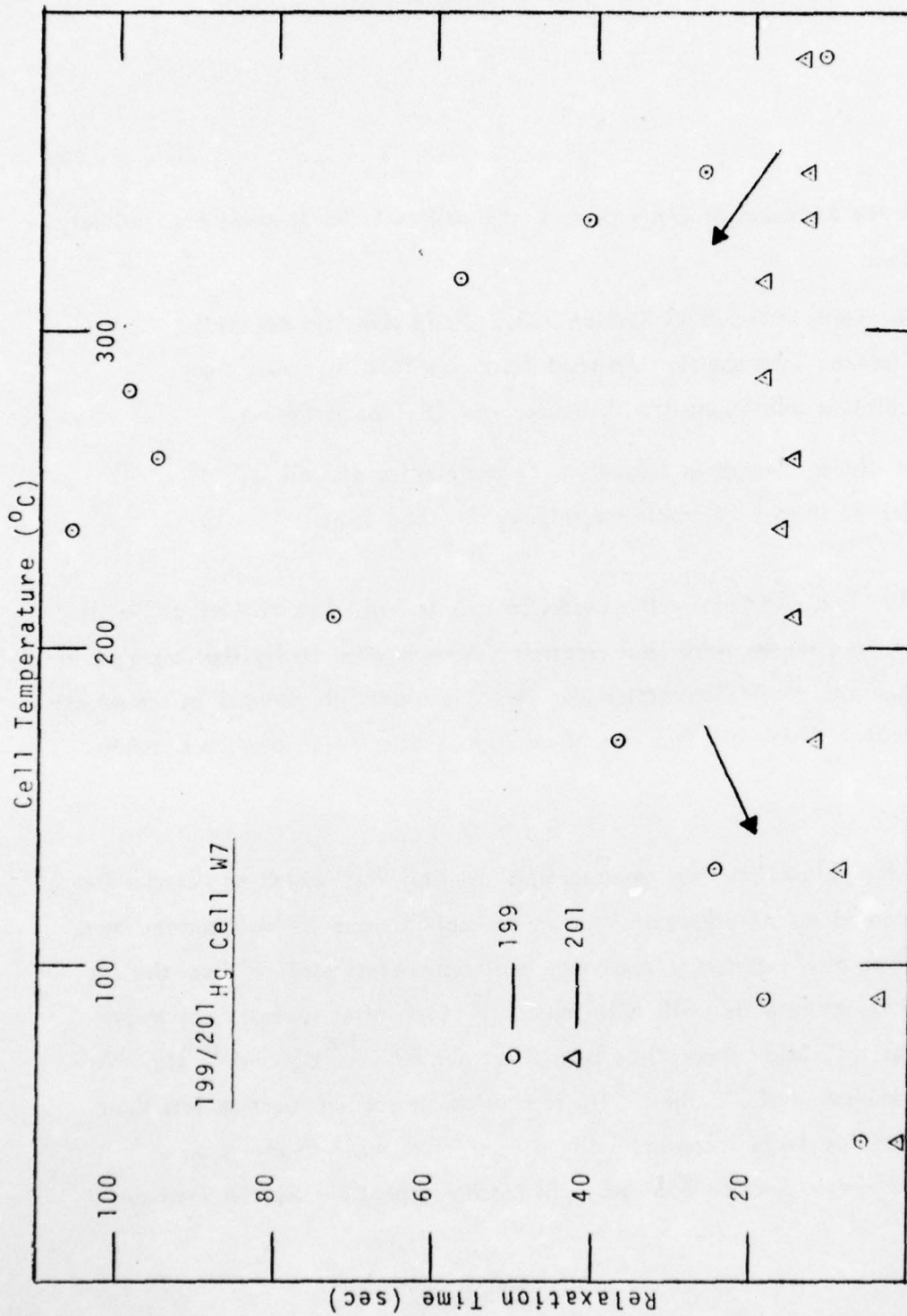


FIGURE 7-7 - Relaxation Time vs Temperature. Cooling Cycle After Third Heat Treatment. (1000°C for 1 hr. UV for 1/2 hr.)

the cell.

A possible correlation between the strength of this magnetic dipole interaction with the ^{199}Hg and ^{201}Hg nuclei and the presence of OH groups in the cell material is considered unlikely for the following reasons:

- a) The results reported in Section 7.3.2 which show no essential difference in relaxation between Tetrasil with a high OH concentration and Suprasil with a very low OH concentration.
- b) The abrupt change in relaxation characteristics of Cell W7 after its third heat treatment (Figures 7-6 and 7-7).

The behavior of Cell W7 and particularly the evidence that it had three distinct cell-wall binding states (Figure 6-8) after its third heat treatment make it more likely that changes in the strength of this magnetic dipole interaction can be correlated with changes in the surface structure of the cell walls. There are two sets of additional data which provide a similar indication.

The first set comprises the relaxation time measurements for Cell W25 which as described in Section 6 was slowly cooled during preparation in an attempt to make its wall surface more quartzlike. This cell was also exposed to resonance radiation before seal off from the Hg reservoir in an attempt to saturate its walls with mercury. Even after several heat treatments this cell had short relaxation times, less than 5 sec for both ^{199}Hg and ^{201}Hg . As the cell temperature approached 400°C the ^{199}Hg relaxation time again became less than that for ^{201}Hg . The possibly large increase in the number of exposed O atoms on a quartzlike surface mentioned in Section 6.6, may have been responsible for the increased relaxation in this cell.

The second set consists of the results obtained with new cells fabricated after the preparation procedure was modified to hold the cell temperature at 1100°C . The fused silica cells

(including W7) originally prepared with this longer bake out were purposely held at a lower temperature of 950°C in order to avoid the possibility of collapse if the oven temperature became too high during the night time periods when the apparatus was unattended. None of these first cells had relaxation times (for ^{201}Hg in particular) as large as those obtained in W1 and W2 which had been baked out at 1100° for a shorter time.

The relaxation times observed for the new cells were comparable with those of W1 and W2 and consistently greater than those prepared with the 950°C bake out. In the Suprasil W2 Cell W23, at temperature of 400°C and after several heat treatments, the ^{199}Hg relaxation time was 50 sec and that for ^{201}Hg was 100 sec, which is comparable with the longest relaxation times observed for this isotope (Ref. 14, for instance). It is to be noted that this ^{201}Hg relaxation time was measured as explained in Section 7.5, in the absence of light-induced or cell-intrinsic quadrupole-splitting of the resonance.

It is also to be noted that again the relaxation time for ^{199}Hg became less than that for ^{201}Hg . This was also the case in the other cells that were subjected to the higher temperature bake out.

It is concluded that although this hotter bake out may have removed some impurities that were increasing the electric quadrupole relaxation of ^{201}Hg (see Section 7.5) it did not reduce the strength of the magnetic dipole interaction to the low level observed in glass cells (Section 7.4). Further experiments, especially, further measurements on GE204 cells, will be required to determine the source of this interaction in fused silica cells and its connection with the inherent or possibly impurity-modified surface structure of the cell walls.

7.4 RELAXATION OF ^{199}Hg AND ^{201}Hg ON GLASS

It has been evident from the beginning of this investigation that the magnetic dipole interaction in cells made of Corning 9741 glass is much weaker than in fused-silica cells. The first results were measurements of the longitudinal relaxation time T_1 in the previously prepared glass cell #49. They are shown in Table 7-9.

THE SINGER COMPANY • KEARFOTT DIVISION

TABLE 7-9. Relaxation of ^{199}Hg on Corning 9741 Glass

Cell Temp. ($^{\circ}\text{C}$)	T_1 (minutes)
24	2.5
49	6.2
72	10.3
94	13.8
115	17.2
136	21.3
156	23.8
176	27.5
194	24.3
213	30.6
232	29.4
250	30.5
268	29.2
285	32.4

Comparison of the results at 250°C with those given in Table 7-2 show that the longitudinal relaxation time T_1 for ^{199}Hg on Corning 9741 glass is 8 times that for GE204 fused silica. At 24°C the corresponding enhancement is 25/1. At 285°C the value, $T_1 \approx 32$ min, is 44 times the corresponding value estimated from the data reported by Bonnot and Cagnac (Ref. 14) for ^{199}Hg on flame formed fused silica. It also exceeds the 30 min value observed by these workers when the temperature of their cell was 600°C .

The longest ^{201}Hg relaxation time observed during these measurements was ~ 20 sec at 285°C , and there was evidence that the relaxation was not exponential. This led to the experiments described in Section 7.5 that show evidence for a cell-intrinsic as well as a light-induced quadrupole splitting of the ^{201}Hg magnetic resonance.

Cell #49 was recently retested to determine whether it still exhibited a 32-min relaxation time for ^{199}Hg and whether it contained a foreign gas.

It was found that cell #49 sometimes did and sometimes did not have a long relaxation time for ^{199}Hg . For instance, a value of 32 min was measured at $\sim 160^\circ\text{C}$ and at another time this relaxation time was 29 min at $\sim 230^\circ\text{C}$. However, when the cell was held too long at temperatures greater than 230°C a sharp change occurred in the cell characteristics that was difficult to reverse. After this a ^{199}Hg relaxation time greater than ~ 6 min could not be obtained at any temperature up to $\sim 300^\circ\text{C}$. (This limit is imposed by charring of the coil forms since the large cell #49 could not be enclosed in the protective fused silica tube used with the smaller 1-cm dia. cells.) A similar reduction in the ^{201}Hg relaxation time also occurred. The long relaxation time characteristics could be restored by slowly increasing the cell temperature up to 200°C . So far this heat treatment has been applied during an ~ 8 hour period. The determination as to whether a shorter time will be successful and of the minimum temperature and time required for onset of the destructive change in cell characteristics requires further investigation.

After the long relaxation characteristics have been restored the ^{199}Hg relaxation time increases with temperature until the destructive change again occurs. During this period there is no evidence for the strong cell-intrinsic and temperature-dependent magnetic dipole interaction that was observed in fused silica cells. Further experiments will be required to determine whether such an interaction is present after the destructive change. Possible evidence against this interaction is that the ^{201}Hg relaxation time decreases in nearly the same ratio.

Measurements of the transmission of cell #49 as a function of temperature showed no indication of any anomalous changes in mercury vapor density. The "dry point" of the cell occurred at 13°C . (The seal off temperature of this old cell was 15°C). Signals observed for 199A and 199B were found to be in phase at all temperatures. There is hence no evidence that an appreciable amount of gas has evolved from the walls of this cell.

THE SINGER COMPANY • KEARFOTT DIVISION

Relaxation time measurements on glass cells given the longer bake out during preparation have just been started. One of these, P26, had a relaxation time of 40.5 min at 300°C. So far the type of destructive changes observed in the old cell #49 have not occurred.

The ^{201}Hg relaxation times of two other glass cells so prepared, P23 and P25, were measured at 400°C and found to be 40 sec and 26 sec, respectively. However, the ^{201}Hg relaxation times of both these cells decreased as the cells were held at this temperature. This could indicate that the destructive changes observed in cell #49 were beginning to occur. It is to be noted that neither cell had a relaxation time comparable to the 100 sec value observed at this temperature in the fused silica cell W23 (Section 7.3.4).

To our best knowledge measurements of the nuclear-spin relaxation of ^{199}Hg and ^{201}Hg on glass have not been reported in the literature. The above new results confirm the initial evidence for a greatly weakened magnetic dipole interaction with glass as compared with fused silica. They show, however, that of the two materials, glass apparently has the stronger electric quadrupole interaction.

Similar results for the nuclear-spin relaxation of gaseous ^3He (whose nucleus, like that of ^{199}Hg , has only a magnetic dipole moment) on glass as compared with fused silica have been reported by Fitzsimmons et al. (Ref. 18). A value of $T_1 > 10^5$ sec was observed for ^3He on Corning 1723 glass as compared with ~3000 sec for fused silica (Suprasil). These authors also found that the relaxation time of ^3He in cells made of Suprasil (also Pyrex glass) went through a maximum at ~150°C. They were able to correlate their results by postulating a second relaxation mechanism in addition to that (Section 7.2) involving the fluctuations in magnetic field generated during the time that an adsorbed Hg atom sticks to the cell wall. They proposed that as the temperature increases more He atoms can diffuse into the cell wall and that these "dissolved" atoms continually change place with those He atoms that strike the surface and have oriented nuclear spins. Since the relaxation rate caused by the diffusion mechanism should increase with temperature it takes over from the adsorptive process at temperatures above that where the maximum relaxation time occurs. In

cells made of Corning 1720 and 1723 glass, which are very impermeable to helium (Ref.19) they found that the ^3He relaxation time continuously increased with temperature.

Such diffusion may indeed be occurring for Hg in the fused silica cells and not in the glass cells. However, the 30-minute ^{199}Hg relaxation time observed at 600°C (Ref. 14) indicates that the diffusion mechanism plays a small part in flame-fused silica. A similar situation should exist in the other grades of fused silica. Also, since the diffusion rate of ^{199}Hg atoms can not differ appreciably from that of ^{201}Hg atoms it is difficult to see how such a mechanism could cause ^{199}Hg nuclei to relax faster than ^{201}Hg nuclei.

7.5 RELAXATION OF ^{201}Hg

7.5.1 Light Induced Quadrupole Splitting

As discussed in Section 7.2 the linearly polarized and non-resonant ^{202}Hg read out light can interact with the electric quadrupole moment of ^{201}Hg and split the resonance into three frequency components. This light induced electric quadrupole splitting of the ^{201}Hg resonance was first observed by B. Cagnac (Ref. 15) who predicted and confirmed that the magnitude of the splitting should be proportional to $IP_2(\cos\theta)$ where I is the light intensity, $P_2(\cos\theta)$ is the Legendre polynomial, $3\cos^2\theta - 1$, and θ is the angle between the plane of polarization of the light beam and the direction of the H_0 magnetic field. Observation of the small ($\sim .06\text{Hz}$) splitting required precise control of the magnitude of the H_0 magnetic field and the frequency of the H_1 magnetic field.

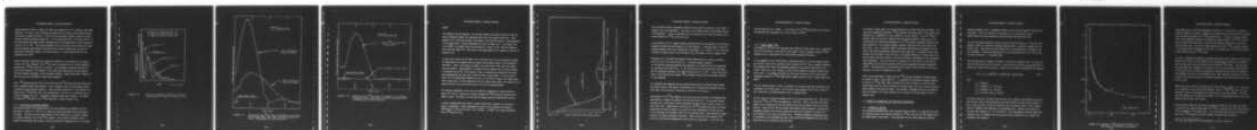
Observation of the decay of the ^{201}Hg signal does not require such precise magnetic field control and the light induced frequency shifts (LIFS) appear as beats in the free precession transient, for instance, as described by equation (7-4). Such a non-exponential decay of ^{201}Hg was observed near the beginning of this investigation in the glass cell #49. Some of the experiments described here were performed in another apparatus since it was equipped with a half-wave plate for rotating the plane of polarization of the incident read out beam. The measurements were made with the fused silica cells W1 and W2.

AD-A033 737

SINGER CO LITTLE FALLS N J KEARFOTT DIV
NOISE SOURCES IN NMR OSCILLATORS AND RELAXATION PHENOMENA IN OP--ETC(U)
AUG 76 D S BAYLEY, I A GREENWOOD, J H SIMPSON F44620-72-C-0047
KD76-31 AFOSR-TR-76-1418 NL

UNCLASSIFIED

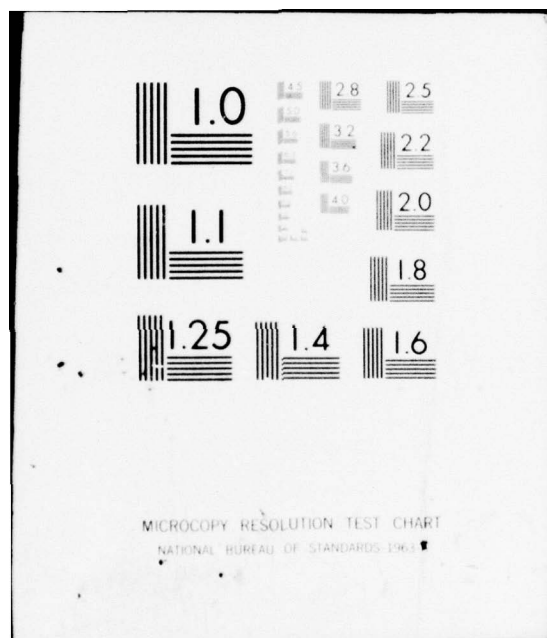
2 OF 2
AD
A033737



END

DATE
FILMED

2-77



Typical results are shown in Figure 7-8 which was prepared from T-Y recordings of the signal amplitude. The start of each recording was delayed until the slope of the transient became flat enough to observe the beats. It shows the free precession transients obtained for three different incident polarization angles (θ). As this angle approached $\sim 55^\circ$ (where $3\cos^2\theta = 1$) the time between the signal minima increased and the curve approached a simple exponential (Curve C at $\theta = 40^\circ$). The initial amplitudes of the curves were not the same for each angle since the relative angle between the polarizer and analyzer changed when the plane of polarization rotated with respect to the fixed analyzer. In these measurements the cell temperature was 135°C .

Similar experiments demonstrating the LIFS were performed in the relaxation time apparatus with cell W6. Alignment of the ^{201}Hg nuclei was produced with a linearly polarized pumping beam (^{198}Hg) along the H_0 direction. The advantage of observing the beat frequency with alignment is the absence of the initial large decay before the beat appears. The light intensity dependence of the quadrupole splitting is clearly observable in Figure 7-9. The two curves are for different readout beam intensities.

With a ^{199}Hg pump lamp both the $F=1/2$ and $F=5/2$ levels of ^{201}Hg were excited (see Figure 5-1), and no alignment signals were observed. This is thought to have occurred because the two components pump in opposite directions. When the light exciting the $F=5/2$ transition was blocked with a ^{204}Hg filter cell in the pumping beam, only the $F=1/2$ transition was excited and alignment occurred. The beating components were again observed. The effect of adding the ^{204}Hg filter in the ^{199}Hg pump beam is shown in Figure 7-10.

7.5.2 Cell-Intrinsic Quadrupole Splitting

The half-wave plate in the readout beam of the other apparatus was adjusted to set the polarization angle at $\theta = 55^\circ$ so as to obtain the purely exponential decay predicted by the theory. The read out beam light intensity was then reduced in an attempt to observe the intrinsic relaxation time of the ^{201}Hg isotope. As the observed relaxation time increased with decreasing light intensity, the beat phenomenon reappeared with a much longer

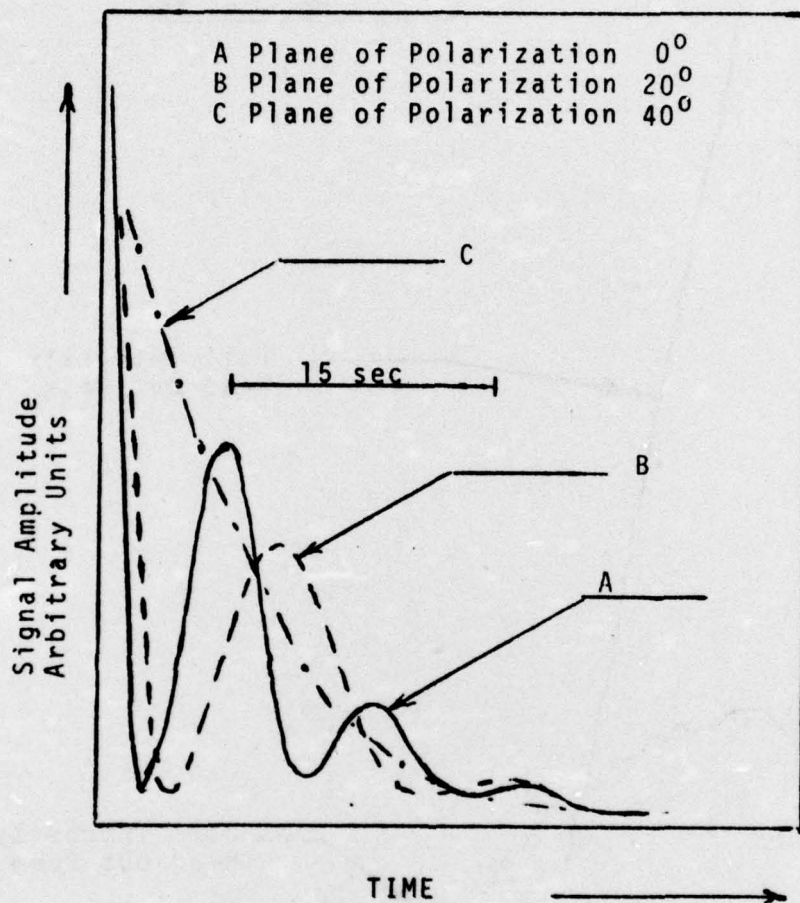


FIGURE 7-8 - Effect of Change in Angle of Plane of Polarization on Shape of Decay Curve

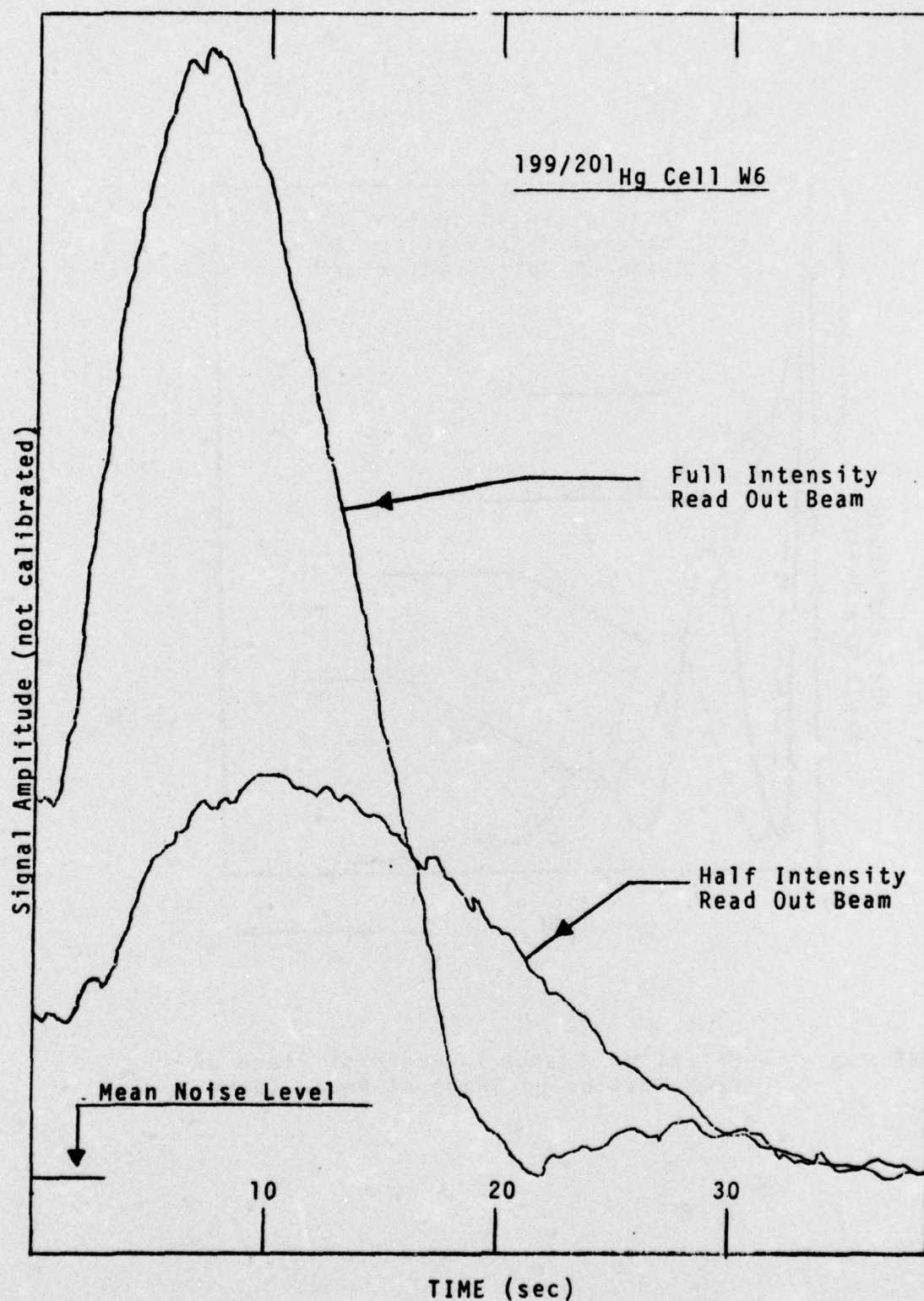


FIGURE 7-9 - Relaxation of ^{201}Hg After Alignment by Linearly Polarized ^{198}Hg Pump Beam and During Read Out With a ^{202}Hg Beam (π polarization).

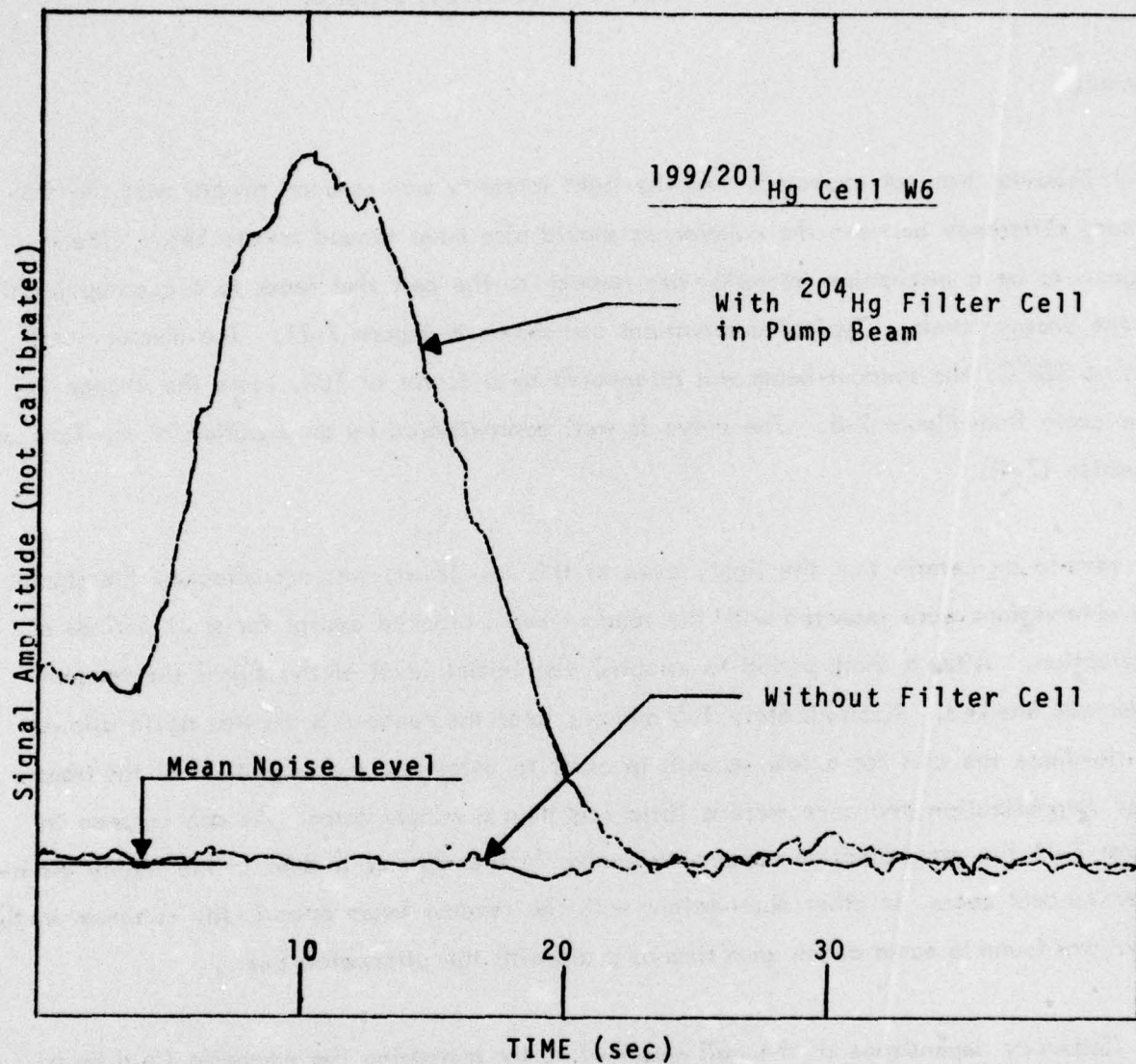


FIGURE 7-10 - Relaxation of ^{201}Hg After Alignment by a Linearly Polarized ^{199}Hg Pump Beam and During Readout With a ^{202}Hg Beam (π polarization).

period.

Such behavior was not expected. As the light intensity was reduced toward zero the frequency difference between the coherences should also have tended toward zero. There appears to be a mechanism intrinsic with respect to the cell that leads to a quadrupole shift in the energy levels. Typical observations are shown in Figure 7-11. The mercury cell was at 328°C , the readout beam was attenuated by a factor of 100. Note the change in time scale from Figure 7-8. The curve is well approximated by an equation of the form of equation (7-4).

In order to be certain that the light, even at this low level, was not affecting the signal, the observations were repeated with the readout beam blocked except for short periods of observation. After a short period to establish the initial level of the signal the readout beam was blocked. Approximately 1.5 minutes later the readout beam was again allowed to illuminate the cell for a few seconds in order to determine the magnitude of the transverse magnetization and once more a little less than a minute later. As can be seen in Figure 7-11 the magnetization appears to evolve in the dark as it does in the highly attenuated readout beam. In other observations with the readout beam pulsed, the minimum in the signal was found to occur at the same time as it did with the attenuated beam.

The frequency dependence of the null was studied by increasing the magnetic field by a factor of 2.7 from 1.3 gauss to 3.5 gauss, changing the ^{201}Hg resonance frequency from 369Hz to 1kHz. The time to the null did not change within the experimental accuracy.

A series of measurements were made at various readout beam intensities as a function of angle of polarization. Within experimental accuracy at all intensities the frequency difference at $\theta \sim 55^{\circ}$ was the same: $6.5 \pm 0.2\text{mHz}$. At 350°C , the intrinsic relaxation time of ^{201}Hg was 77 sec.

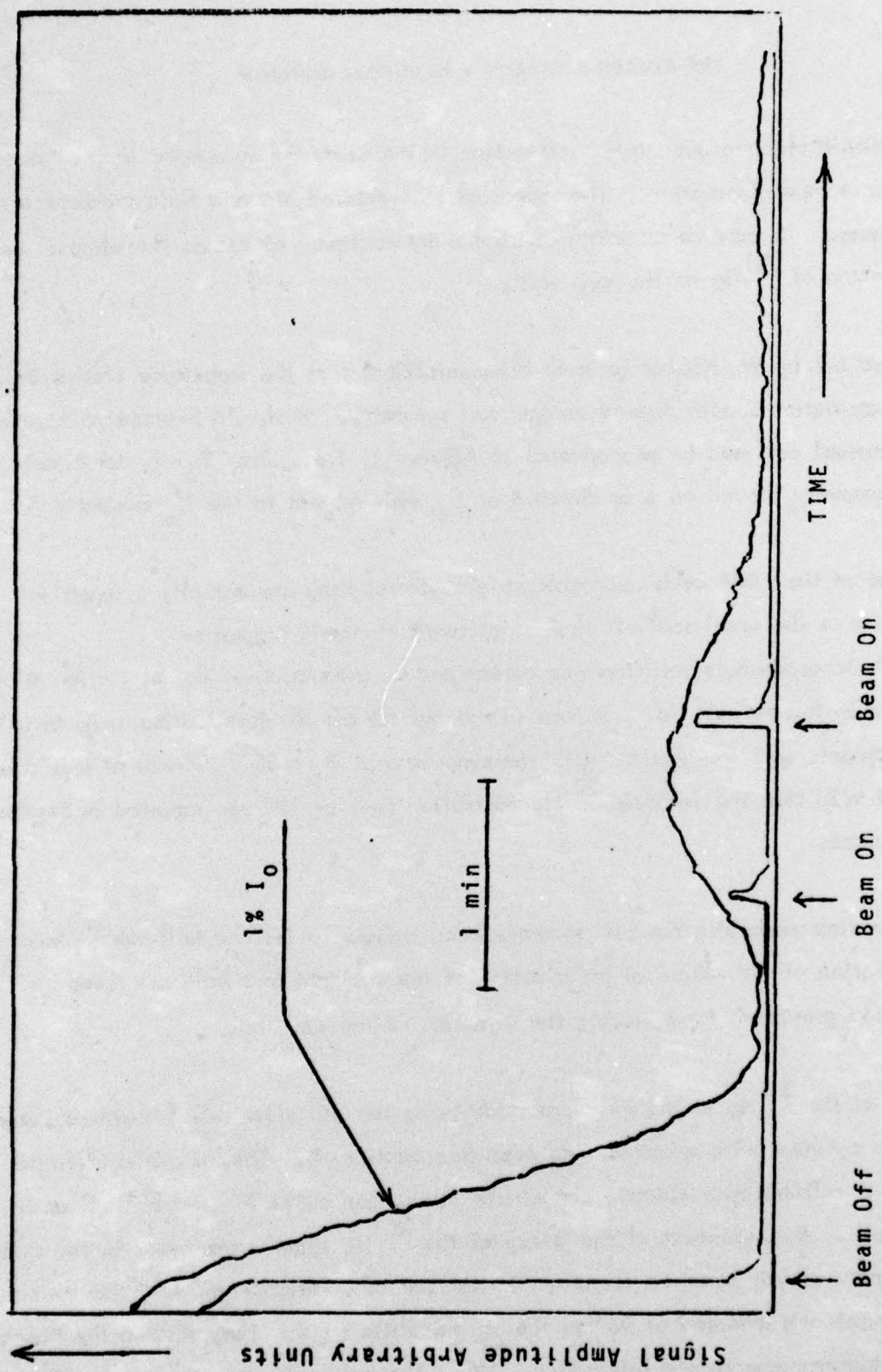


FIGURE 7-11 - Signal Decay With Readout Beam Attenuated to 1% and Beam Blocked.

THE SINGER COMPANY • KEARFOTT DIVISION

The cell-intrinsic electric quadrupole interaction which splits the resonance in the "dark" is thought to be a new observation. The source of the required electric field gradient remains to be determined. It may be associated with the interaction that causes the electric quadrupole relaxation of ^{201}Hg on the cell wall.

It was pointed out by W. Happer (private communication) that the magnitude of this intrinsic quadrupole interaction should depend on the cell symmetry. It should average to zero for a perfectly spherical cell and be proportional to $P_2(\cos\theta_c)$, i.e., $3\cos^2\theta_c - 1$, for a cell with cylindrical symmetry around an axis directed at θ_c with respect to the H_0 magnetic field.

Although most of the NMR cells approach perfect spheres they are actually symmetrical around the axis of the small seal-off tip. Following Happer's suggestion the cell-intrinsic quadrupole splitting was determined as a function of the cell orientation θ_c as defined by this seal off tip. It was found that for all the fused silica cells tested that the quadrupole splitting in the "dark" became zero at $\theta_c = 55^\circ$. It was at this orientation of cell W23 that the intrinsic ^{201}Hg relaxation time of 100 sec reported in Section 7.3 was measured.

The relaxation time apparatus has just recently been revised to include half-wave plates that allow rotation of the planes of polarization of the incident and transmitted read out beam light, and provisions for adjusting the direction of the cell axis.

Measurements of the ^{201}Hg relaxation were made using the old glass cell #49 whose shape approximates a cylinder with spherical end caps (see Section 4). They provided definite evidence that a cell-intrinsic electric quadrupole interaction exists in glass as well as in fused silica cells. Measurements of the decay of the ^{201}Hg signal were made in the dark (pump beam and read out beam on for only 0.5 sec per observation), and with the axis of this cylindrical cell oriented at 90° to the H_0 magnetic field. They showed the "beats" caused by an electric quadrupole interaction. When the cell axis was oriented at 55° to the H_0 field the beats disappeared and the decay was exponential. In the first case

the beat frequency was $\sim 1/60\text{Hz}$. In the second case the ^{201}Hg relaxation time increased monotonically with temperature to a value of 50 sec at 300°C .

7.5.3 "Magic Angle" Cells

The angle $\theta_c = 55^\circ$ has in this laboratory been called the "magic angle" since it was found that at this orientation of the cell axis with respect to the H_0 magnetic field the ^{201}Hg resonance was no longer split by the cell-intrinsic quadrupole interaction.

It was suggested by one of the authors (I. Greenwood) that if a cell were shaped so that the normal to each surface element could be oriented at 55° to the H_0 magnetic field then the interaction that causes this quadrupolar splitting would vanish at each point of the surface, rather than on the average as is the case for spherical or properly oriented cylindrical cells. It is possible, therefore, that the surface interaction which causes electric quadrupole relaxation of ^{201}Hg might also be greatly reduced in such a "magic angle cell" (MAC).

One such possible shape is a cube, and another is a bi-cone whose half-cone angle is the complement of the magic angle. For the cube a body diagonal, and for the bi-cone the axis, would then be oriented parallel to the H_0 magnetic field.

The first tests of a MAC were performed with an old cubic fused-silica cell. This was re-filled with ^{199}Hg and ^{201}Hg and prepared as a wet cell. After it was found that NMR signals could be obtained the cell was sealed off with the Hg reservoir held at room temperature. Before this dry cell was heated NMR signals could be observed. However they disappeared rapidly as the cell was heated and could not be restored by cooling or by heat treatment of the cell in an external oven. Although transmission measurements were not performed it was concluded that most of the Hg atoms had disappeared from the vapor phase and were now attached to the cell walls.

A bi-conical "magic angle" dry cell was prepared from Corning 9741 glass and tested. The results were disappointing because a ^{201}Hg relaxation time greater than ~ 8 sec could not be obtained and no dependence on cell orientation could be observed. Since the ^{199}Hg relaxation times were also short compared with those usually observed in glass cells it was concluded that the directional dependence of the ^{201}Hg electric quadrupole interaction was being masked by a much stronger magnetic relaxation mechanism that could interact with both nuclei. Such a mechanism might be associated with particular characteristics of the interior cell surface produced by blowing the molten glass into a considerably cooler mold. Evidence that the surface of this cell had a much greater attraction for mercury atoms than exists in glass cells blown without a mold was provided by measurements of cell transmission versus temperature. Not only was there no evidence for a "dry point" but also the Hg vapor density did not reach its maximum until the cell temperature had been increased to $\sim 220^\circ\text{C}$. Had there been no wall attraction all Hg atoms would have been in the vapor phase above the seal off temperature of $\sim 35^\circ\text{C}$.

There is some experimental evidence that the ^{201}Hg electric quadrupole relaxation might be reduced in such a magic angle cell. In comparing the exponential envelope enclosing the beats of a ^{201}Hg "dark" decay transient, such as that of Figure 7-11, with the exponential decay when the cell was oriented at the magic angle, the former typically showed a shorter relaxation time than the latter. This increase in relaxation time may be enhanced when the normals to all surface elements can be oriented at 55° with respect to the H_0 magnetic field.

7.6 EFFECTS OF RADIATION ON CELL-WALL RELAXATION

7.6.1 Radiation at 253.7nm

The experiments described herein were concerned with the effects of uv light from the read out and pump beams on the intrinsic relaxation of ^{199}Hg in the old cell #27 prepared from the GE204 grade of fused silica. They developed from the initial observations that the

transverse relaxation time τ_2 gradually decreased as the cell was exposed to light from the pump beam. When the pump beam was blocked the cell would slowly recover. Similar results have been reported by Cohen-Tannoudji and Brossel (Ref. 20).

The cell was initially exposed to both the pump and read out beams for ~ 1 hour at a temperature ($\sim 70^\circ\text{C}$) for which the transverse relaxation time τ_2 was short compared with the recovery time. Both beams were then blocked and τ_2 was measured as a function of the time thereafter. During each measurement of τ_2 the pump beam was on for ~ 30 sec and the read out beam for ~ 2 relaxation times.

The results are shown in Figure 7-12 which is a plot of the relaxation rate $1/\tau_2$ versus the time the cell had recovered in the dark. It was found that at least three exponential time constants were involved in the recovery. A good fit to the data was provided by the equation,

$$1/\tau_2 = a_0 + a_1 \exp(-t/t_1) + a_2 \exp(-t/t_2) + a_3 \exp(-t/t_3), \quad (7-5)$$

with

$$\begin{aligned} a_0 &= 0.241/\text{sec}, \\ a_1 &= 0.437/\text{sec}, \quad t_1 = 0.42 \text{ min}, \\ a_2 &= 0.533/\text{sec}, \quad t_2 = 3.6 \text{ min}, \\ a_3 &= 0.311/\text{sec}, \text{ and } t_3 = 25 \text{ min}. \end{aligned}$$

The French group (Ref. 20) also found that three time constants could describe the recovery, that the same values of these parameters would also describe the decay during exposure to the uv light, and that not only the values but also the required number of time constants varied in "different" (the difference is not specified) cells. However, they report only the three time constants of 2, 19, and 150 min. Their measurements were also made after exposure to the uv irradiation from the pump and read out beams and at a constant cell temperature (not reported).

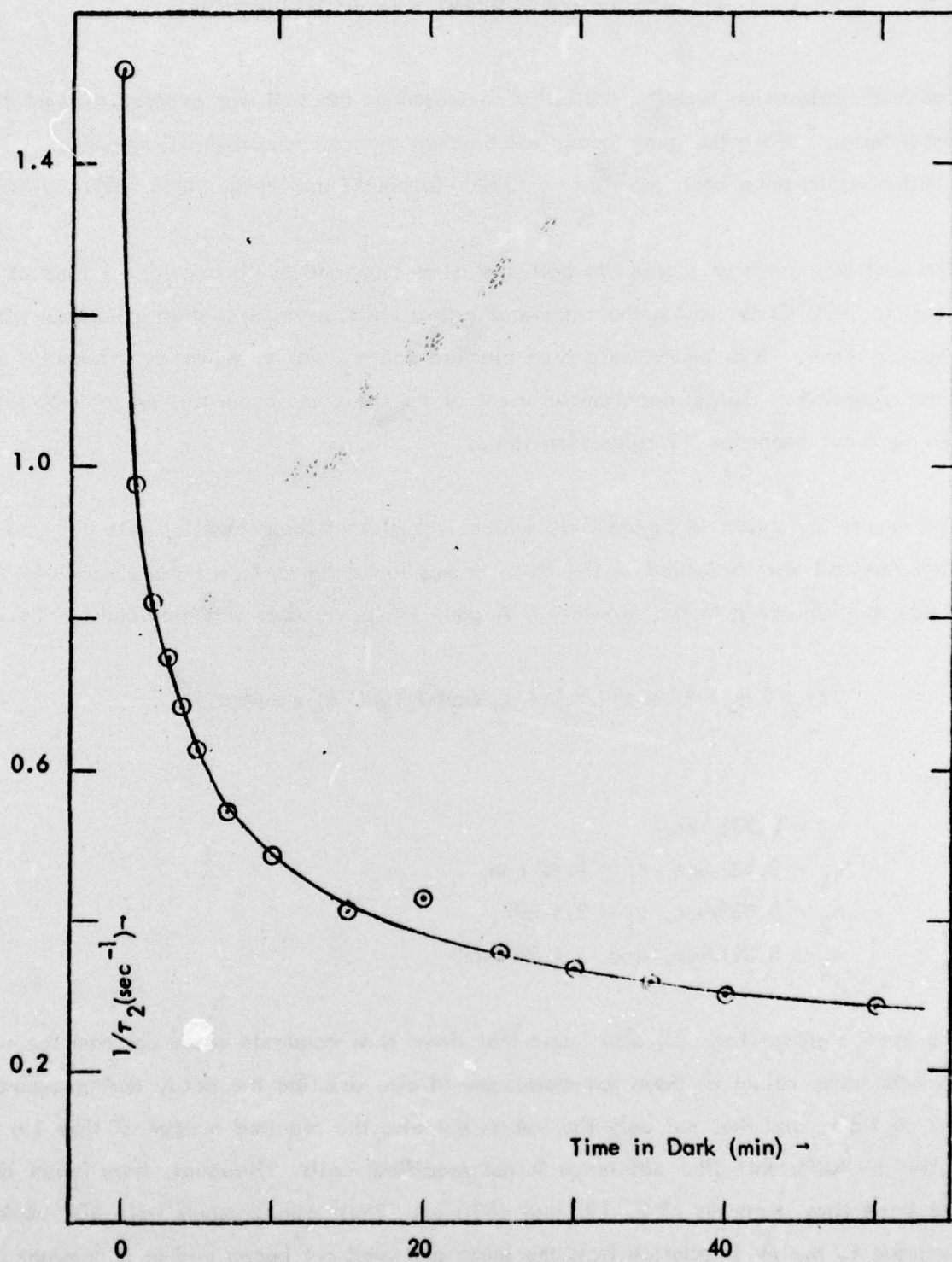


FIGURE 7-12. Decrease in ^{199}Hg Relaxation Rate With Time After Exposure of the Cell to uv Radiation.

THE SINGER COMPANY • KEARFOTT DIVISION

These authors point out that the photoelectric efficiency of a silica surface is greatly enhanced by exposure to intense uv radiation and suggest that this process could be associated with the observed increase in the ^{199}Hg relaxation rate. However, during our measurements it was consistently observed that despite its greater intensity at the ^{199}Hg cell the read out beam had far less effect on the cell wall relaxation than did the pump beam. Since the filter cell in the read out beam removed most of the ^{199}Hg resonance radiation it was suspected that at least part of the effect was associated with an interaction between the cell walls and excited ^{199}Hg atoms.

In order to investigate this apparent wavelength dependence more carefully and still use the filtered read out beam for the relaxation time measurements the apparatus was modified so that the pump beam could be obtained from two different ^{204}Hg lamps. The light beams from both lamps were arranged to be incident on the same beam-splitting linear polarizer and directed so that one beam was polarized by reflection and the other by transmission. A photodiode* was set up in the transmitted beam whose reflected component was used for pumping and could thus monitor the individual intensities or the total intensity of the light from the lamps.

Either lamp could be used for pumping and the other used as a "spoiler", i.e., to provide the uv radiation to which the cell was exposed. Either a $^{199}\text{Hg}/^{201}\text{Hg}$ filter cell or an attenuator could be inserted between the spoiler lamp and the beam splitter. The attenuator was selected so as to reduce the intensity of the unfiltered spoiler beam to the level obtained with the filter cell in place.

When the spoiler lamp was only used for pumping the presence of the filter cell caused a reduction in the observed NMR signal from ^{199}Hg to less than 2% of the value obtained with the attenuator in the spoiler beam. This demonstrated that the filter cell removed most of the ^{199}Hg hyperfine resonance radiation components from the beam.

*This was later replaced by the photomultiplier P_1 shown in Figure 3-1.

THE SINGER COMPANY • KEARFOTT DIVISION

In the experiment the ^{199}Hg cell was exposed to both the pump and spoiler beams until the relaxation rate had been increased to $\sim 3/\text{sec}$. After 45 minutes in the dark the cell had so recovered that the relaxation rate was only $0.36/\text{sec}$. Following this, the cell was exposed continuously to the filtered spoiler beam until the relaxation rate had reached an approximately steady-state value of $0.53/\text{sec}$. Further exposure to the unfiltered but attenuated spoiler beam increased this steady-state level to $0.69/\text{sec}$.

Since removal of the filter cell from the spoiler beam increased the steady-state relaxation rate by $\sim 30\%$, it is concluded that production of at least one type of ^{199}Hg cell-wall relaxation center requires the presence of ^{199}Hg resonance radiation and very probably involves an interaction between the walls and excited ^{199}Hg atoms.

In the light of information obtained since this experiment was performed (1974), particularly those experiments showing that excited Hg atoms are also involved in producing changes in Hg vapor density (Section 6), it is considered important to extend the measurements to cells made of glass as well as the other grades of fused silica.

7.6.2 High Energy Radiation

Preliminary tests were made of the effects of high energy radiation on the cells, W1 and W2, made of the Suprasil W2 grade of fused silica. The relaxation times for these cells had been previously measured over a period of many months and found to be stable before the tests. The cell W1 was exposed to gamma rays and neutrons at the White Sands Missile Range Nuclear Weapons Effects Division Labs. The cell was exposed to the neutron source three times about one hour apart. The fluence was estimated to be 5×10^{13} for each exposure. This was followed by exposure to gamma rays from ^{60}Co for a total dose of $2.35 \times 10^6 \text{R}$.

No visible changes were observed in the cell. Several weeks after the exposure the NMR relaxation times were again measured and found to be the same as before exposure.

THE SINGER COMPANY • KEARFOTT DIVISION

In a second test, cell W2 was irradiated with 800,000 Rad (Si). The source was 10Mev electrons from a Linear Accelerator. Again no change in the cell's appearance or performance was found.

THE SINGER COMPANY • KEARFOTT DIVISION

8. REFERENCES

1. J. Simpson, L. Ferriss, and I. Greenwood, KD-75-31, "Final Report - Experimental Test Results on Test Bed Model of Magnetic Resonance Gyro, Magnetic Resonance Gyro Development," Contract N62269-73-C-0408, The Singer Company, Kearfott Division, June 19, 1975.
2. S. Sherman, "Interim Technical Note on Nuclear Gyroscope Study," Appendix 6, WADD-TN-60-120, March 1960.
3. H. Strell, "Analysis of D-I and Inertial Systems," General Precision Laboratory Internal Technical Memorandum, September 17, 1956, unpublished.
4. S. Goldman, "Laplace Transform Theory and Electrical Transients," Dover, 1966.
5. C. Kittel, "Elementary Statistical Physics," John Wiley, 1958.
6. D. I. Shernoff, Rev. Sci. Instr., 40, 1418 (1969).
7. B. Cagnac, "Orientation Nucleaire par Pompage Optique des Isotopes Impairs du Mercure," Doctoral Thesis, University of Paris, December 1960.
8. A. G. G. Mitchell and M. W. Zemansky, "Resonance Radiation and Excited Atoms," The Macmillan Co., New York, 1934.
9. S. Dushman, "Vacuum Technique," p. 804, John Wiley & Sons, New York, 1949.
10. R. B. Sosman, "The Phases of Silica," Rutgers University Press, New Brunswick, N.J., (1965).
11. F. M. Ernsberger, J. Phys. Chem. Solids, 13, 347 (1960).
12. W. Happer, Rev. of Mod Phys. 44, 169 (1972).
13. C. Cohen-Tannoudji, Journal de Physique, 24, 653 (1963).
14. A. M. Bonnot and B. Cagnac, C.R. Acad. Sc., Paris, 274, 947 (1972).
15. B. Cagnac, in "Proceedings of the International Conference on Optical Pumping and Atomic Line Shape," Ed. T. Skalinski, IUPAP Warsaw, Poland, 25-28 June 1968, "Separation of Magnetic Resonance Lines by the Method of Light Shifts."

THE SINGER COMPANY • KEARFOTT DIVISION

16. B.Cagnac and G. Lemeignan, C.R. Acad. Sc. Paris 264, 1850 (1967).
17. D.E. Swets, R.W. Lee, and R.C. Frank, J. Chem. Phys. 34, 17 (1961).
18. W.A. Fitzsimmons, L.L. Tankersley, and G.K. Walters, Phys. Rev. 179, 156 (1969).
19. V.O. Altemose, J. Appl. Phys. 32 (1961).
20. C.Cohen-Tannoudji and J. Brossel, C.R. Acad. Sc. Paris 258, 6119 (1964).

THE SINGER COMPANY • KEARFOTT DIVISION

9. PARTICIPANTS IN THE PROGRAM

In addition to the authors, the following people have participated in this program:

- a) Vincent Benischek
- b) Lincoln Ferriss
- c) Edward Kling
- d) Donald Shernoff
- e) James Stevens
- f) Michael Tarasevich
- g) Professor Robert Novick

All are employees of The Singer Company, Kearfott Division except Professor Novick of Columbia University who participates as a consultant.

UNCLASSIFIED

SECURITY CLASSIFICATION OF THIS PAGE (When Data Entered)

REPORT DOCUMENTATION PAGE

READ INSTRUCTIONS
BEFORE COMPLETING FORM1. REPORT NUMBER
(18) AFOSR - TR - 76 - 1418

2. GOVT ACCESSION NO.

3. RECIPIENT'S CATALOG NUMBER

4. TITLE (and Subtitle)

Noise Sources in NMR Oscillators and Relaxation
Phenomena in Optically Pumped Mercury Isotopes.

5. TYPE OF REPORT & PERIOD COVERED

Final Scientific Report.
June 1972 - July 1976.

6. AUTHOR(s)

Donald S. Bayley, Ivan A. Greenwood,
James H. Simpson

7. PERFORMING ORG. REPORT NUMBER

KD 76-31

8. CONTRACT OR GRANT NUMBER(s)

F44620-72-C-0047

9. PERFORMING ORGANIZATION NAME AND ADDRESS

The Singer Company, Kearfott Division
1225 McBride Avenue
Little Falls, New Jersey 0742410. PROGRAM ELEMENT, PROJECT, TASK
AREA & WORK UNIT NUMBERS

61102F

9767-01

11. CONTROLLING OFFICE NAME AND ADDRESS

Air Force Office of Scientific Research/NP
Bolling AFB
Washington, D.C.

12. REPORT DATE

August 1976

13. NUMBER OF PAGES

110

14. MONITORING AGENCY NAME & ADDRESS (if different from Controlling Office)

15. SECURITY CLASS. (of this report)

UNCLASSIFIED

15a. DECLASSIFICATION/DOWNGRADING
SCHEDULE

16. DISTRIBUTION STATEMENT (of this Report)

(16) 9767

Approved for public release;
distribution unlimited.

(17) 01

17. DISTRIBUTION STATEMENT (of the abstract entered in Block 20, if different from Report)

18. SUPPLEMENTARY NOTES

19. KEY WORDS (Continue on reverse side if necessary and identify by block number)

Nuclear Gyroscope, Nuclear Magnetic Resonance, Nuclear Quadrupole Resonance,
Nuclear Spin Polarization, Nuclear Spin Relaxation, Mercury Isotopes, Mercury Resonance
Radiation, Optical Pumping, Solid Phases of Silica, Surface Properties of Fused Silica,
White Noise.

20. ABSTRACT (Continue on reverse side if necessary and identify by block number)

Two investigations are described: the effects of noise in NMR oscillators, and spin
relaxation of optically pumped Hg nuclei.A suitable noise model was provided by white-noise forcing of an NMR oscillator
based on linearized Bloch equations. Experimental confirmation at the microhertz
level was obtained.

UNCLASSIFIED

SECURITY CLASSIFICATION OF THIS PAGE(When Data Entered)

Block 20 (continued)

Measurements of Hg vapor density in one fused silica cell indicated the existence of three Hg-wall binding states. Excited Hg atoms were required to stimulate interstate transitions. Maximum spin-relaxation times for ^{199}Hg measured in glass and fused silica cells were, respectively, 40 and 11 min for ^{199}Hg and 50 and 100 sec for ^{201}Hg . In some fused silica cells evidence was found for a magnetic relaxation mechanism whose strength increased rapidly with temperature and may depend on the surface structure of the cell walls. By observing beats in free precession decay of ^{201}Hg electric quadrupole splittings as small as 1mHz were measured. Cell-intrinsic quadrupole splittings as large as 6.5mHz for fused silica and 17mHz for glass were observed. The cell-intrinsic splitting approached zero as the cell-axis-magnetic-field angle approached 55°. The relaxation rate on fused silica was enhanced after excited Hg atoms had been present in the cell.

55 deg